1-1-2016

Development Of Single And Array Electro-Chemical Sensors For Real-Time Trace Metal Analysis In Aqueous Environmental Media

Yuanyuan Yang
Wayne State University,

DEVELOPMENT OF SINGLE AND ARRAY ELECTRO-CHEMICAL SENSORS FOR REAL-TIME TRACE METAL ANALYSIS IN AQUEOUS ENVIRONMENTAL MEDIA

by

YUANYUAN YANG

DISSERTATION

Submitted to Graduate School

of Wayne State University,

Detroit, Michigan

in partial fulfillment of the requirements

for the degree of

DOCTOR OF PHILOSOPHY

2016

MAJOR: CHEMISTRY (Analytical)

Approved By:

_____

Advisor Date

_____

_____

_____

_____

DEDICATION

To Nian Liu

ACKNOWLEDGEMENTS

First and foremost, I would like to express my special appreciation and thanks to my advisor Dr. Parastoo Hashemi. It has been an honor to be one of her first Ph.D. students. She has always been extraordinarily patient and supportive in mentoring me to become an independent and confident scientist. Her joy and enthusiasm for research as well as life has always motivated me. She provided me the best opportunities and experiences I could ever ask for.

I would like to thank my co-advisor Dr. Jennifer L. Stockdill. She has guided, supported, and encouraged me throughout these years. I appreciate all her contribution of time, ideas, and energy to achieve our shared goals in research. I would like to acknowledge all my colleagues in Hashemi group and Stockdill group, especially Pavithra, Thushani, Srimal, Aya, Ahmad, Audrey, Kevin, Anisa, Matt, Megan, Christine. You all have provided selfless support and sincere friendship over these years.

I have had pleasure of working with many talented collaborators on different projects. Dr. Shawn P. McElmurry introduced me to the world of environmental chemistry. Dr. Mark Cheng and Wenwen Yi taught me advanced engineering techniques and provided numerous intellectual ideas.

I am very grateful to the remaining members of my committee, Dr. Stephanie L. Brock and Dr. Colin F. Poole. They have provided numerous brilliant comments and feedback. My gratitude is also extended to Dr. Munk for guiding me in teaching. It has been so inspiring and cheerful to work with her. I also want

to thank Melissa and Bernie for giving tremendous help no matter what task or circumstance I brought to them.

Last but not the least, I would like to thank my family: my parents and my grandparents for endless love and trust, my boyfriend Da Li for unconditional caring and accompany. This acknowledgement would not be complete if I did not mention my friends, Beixi Wang, Yueting Zhao, Wenjing Zhang, Tian Shi, Chenchen He, and Habib Baydoun. They all have made indirect but important contributions to my doctoral degree's completion.

PREFACE

This dissertation is based closely on the following refereed publications:

Chapter 2: Pathirathna, P., Yang, Y., Forzley, K., McElmurry, S. P., Hashemi, P., Fast-Scan Deposition-Stripping Voltammetry at Carbon-Fiber Microelectrodes: Real-Time, Subsecond, Mercury Free Measurements of Copper, *Analytical Chemistry*, **2012**, 84(15): 6298-6302.

Chapter 3: Yang, Y., Pathirathna, P., Siriwardhane, T., McElmurry, S. P., Hashemi, P., Real-Time Subsecond Voltammetric Analysis of Pb in Aqueous Environmental Samples, *Analytical Chemistry*, **2013**, 85(15): 7535-7541.

Chapter 4: Yang, Y., Ibrahim, A. A., Stockdill, J. L. and Hashemi, P. A Density-Controlled Scaffolding Strategy for Covalent Functionalization of Carbon-Fiber Microelectrodes, *Analytical Methods*, 2015, 7: 7352-7357.

Chapter 5: Yang, Y., Ibrahim, A. A., Hashemi, P. and Stockdill, J. L., Real-Time, Ultra-Selective Detection of Copper(II) using Ionophore-Grafted Carbon-Fiber Microelectrodes, *In preparation.*

Chapter 6: Yang, Y.,* Yi, W.,* Hashemi, P., Cheng, M., A Novel Carbon Nanofiber Pyrolyzed Photoresist Microelectrode Array for Fast Scan Cyclic Voltammetry Analysis, *In preparation,* *Contributed equally.

TABLE OF CONTENTS

LIST OF SCHEMES AND TABLES

LIST OF FIGURES

LIST OF ABBREVIATIONS

ASV	anodic stripping voltammetry
CAN	acetonitrile
AFM	atomic-force microscopy
BFE	bismuth film electrode
CuAAC	copper-catalyzed azide alkyne cycloaddition
CFM	carbon fiber microelectrode
CV	cyclic voltammogram
DOS	density of state
DSV	deposition-stripping voltammogram
EDTA	ethylenediaminetetraacetic acid
EDS	energy dispersive x-ray spectroscopy
Fc	ferrocene
FIA	flow injection analysis
FSCV	fast-scan cyclic voltammetry
FSDSV	fast-scan deposition-stripping voltammogram
GF-AAS	graphite furnace atomic absorption spectroscopy
HMDE	hanging mercury drop electrode
HPLC	high-performance liquid chromatography
ICP-MS	inductively coupled plasma mass
ISE	ion selective electrodes
LOD	limit of detection
LPCVD	low-pressure chemical vapor deposition
MEA	microelectrode array

XPS	X-Ray photoelectron spectroscopy
PECVD	plasma enhanced chemical vapor deposition
ppb	parts-per-billion
PPF	pyrolyzed photoresist film
SA	stripping analysis
SD	standard deviation
SEM	scanning electron microscopy
SHE	standard hydrogen electrode
$TBAPF_6$	tetrabutylammonium hexafluorophosphate
TBAF	tetrabutylammonium fluoride
TMS	trimethylsilyl
TBS	*t*-butyldimenthylsi
TIPS	triisopropylsilyl

CHAPTER 1. INTRODUCTION

1.1 Electrochemical Detection of Trace Metals

Detection of trace metals (i.e., Cu, Pb, As, etc.) has significant importance for studying biological and environmental processes.[1-3] Trace metals, as essential micronutrients for human beings, are required in numerous metabolic and physiological systems. A lack or an excess of trace metals can lead to serious diseases such as gastrointestinal disease, liver and kidney damage, neurological deficits and neurodegenerative diseases.[1] High concentrations of trace metals are introduced to the environment by anthropogenic activities such as mining, smelting and industrial processes. Mobilized metals are pervasive, often reaching and contaminating natural waters.[4] Unlike organic pollutants, natural degradation of metal does not occur, thus metal pollution is persistent.[4] Removal of metals from aqueous systems is essential to mitigate their negative impact on the environment and on humans. Typical mitigation strategies include immobilization and concentration via suitable sorbents to keep toxic metals at low levels prior to release into the environment.[5] Quantitative analysis of the trace metals is a fundamental requirement to treat and remove trace metals most effectively.

Because the toxicity of trace metals strongly depends on their physio-chemical forms, including particulate (> 1 μm), colloidal (1 nm-1 μm) and dissolved (≤ 1 nm) species, measurements of total metal concentrations are not sufficient to understand metal mobilization and transport.[6] Speciation (specific species or groups of homologous species), therefore, is the essential information required to apply mitigation methods.

Current analytical techniques for metal determination can be divided into two major categories: spectroscopy[7,8] and electrochemistry.[6,9,10] The major spectroscopic methods are UV-Vis Spectroscopy, graphite furnace atomic absorption spectroscopy (GF-AAS) and inductively coupled plasma mass spectroscopy (ICP-MS). They have extensive applications in laboratory examinations for a variety of elements and offer high sensitivity and selectivity. Their applications in the field, however, are limited due to poor portability associated with instrumentation, high energy consumption and costs, and elaborate sample preparation.[11] Furthermore, these methods only determine total metal concentrations unless they are coupled with separation and extraction techniques that enable speciation analysis.[11] Additional analysis steps significantly increase the risk of contamination during sample storage and handling, as well as analysis time and budget.

Electrochemistry is another widely accepted analysis method that is typically low cost, instrumentally compact, and technically simple. Electrochemical methods are particularly suitable for *in-situ* metal monitoring in real natural systems, because they do not normally require sample collection or complicated pre-treatment, and can be used to probe environmental water samples directly. Moreover, they are especially powerful for speciation analysis. The sections below summarize the fundamental theory, fabrication, and applications of electrochemical techniques for trace metal measurements.

1.2 Conventional Electrochemical Approaches for Trace Metal Analysis

In the field of metal analysis, a variety of different electrochemical methods have been developed to quantify and/or identify trace metals and their corresponding ions.[12] Among a variety of electrochemistry-based methods, stripping analysis (SA) and ion selective electrodes (ISEs) have been well established for both laboratory and field tests. SA is especially advantageous in speciation studies and for simultaneous detection of several different metals. Potentiometric ISEs are favored for rapid and selective quantification of certain analytes. Since these two methods have inspired and influenced a number of advancements in this field, they are specifically discussed in detail.

1.2.1 Stripping Analysis

Electrochemical SA was firstly reported at Pt electrodes for measurement of low concentrations of copper by Zbinden et al. in 1931.[13] However, it wasn't until Heyrovsky's dropping mercury electrode (DME) that SA was popularized.[14] In SA, a pre-concentration step is critical in accumulating analyte onto the surface of the working electrode. A detection step follows that identifies and quantifies the analyte of interest via voltammetry or chronopotentiometry. Trace metal analysis is typically carried out via Anodic Stripping Voltammetry (ASV) as shown in **Scheme 1.1**. In ASV, the pre-concentration step involves holding the electrode potential at a negative value for up to 20 minutes to electrodeposit (reduce) metal ions onto the electrode surface. The applied potential is subsequently swept in a positive direction to oxidize the metals to cations and strip them off the electrode. Mercury based electrodes are favorable because mercury creates an amalgam with the deposited metal ions. This amalgamation fundamentally stabilizes the

electrolytic deposition, and leads to sharp and theoretical shaped stripping peaks. Finally, different metal ions can be differentiated and quantified via the potential position of their anodic stripping peaks.

Scheme 1.1. Schematic representation of the three steps in anodic stripping voltammetry (ASV) for metal analysis.

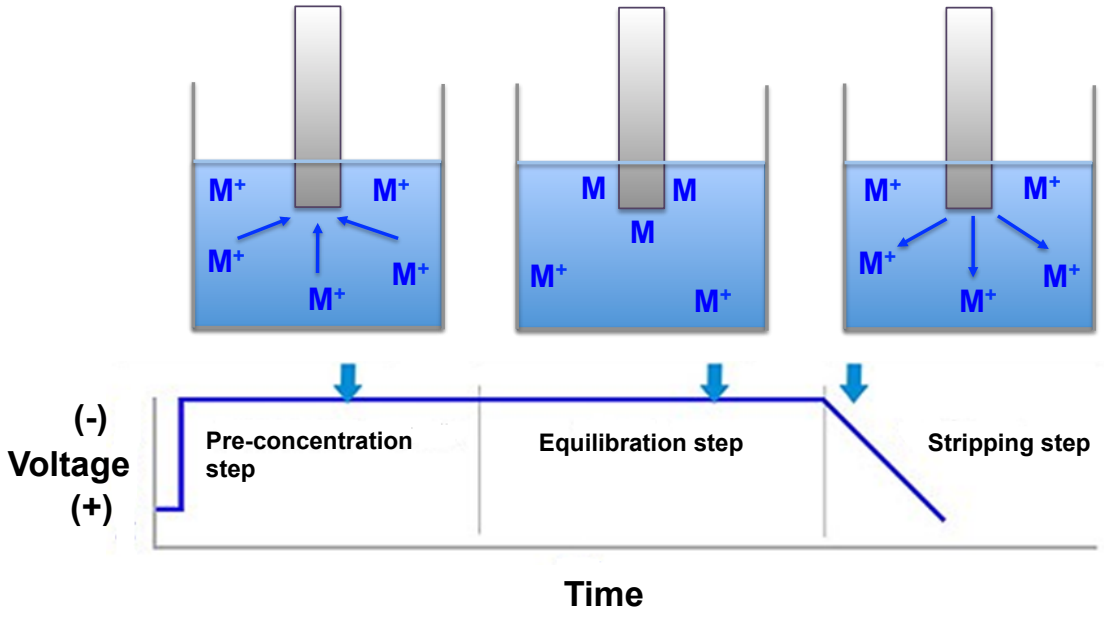

Improvements in sensitivity are usually achieved by controlling the accumulation step and two major modifications have been described in this context: (a) addition of adsorptive materials in solution[15] and (b) attachment of selective accumulation agents (i.e., ligand, ion-exchanger) on electrodes.[16] In method (a), a selective complexing ligand is added to the sample and forms a complex with the metal; this complex is then physisorbed on the electrode surface. Here, either the metal cation or the ligand can be reduced for analysis. Method (b) is based on chemically modified electrodes. Both methods can assist detection of the metals that are not readily oxidized during the stripping step, or species that produce overlapping stripping peaks.[12]

Over the last few decades, major efforts have been made in finding an environmental-friendly alternative to Hg as an electrode material. Although Hg electrodes provide excellent sensitivity, selectivity, stability, and a wide potential window, they are undoubtedly hazardous and toxic to use. Carbon electrodes,[17] screen-printed electrodes,[18] solid amalgam electrodes,[19] bismuth film electrode,[20] microelectrodes,[21] and microelectrode arrays[22] have been actively investigated, representing various levels of promise as alternatives to Hg.

1.2.2 Ion Selective Electrode

ISEs are analytical potentiometric electrochemical sensors with numerous applications in environment, clinical chemistry, biochemical and physiological researches.[23] The history of ISEs can be traced back to the 1930s, when the first glass electrodes became commercially available.[24] The field of ISEs has progressively grown since the invention of ion-binding receptors (i.e., ionophore or ion carriers).[25] For either type, ISEs report electrical potential depending on the type and concentration of the analyte ion.[26]

For selective metal analysis, ionophores (e.g., crown ethers) or chelating agents can complex selectively to a particular metal ion of specific dimensions that bind into the cavities of the ionophore's molecule structures.[27] A large number of ionophore-based ISEs with selectivities for alkali metal cations (e.g., K^+, Na^+, Li^+)[28] and alkaline earth metal cations (e.g., Mg^{2+}, Ca^{2+})[29] have been described and successfully commercialized. For example, a valinomycin-based potentiometric ISE has replaced flame atomic emission spectroscopy as the standard analytical instrument in measurement of K^+ in biological samples, such

as blood and urine.[30] For transition metal ions (e.g., Cu^{2+}, Ag^{+}, Zn^{2+}, Cd^{2+}, Hg^{2+}, Pb^{2+}), advancements in ionophore designs and electrode constructions are still in progress.[25]

Polymers[31] and nano-materials[9] are commonly used as ionophore-doped membranes to create solid-contacts. They are ideal transduction materials because of their highly efficient electrochemical conductivity.[32] Solid contacts have significantly improved the mechanical stability of ISEs, however, there remain two critical technical issues. First, the thickness of the polymeric membrane usually extends the electrode response time to minutes. Next, formation of a water layer at the metal-membrane interface leads to instabilities, which shortens ISEs' shelf life.

ISEs provide a simple and low-cost option for ion detection in aqueous media. Good portability also makes ISEs suitable for online and field analysis. Major concerns remain in understanding the thermodynamics and kinetics that describe the electrochemical response and the selectivity of ISEs. For trace metals, new sensing modes and electrode designs, in additional to the use of novel materials, such as novel polymer matrixes, nanostructured materials, or biomaterials still are the subject of continued studies.[23] Moreover, in order to develop ISEs with real utility for trace metal analysis, substantial progress will be required in many aspects such as lowering detection limits, improving selectivity, biocompatibility, and long-term stability.

1.3 Fast-Scan Cyclic Voltammetry at Carbon-Fiber Microelectrodes

A number of endeavors have been made to improve electroanalysis in terms of sensitivity, selectivity, stability, and speed. Fast scan cyclic voltammetry (FSCV) at carbon fiber microelectrodes (CFMs) is a powerful method that fulfills these criteria. FSCV at CFMs was first introduced for neuroscience applications in 1979;[33] however, the high scan rates utilized generate a large, capacitive background current that drastically interferes with observation of the faradaic signal. In order to extract the small faradaic current from the huge charging current, a digital data processing program was developed to subtract out the background current.[34]

In FSCV, an electrochemical waveform is applied to the CFM at a high scan rate (> 100 V/s) for rapid analysis. The waveform usually has a width of several ms and is applied at 10 Hz. In between each waveform application, the CFM is held at a resting potential and provides the time for the analyte to adsorb onto the CFM.[35-37] When the waveform is applied, the adsorbed analyte undergoes redox reactions at the surface of CFM. Through optimization of the potential limits, scan rate and frequency, analytical performances in sensitivity, selectivity, and temporal resolution can be controlled. The FSCV signal is usually interpreted via cyclic voltammogram (CV) and color plot. For instance, **Figure 1.1** is a typical FSCV data set for 1.0 μM dopamine analysis. **Figure 1.1.A** is a CV of dopamine, the peak potentials provide a chemical signature to identify the species detected. Peak current is proportional to concentration within the detection limits. **Figure 1.1.B** is a color plot, which is digitally constructed through stacking a series of CVs in the sequence of time. It provides information for each measurement in

three dimensions: current, voltage, and time. **Figure 1.1.C** is a plot of current vs. time. It can be used to monitor the concentrations of the analyte.

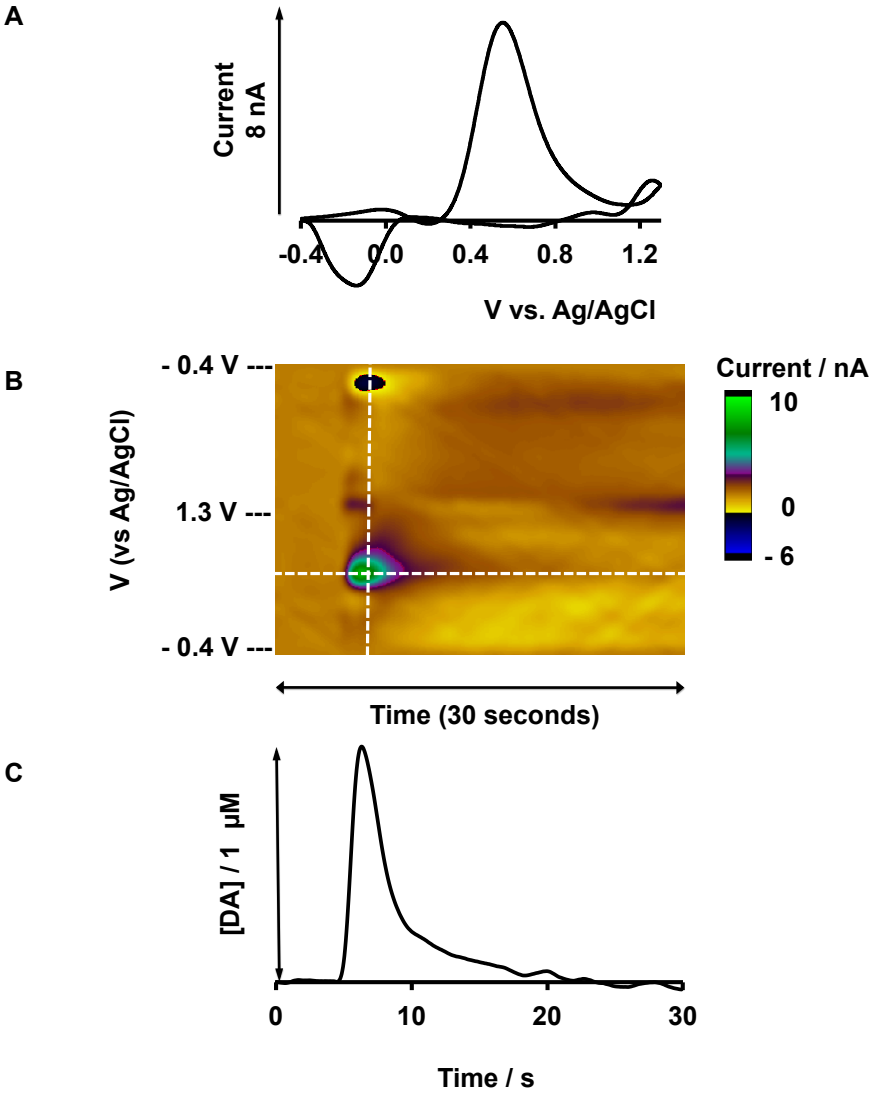

Figure 1.1. (**A**) CV (i vs v) taken from the white vertical dashed line in part B. (**B**) Color plot with potential on the y-axis plotted against time on the x-axis and the current response represented in false color. Dopamine (1.0 µM) is injected over the period spanning 5 to 10 s. (**C**) i vs time from the horizontal white dashed line at peak reduction potential.

FSCV has been mainly employed for detecting electroactive species *in vitro* and *in vivo*, such as neurotransmitters[38] (e.g., dopamine,[39] serotonin,[40] histamine[41]), O_2,[42] and pH changes.[43] Most recently, as I describe in this thesis,

our lab has extended FSCV to monitoring fluctuations of Cu^{2+} and Pb^{2+} in environmentally relevant studies.[35,44,45]

CFMs are the conventional electrodes used in FSCV. Their micron dimensions render them minimally impactful on their surroundings. CFMs own all the advantages of carbon electrode materials such as low cost, excellent electrochemical behaviors, and biological compatibility. CFMs can be fabricated in a variety of ways, either through insulation of a carbon fiber (5 – 35 μm diameters) in a glass capillary and cutting the protruding fiber to form a cylindrical electrode (as shown in **Figure 1.2**), or by treating the seal with epoxy and polishing the tip to form an elliptical surface. The exposed carbon fiber is rich in surface oxygen groups, which facilitate analyte adsorption onto the electrode surface.[35-37]

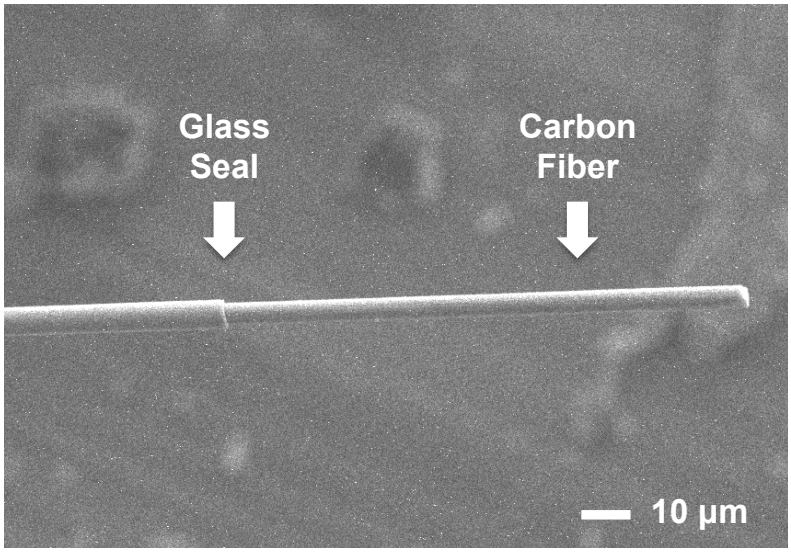

Figure 1.2. SEM image of a glass capillary sealed CFM.

To meet lower detection limits, a number of novel FSCV compatible sensors have been developed. For instance, carbon-nanotube based microelectrodes have shown increased electron-transfer kinetics and sensitivity for adsorption-

controlled species such as dopamine.[46] Microelectrode arrays (MEAs), which incorporate multiple sensing elements onto a single device, have also been developed to resolve spatial profiles, and own great potential for simultaneous detection for different analytes.[47]

1.4 Covalently Modified Carbon Electrodes

Electrode materials play vital roles in the production of high performance electrodes, particularly those requiring high selectivity[48,49] and those used in catalysis.[50,51] Different methods have been applied for surface modifications, which includes electrostatic interactions,[52] adsorption,[53] non-covalent interactions,[54] as well as covalent modifications.[55] Most non-covalent methods share intrinsic weaknesses of slow response, short lifetime, degradation, and bad stability. Conversely, covalent modification is especially effective in terms of stability and reproducibility.[56]

Herein the discussion is focused on covalent modifications of carbon electrodes. Carbon electrode have a number of allotropic forms such as glassy carbon, carbon fibers, boron doped diamond, powdered graphite, and highly ordered pyrolytic graphite. Since electrochemistry is fundamentally based on surface interactions, the nature and structure of the carbon surface significantly affect electrochemical behavior.[57] One impacting factor is the effect of electronic density of state (DOS) on electron transfer.[56] Another important feature of the carbon surface is the natural occurrence of oxygenated functional groups, including carboxyl, hydroxyl, ester, ketone and ether as shown in **Figure 1.3**.[56] These oxygenated groups influence not only electron transfer rates but also

adsorption. A better control of the surface properties by means of covalent modification is desirable to us for analysis of real samples where several similar metals are often present.

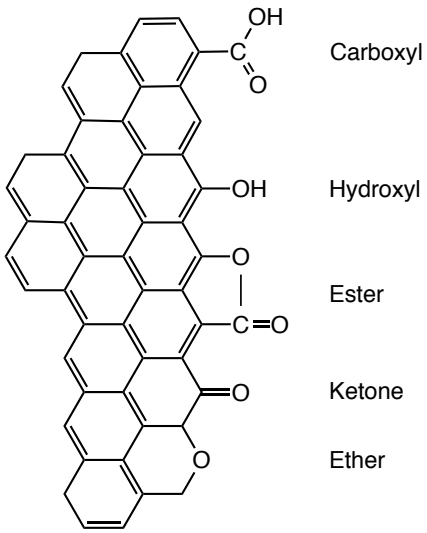

Figure 1.3. Oxygenated groups presented at carbon material surfaces.

There have been limited methods enabling covalent modification of carbon surfaces with organic molecules for improved performances. Several early covalent modifications include the creation of amide bonds[49] and the bonding of acid chloride with surface hydroxyl groups.[58] However, the application of these reactions has been fundamentally limited by low reaction yields, harsh conditions, and side reactions.[56]

The most widely accepted covalent modification of carbon is electrochemical reduction of diazonium reagents created by Saveant et al. in 1992.[59] This reaction can introduce a persistent and condensed layer of aryl molecules on carbon electrode surfaces through C-C bonding. Aryldiazonium functionalization is applicable to carbon electrodes in which the carbon atom hybridization is sp^2 (graphene, carbon nanotube, graphite) or sp^3 (diamond). Different covalent

modification strategies using diazonium, amine, azide, and olefins have been tested both individually and compared to one another.[60,61] Diazonium electrochemical reduction produced a significantly higher density of functionalities on electrode surfaces with improved stability.[60,61]

Click chemistry, which often follows diazonium reduction to achieve post-functionalization, carries advantages of mild reaction conditions, high efficiency and good selectivity. Copper-catalyzed azide alkyne cycloaddition (CuAAC), as the first reaction in click chemistry, occurs between azide groups and terminal alkynes in the presence of a Cu(I) catalytic system and moderate reaction conditions.[62,63] CuAAC provides a fast and reproducible coupling strategy with few side reactions in a variety of reaction conditions. While most chemical modifications lead to the formation of thick, disorganized multilayer films, which may bring uncertainty and inconsistency to the electrode behavior, Leroux *et al.* developed a protection - deprotection method through electrochemical reduction of protected aryldiazonium ions followed by click chemistry to obtain monolayers.[64,65]

Chemically modified carbon electrodes have fundamentally expanded and improved electrochemical sensors and biosensors. As mentioned in **1.2.1**, adsorptive stripping voltammetry has employed ligand-grafted electrodes for detection of certain types of trace metals.[66] Diazonium reduced modified CFMs were employed to achieve an accelerated adsorption rate and increased sensitivity for dopamine detection.[67] Mediator-free biosensors have been developed through immobilizing enzymes directly on conducting substrates for

more efficient and stable glucose detections.[68] In general, covalent modification has provided an innovative electroanalysis platform for improved electrochemical selectivity.

1.5 Scope of This Dissertation

This dissertation presents the fundamental theory, development, and applications of a FSCV based electrochemical technique at CFMs for real-time, sensitive, selective, and stable analytical trace metal measurements.

Chapter 2 presents a Hg-free voltammetric technique that can measure Cu(II) with ppb sensitivity at 100 ms temporal resolution. This chapter reports the first example of using FSCV for the determination of trace metal species. We optimized electrochemical parameters including potential limits and scan rates for Cu(II) analysis. Our initial understanding of the mechanism of metal ions at the CFM interface is explained. We also described the application of using this technique for monitoring dynamic chemical speciation.

Chapter 3 presents a rapid and sensitive approach using FSCV at CFMs to analyze Pb(II) in both model and authentic environmental solutions. In this chapter, we described two novel methodological advances. First, we created an environmentally relevant buffer solution based on geochemical models to enable electrochemical analysis for dissolved Pb(II). Secondly we improved FSCV parameters to assess the method's sensitivity and stability while taking into account Pb speciation. The applicability of our novel method for monitoring rapid Pb fluctuations in real environmental samples was presented.

Chapter 4 reports a scaffolding strategy for covalent modification of CFMs. Although FSCV and CFM showed benefits in ultrafast and sensitive detection of trace metal ions, their application in more complex samples has been limited by analytical selectivity. Our innovative strategy provided the groundwork to generate analyte-selective CFMs based on a universal scheme. We expanded diazonium electrochemical reduction and CuAAC for covalent modification on CFMs. As a proof of principle, CFMs were covalently modified with ferrocene as an *in-situ* redox label through our density-controlled modification strategy.

Chapter 5 describes the generation of ionophore-grafted CFMs for selective detection of Cu(II) by FSCV. Building upon our scaffolding covalent modification strategy, this chapter represents the first example of attaching ionophores onto CFMs for selective analysis in a media of mixed metal ions. We optimized not only organic reaction conditions but also electrochemical analysis parameters to achieve rapid, selective, sensitive, and stable metal measurements. This method will be amenable to grafting a variety of recognition components onto CFMs in a robust manner, and will ultimately allow real-time detection of target analytes in complex environmental systems.

Chapter 6 shows the development of FSCV compatible pyrolyzed photoresist film (PPF) microelectrode arrays (MEAs) towards simultaneous detection of multiple different analytes. In this chapter, we designed a highly reproducible method to produce MEAs with controlled electrode surface areas without compromising device dimensions. A two-step pyrolysis process and a dual O_2 plasma treatment was employed to improve film adhesion and surface reactivity.

As a proof of principle, the compatibility of MEAs for FSCV analysis was demonstrated through highly sensitive and stable dopamine measurements on 4-channel arrays.

Chapter 7 summarizes our work and proposes future research directions.

CHAPTER 2. FAST-SCAN CYCLIC VOLTAMMETRY AT CARBON-FIBER MICROELECTRODES FOR REAL-TIME, SUBSECOND, MERCURY FREE MEASUREMENTS OF COPPER(II)

Elevated concentrations of hazardous metals in aquatic systems are known to threaten human health. Mobility, bioavailability, and toxicity of metals are controlled by chemical speciation, a dynamic process. Understanding metal behavior is limited by the lack of analytical methods that can provide rapid, sensitive, in situ measurements. While electrochemistry shows promise, it is limited by its temporal resolution and the necessity for Hg modified electrodes. In this letter, we apply fast- scan deposition-stripping voltammetry at carbon-fiber microelectrodes for in situ measurements of Cu(II). We present a novel, Hg-free technique that can measure Cu(II) with ppb sensitivity at 100 ms temporal resolution.

Pathirathna, P., Yang, Y., Forzley, K., McElmurry, S. P., Hashemi, P. *Anal. Chem.* **2012**, 84(15): 6298-6302.

2.1 Introduction

In urban areas, anthropogenic sources of heavy metals are a significant public health concern. Mobility, bioavailibity, and toxicity of metals depend on speciation, including complexation with inorganic and organic ligands.[69,70] The ability to dynamically assess low metal concentrations in aqueous solutions is critical for characterizing environmental processes, assessing risks, and mitigating their impact. Spectroscopic techniques study heavy metals with high sensitivity.[71-73] These instruments typically have limited portability and require significant sample handling, which may alter speciation. The majority of in situ research, aiming to understand "unaltered" speciation, has aggressively employed electrochemistry with the ultimate goal of a submersible field device (see review[6] for details). While ion selective electrodes provide high sensitivity with temporal resolution of seconds, their response time (10 – 15 s) limits their application for real-time studies.[74] Techniques such as anodic stripping voltammetry (ASV) have shown promise for environmental applications. ASV involves "deposition" of metal onto an electrode during a negative potential sweep. The metal is subsequently "stripped" off during a positive sweep. A Faradaic current during stripping is typically used to quantify the metal. The extreme sensitivity of ASV has hinged upon two critical factors: (a) Hg (mercury) modification: The "deposition" process can be unstable on conventional electrodes leading to inconsistencies in analyses. Hg on the electrode surface significantly stabilizes this process by creating an amalgam with the depositing metal. (b) Preconcentration: Conventional electrodes are held at a negative

potential for several minutes in order to preconcentrate the heavy metal on the electrode yielding high sensitivity.[75]

Until now, few alternatives existed that could detect low metal levels without Hg (an environmental hazard) and with high temporal resolution (faster than minutes required for preconcentration). In this chapter, we present a Hg-free electrochemical technique that can measure [Cu(II)] with environmentally relevant parts-per-billion (ppb) sensitivity and importantly, a temporal resolution of 100 ms. This temporal improvement, of greater than 3 orders of magnitude, allows real-time metal speciation to be studied.

2.2 Materials and Methods

2.2.1 Solutions

All chemicals were purchased from Sigma Aldrich (St. Louis, MO). The flow injection buffer, Tris buffer, was constituted of the following: $H_2NC(CH_2)OH)_3 \cdot HCl$ (15 mM), NaCl (140 mM), KCl (3.25 mM), $CaCl_2$ (1.2 mM), $NaH_2PO_4 \cdot H2O$ (1.25 mM), $MgCl_2$ (1.2 mM), and Na_2SO_4 (2.0 mM). All solutions were at pH 7.4, at room temperature and atmospheric pressure. For most experiments, Cu was injected at a concentration of 10 μM $Cu(NO_3)_2$ (Sigma-Aldrich, St. Louis, MO, USA). For calibration experiments, $Cu(NO_3)_2$ was injected in different sample concentrations in Tris buffer.

2.2.2 Data Acquisition and Analysis

In order to construct carbon-fiber microelectrodes, a single carbon fiber of 3 μm radius (T-650, Thornel, Amoco Co.) was aspirated into a glass capillary (0.6 mm external diameter, 0.4 mm internal diameter, A-M Systems, Inc., Sequim,

WA). The glass was tapered to form a carbon-glass seal with a micropipette puller (Narishige, Tokyo, Japan). The exposed carbon fiber was cut to approximately 150 μm in length under a microscope. Customized software, TH-1 (ESA, Chelmsford, MA) written in LABVIEW (National Instruments, Austin, TX) was used for waveform generation and data acquisition. A custom-built UEI potentiostat (University of North Carolina at Chapel Hill, Department of Chemistry Electronics Facility) was employed. Signal processing (background subtraction, signal averaging, and digital filtering (4-pole Bessel Filter, 5 kHz)) was performed in TH-1 software.

2.2.3 Flow Injection Analysis

The carbon-fiber microelectrode was placed in a modified HPLC union (Elbow, PEEK 3432, IDEX, Middleboro, MA) and in the output of a manual six-port HPLC loop injector valve (VICI, 6223186, Houston, Texas). The apparatus enabled the introduction of a pulse of analyte to the microelectrode surface using a syringe infusion pump (Harvard Apparatus model 940, Hollison, MA) at a flow rate of 2 mL min^{-1}. In optimizing the system, longer sample loops were used to establish the maximum delivery of analyte to the electrode; the length of the loop was subsequently reduced to provide the maximum signal with the shortest loop length.

2.2.4 SEM-EDS

Scanning electron microscopy and energy dispersive x-ray spectroscopy (SEM-EDS) were performed on a Jeol JSM-6510LV/LGS Scanning Electron Microscope (Peabody, MA). SEM images were collected under high vacuum,

using an excitation voltage of 25 kV and Au sample sputtering. EDS data were collected using a SDD detector. EDS spectra were collected at three distinct locations on each electrode and the values for atomic % Copper were averaged.

2.3 Results and Discussion

Our method is based on fast-scan cyclic voltammetry (FSCV) at carbon-fiber microelectrodes (CFM). FSCV has largely been developed for biological applications[76,77] and employs scan rates between 400 and 1000 V s^{-1}. The time to acquire one cyclic voltammogram is approximately 20 ms. A large charging current can be eliminated by background subtraction when cyclic voltammograms are collected in quick succession (every 100 ms).[78] We now apply this technique, which we refer to as fast-scan deposition-stripping voltammetry (FSDSV), to detect Cu(II) in real-time.

2.3.1 FSCV Characterization for Cu(II)

Deposition-stripping voltammograms (DSVs) collected every 100 ms serve two important purposes, identification and quantification, illustrated in **Figure 2.1**. Here DSVs were collected for 30 s during a flow injection analysis (FIA) of Cu(II) (10 μM) onto a CFM. The potential of the CFM was initially swept in the negative direction from 0 to −1.0 V and then subsequently reversed to +1.0 V at a scan rate of 400 V s^{-1}. The middle panel of **Figure 2.1** provides a representation of all of the background-subtracted DSVs. The interpretation of this color plot is described in detail elsewhere.[79] Cu(II) was injected at the time point indicated by the star.

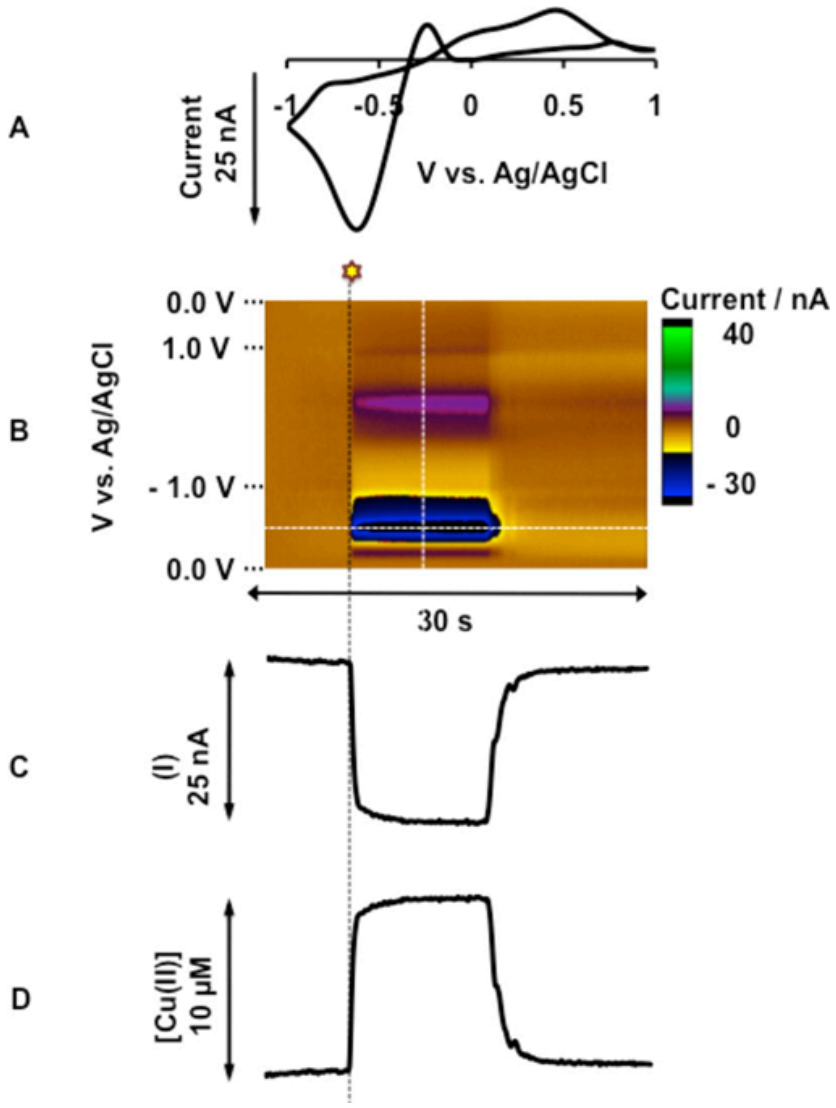

Figure 2.1. (**A**) DSVs (i vs v) taken and reconstructed from the white vertical dashed line in part B. (**B**) Color plot with potential on the y-axis plotted against time on the x-axis and the current response represented in false color. Cu(II) (10 µM) is injected at the time indicated by the black vertical dashed line and star. (**C**) i vs time from the horizontal white dashed line at peak reduction potential. (**D**) [Cu(II)] obtained by taking the reverse of part C and standard calibrations.

Figure 2.1.A is one DSV taken during the Cu(II) injection, indicated by the vertical white dashed line. Peaks corresponding to deposition (−0.6 V) and stripping (0.5 V) are visible as reduction and oxidation peaks. **Figure 2.1.C** is the current taken at the maximum reduction potential for each DSV plotted with time.

Because we are measuring Cu(II) reduction, the current is in the negative direction; however, the signal corresponds to an increase in [Cu(II)]. **Figure 2.1.C** can be converted to [Cu(II)] first with standard calibrations and then via reversal of the current direction. This analysis now represents the sub-second measurement of [Cu(II)] and is shown in **Figure 2.1.D**. FSCV at CFM has been found to be highly sensitive for neurotransmitters,[80] and we found the same for Cu(II), in this example 28.7 nA was obtained for a 10 μM Cu(II) injection. Hemispherical diffusion of the analyte to the CFM surface creates increased mass transport hence increased response. In addition, Faradic current is proportional to the scan rate for absorbed species and again results in an increased response. Moreover, the increased convection effects of flow injection analysis can contribute to an increased signal.

2.3.2 Copper at Carbon-fiber Microelectrodes

In classical ASV, the magnitude of the stripping peak is used for quantification; this is because it is not feasible to quantify deposition due to the pre-concentration that lasts several minutes. The length of our negative sweep is around 2.5 ms, therefore it is possible to acquire a well-defined deposition peak. This peak is advantageous for two reasons. First, the deposition peak has a higher magnitude than the stripping peak, presumably due to kinetics (with an optimized waveform described below, deposition and stripping have magnitudes of 55.8 ± 0.96 nA and 18.0 ± 0.39 nA, respectively (n = 50 ± standard error of the mean)); hence, employing the deposition peak for quantification improves sensitivity. Second, this technique has two characteristic voltages by which to

identify a process. Our future focus is to characterize multiple metals in environmental samples simultaneously. Therefore having both peaks will be particularly important for distinguishing between them.

To analyze multiple metals with both deposition and stripping peaks, it is essential that deposition is stable over multiple readings in the absence of Hg. To establish whether this holds for CFMs, we tested the reproducibility of Cu(s) electro-deposition on CFMs. We applied −1.4 V to the CFM for 0, 1, 5, and 10 min in a solution of Cu(II) (100 μM) and assessed the electrode surface with scanning electron microscopy (SEM) and energy dispersive X-ray spectroscopy (EDS). There is a proportional relationship between the deposition time and % Cu(s) as shown in **Figure 2.2.A**; a visual confirmation of this relationship is observed in the representative scanning electron micrographs (SEMs) for each time group. Here, the SEMs clearly show presence of Cu(s) clusters on the carbon-fiber striations even after 1 min. Trace levels of Cu(s) at 0 min can be attributed to the sample holder material of the instrument. After 1 min, the surface Cu(s) was 1.2 ± 0.2%; after 5 min, 3.2 ± 0.4%; after 10 min, 6.9 ± 1.1%. This shows that we can control the deposition process, an indication of its high stability.

To further validate the stability of deposition, we used an optimized waveform (−1.4 to 1.3 V at 600 V s with a resting potential of 0 V, as described below), we repeatedly injected Cu(II) (10 μM) onto a CFM (50 times), and we recorded the peak reduction current each time. The magnitude of the current observed is plotted against injection number in **Figure 2.2.B**. The response is 55.2 ± 2.1

(standard deviation) ± 0.29 (standard error of the mean) nA (n = 50). The low standard deviation and standard error confirm that this is a stable process. The DSVs exhibited a robust deposition/stripping peak ratio of 3.1 ± 0.03 (n = 50 ± standard error of the mean). Again, the low standard error indicates that deposition is as stable as oxidation, a further index of its high stability.

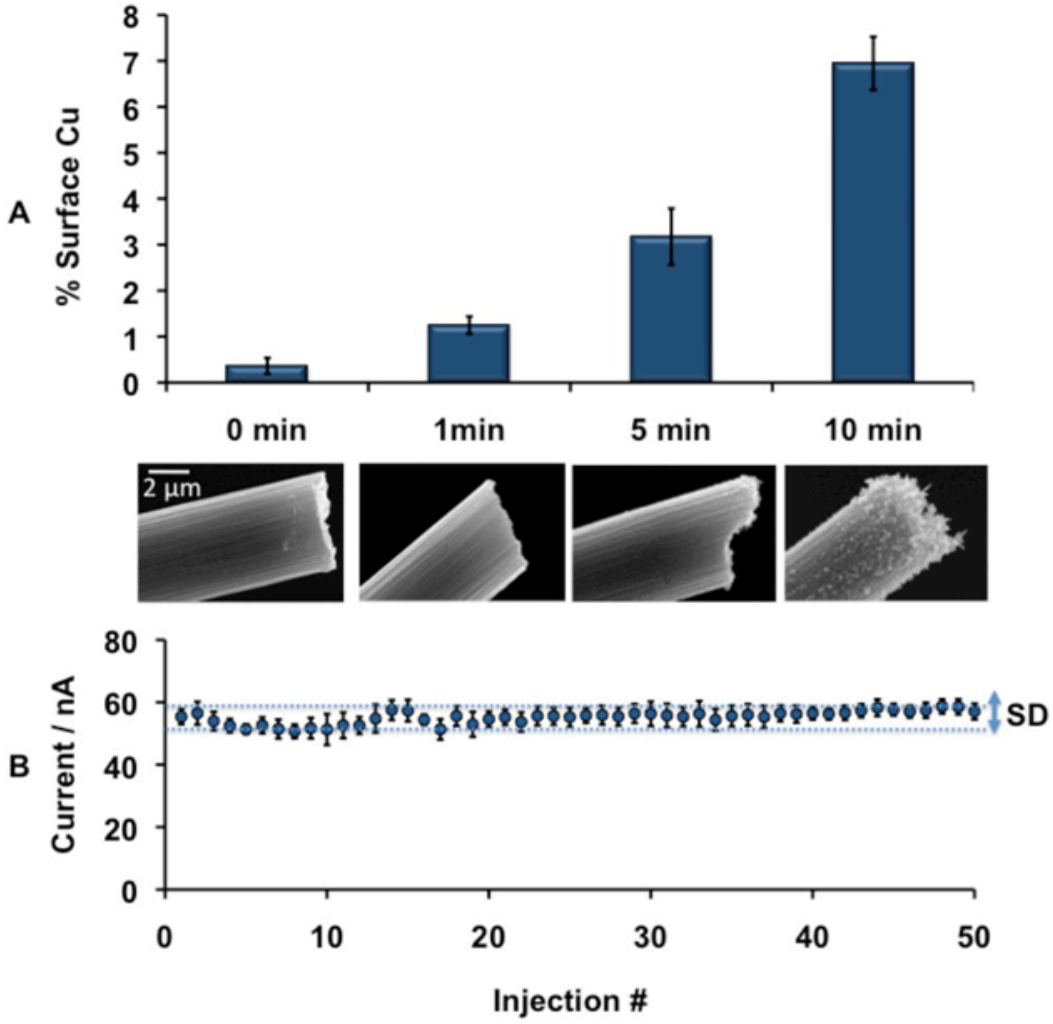

Figure 2.2. (**A**) Histogram showing % surface $Cu_{(s)}$ vs deposition time (0, 1, 5, and 10 min) (n = 3 ± standard error of the mean). Representative SEMs, taken at 8000× magnification for each group are displayed under each histogram block. (**B**) Peak reduction current of successive Cu(II) (10 µM) injections onto a CFM with FIA. (Positive potential limit +1.3 V, negative potential limit −1.4 V, resting potential 0 V, scan rate 600 V s^{-1}). Horizontal lines indicate SD limits.

2.3.3 Waveform Optimization for Cu(II)

Cu(II) reduction is described below:

$$Cu(II) + 2e^- \rightarrow Cu_{(s)} \qquad E^\circ = 0.34 \text{ V vs. SHE}$$

We initially chose waveform parameters that are well established in FSCV. We observed Cu(s) deposition over −0.3 to −0.8 V. The discrepancy may be due to the difference in reference material (SHE vs Ag/AgCl). Another possibility is an iR drop due to slow electron transfer kinetics at high scan rates, during the deposition scan that creates a wide peak separation. The mechanism of this process is a focus of our ongoing studies. With this waveform, the response to Cu(II) (10 μM) is 33.9 ± 4.1 nA (n = 4 ± standard error of the mean).

We varied our waveform parameters to optimize sensitivity to Cu(II). **Figure 2.3.A** shows the averaged current response to Cu(II) (10 μM) when the positive and negative potential limits were varied (n = 4). Each point on the topograph in **Figure 2.3.A** shows the current response at a particular combination of the positive and negative limits. The current is modestly augmented with increasing negative potential; we postulate that this is due to maximized Cu(II) adsorption. There is a more defined trend with an increasing positive limit, with two clear "breaks". First, there is a drop-off at around 0.8 V. This may be due to incomplete stripping, which would reduce the surface available for deposition on subsequent scans. Second, there is an exponential increase after 1.2 V. This has previously been observed for neurotransmitters and is due to overoxidation of the carbon surface. The overoxidation process renders the surface more sensitive due to increased absorption to catalytic oxygen groups[80] and regeneration of the carbon

surface with each scan.[81] Therefore, we set the optimal potential limits to −1.4 to 1.3 V vs Ag/AgCl. However, we found that the response to Cu(II) (10 μM) at 1.3 V, 53.2 ± 10.9 nA (n = 4 ± standard error of the mean), was variable. The metal has a complex interaction with the carbon surface under these conditions; we are currently studying the surface catalysis at 1.3 V to better understand this.

In **Figure 2.3.B** we varied the resting potential from −0.6 to 0.6 V. We found that the optimal resting potential was 0 V (for 10 μM, 36.1 ± 2.0 nA, n = 4 ± standard error of the mean) with two different slopes governing the drop-off in the positive and negative directions. When the rest potential is held at positive potentials, Cu(II) is correspondingly repelled. FSDSV only detects differential responses; therefore, when scanning negatively, there will be a background Faradaic current arising from the deposition that will effectively be subtracted out, manifesting itself as a reduction in signal.

Finally, we varied the scan rate from 100 to 1200 V s^{-1}. There is a linear relationship between scan rate and current up to 1000 V s^{-1} (**Figure 2.3.C**). The slope of log current vs log scan rate is 0.9, close to 1, confirming adsorption driven electro-chemistry. At 1200 V s^{-1} the current is reduced, possibly because of a temporal limitation for deposition (time for the negative sweep at this scan rate is less than 1 ms). At 1000 V s^{-1}, the peak separation was significant enough to cause inconsistencies in the shapes of the DSVs. At 600 V s^{-1}, there were still advantageous current gains, but the shapes of the DSVs were consistent. Therefore, we chose 600 V s^{-1} as our optimal scan rate. Here the current response to 10 μM was 48.7 ± 5.1 nA (n = 4 ± standard error of the mean) and

the limit of detection was 250 nM or 15.8 ppb. Therefore, we present a unique, optimized waveform for online Cu(II) detection, −1.4 to 1.3 V at 600 V s with a resting potential of 0 V.

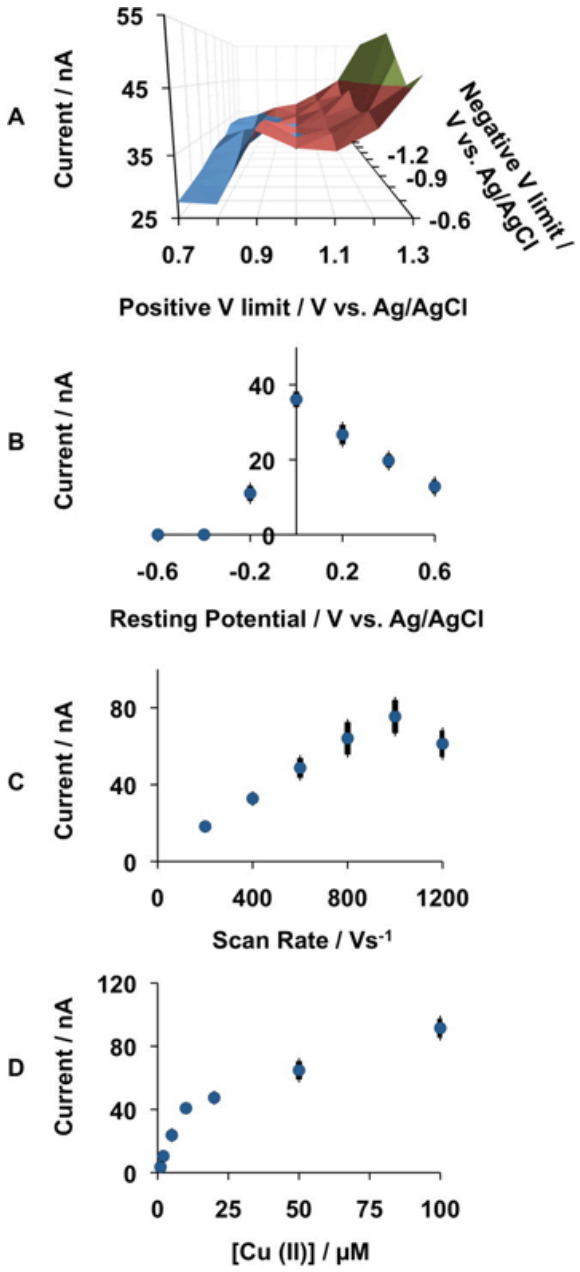

Figure 2.3. (**A**) 3-D representation of peak reduction current of background-subtracted in vitro DSVs of Cu(II) (10 µM) vs positive potential limit (x-axis) and negative potential limit (z-axis) (n = 4).(Resting potential 0 V, scan rate 400 V s^{-1}). (**B**) Variation in peak reduction current when resting potential is varied (n = 4 ± standard error of the mean). (Positive potential limit +1.3 V,

negative potential limit −1.4 V, scan rate 400 V s^{-1}). (**C**) Variation in peak reduction current when the scan rate is varied (n = 4 ± standard error of the mean). (Positive potential limit +1.3 V, negative potential limit −1.4 V, resting potential 0 V). (**D**) Standard calibrations (n = 4 ± standard error of the mean). (Positive potential limit +1.3 V, negative potential limit −1.4 V, resting potential 0 V, scan rate 600 V s^{-1}).

Standard calibrations with this waveform are presented in **Figure 2.3.D** (n = 4 ± standard error of the mean). A linear calibration range up to 5 μM or 318 ppb is suitable for environmental Cu(II) analyses, the sensitivity (slope) in this range is 4.9 nA μM or 0.077 nA ppb.

2.3.4 Speciation Study

The strength of our technique is its time resolution because it is critical for studying speciation, and we demonstrate this in **Figure 2.4.B**. Here, the CFM was immersed into a well-stirred 20 mL of 200 mM $Cu(NO_3)_2$ solution. We injected 1 mL of 1mM ethylenediaminetetraacetic acid (EDTA) at the time point indicated by the star and this created an immediate change. The DSV taken at the vertical white dashed line shows the reverse DSV of Cu(II) indicating that the concentration of Cu(II) decreased (**Figure 2.4.A**). The identity of Cu(II) was verified by the close agreement of peak positions in the inset of **Figure 2.4.A**. Here, the current of the experimental DSV (black solid) was reversed and superimposed onto an DSV of Cu(II) (10 μM) collected in vitro (dashed), both were normalized to the maximum negative current. In **Figure 2.4.C**, the maximum deposition current (reversed) decreased with time reaching a new level indicating less free Cu(II). This is a novel subsecond electrochemical measurement of the Cu(II) binding process by EDTA. We repeated this experiment with four different electrodes and found similar results.

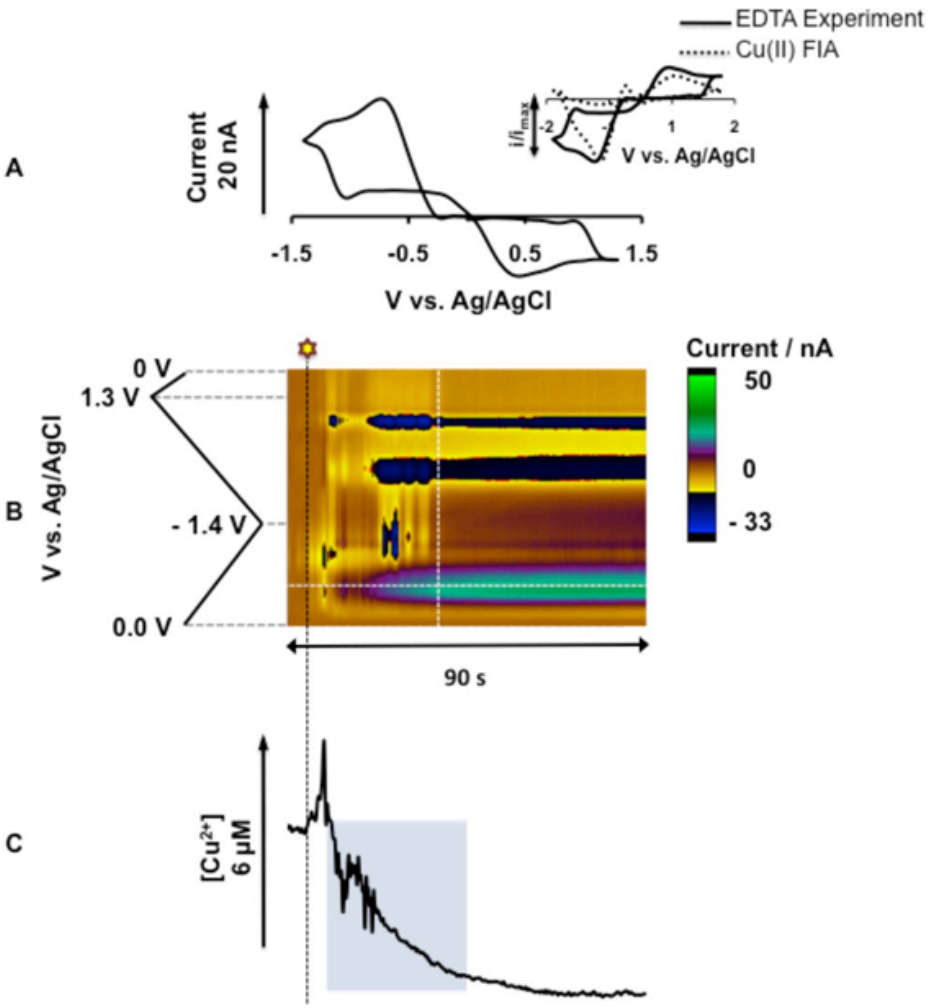

Figure 2.4. (**A**) DSVs (i vs v) taken and reconstructed from the white vertical dashed line in part B. Inset: DSV of Cu(II) (10 µM) taken by FIA (dashed) superimposed on the reverse current DSV taken from white vertical dashed line in part B. (**B**) Color plot with potential on the y-axis plotted against time on the x-axis, and the current response represented in false color. CFM is immersed into a well stirred solution of Cu(II) (20 mL of 200 µM). EDTA (1 mL of 1 mM) is injected at the time indicated by the black vertical dashed line and star.(**C**) [Cu(II)] vs time taken and reversed from the horizontal white dashed line at peak reduction potential.

Quantitative measurements of Cu-EDTA complexation are routinely performed during titrations, where specific points are monitored at equilibrium. The slope in **Figure 2.4.C** represents the magnitude of Cu(II) bound with time or the rate at which EDTA binds Cu(II). This real-time kinetic information is fundamentally novel with electrochemical techniques. Such information is

dependent on a complex variety of information about the system, including temperature, flow, pH, ionic strength, and complexation. These can now be studied using well-established models for Cu(II) speciation. Real environmental samples contain a variety of electroactive interferences; therefore, we are currently identifying and characterizing these substances in order to separate out specific effects of interest.

2.4 Conclusion

In conclusion, studying metal speciation is essential for mitigating the impact of metals in environmental systems. However field technology that provides real-time information on metal speciation has been limited. While portable and low cost, electrochemical techniques have traditionally been limited by their temporal resolution and necessity for Hg. In this chapter, we reported a novel Hg-free technique, FSDSV at CFMs, to perform electrochemical measurements of Cu(II) every 100 ms, without toxicity concerns. We anticipate that our technology will open new frontiers for studying speciation, advancing our ability to reduce the environmental impact of metals.

CHAPTER 3. REAL-TIME SUBSECOND VOLTAMMETRIC ANALYSIS OF LEAD(II) IN AQUEOUS ENVIRONMENTAL SAMPLES

Lead (Pb) pollution is an important environmental and public health concern. Rapid Pb transport during stormwater runoff significantly impairs surface water quality. The ability to characterize and model Pb transport during these events is critical to mitigating its impact on the environment. However, Pb analysis is limited by the lack of analytical methods that can afford rapid, sensitive measurements in situ. In this chapter, we describe two novel methodological advances that bypass the limitations of conventional electrochemical methods. Using geochemical models, we firstly created an environmentally relevant test solution that can be used for electrochemical method development and characterization. We secondly developed a fast-scan cyclic voltammetry (FSCV) method for Pb detection on Hg-free carbon fiber microelectrodes. We assessed the method's sensitivity and stability, taking into account Pb speciation, and utilized it to characterize rapid Pb fluctuations in real environmental samples. We thus present a novel real-time electrochemical tool for Pb analysis in both model and authentic environmental solutions.

Yang, Y., Pathirathna, P., Siriwardhane, T., McElmurry, S. P., Hashemi, P. *Anal. Chem.* **2013**, 85(15): 7535-7541. Reprinted with permission from Copyright (2013) American Chemical Society.

3.1 Introduction

Lead (Pb) is a toxic pollutant commonly found in post-industrial urban watersheds because of its historical use in paints and automotive gasoline and batteries.[82,83] Despite efforts to reduce Pb loadings to the environment, Pb exposure continues to be of great concern to public health. In particular, there is increasing evidence that children exposed to Pb, even at levels previously considered safe, have a high risk for developing adverse neurological and systemic health problems.[84] These concerns, in addition to newly recognized exposure paradigms[85] have created a critical interest in better defining Pb cycling in the environment.

One of the most significant transport processes in urban systems is stormwater runoff. Urban stormwater is the primary source of water quality impairments for 13% of all rivers, 18% of all lakes, and 32% of all estuaries in the United States, despite urban land use constituting only 3% of the land cover.[86] The discharge of metals in stormwater is one of the primary causes for these water quality impairments.[87] In order to prevent the damaging environmental effects of Pb, it is vital to understand the mechanisms of Pb transport during environmental events such as stormwater runoff where solution chemistry is often in disequilibrium.[88] To understand Pb transport, it is necessary to quantify the interactions of Pb with organic ligands and soils dynamically because these reactions have rapid kinetics.[89,90] The lack of analytical methods that can continuously monitor Pb *in situ* with high time-resolution has traditionally limited this goal.

While spectroscopy provides highly sensitive and selective metals measurements, on-site analysis is difficult due to limited portability of the instruments. Moreover, sample collection and preparation do not allow *in situ* analysis. Electrochemistry has shown promise for such measurements,[91-93] because electrochemical reactions occur at a submersible surface. However, concerns about stability, Hg-electrode toxicity and low temporal resolution have severely limited the application of electrochemistry to environmental analyses.

We recently described the application of fast-scan cyclic voltammetry (FSCV) to real-time, sub-second Cu detection.[94] Our method is fast, robust and Hg-free. In this work, we applied a similar approach to Pb characterization. We faced two discrete challenges for experimental FSCV analysis. First, aqueous systems were not available to analyze Pb under conditions that are representative of real natural water systems like those in which we ultimately seek to understand Pb's behavior. Due to Pb's limited aqueous solubility, other researchers performing Pb electrochemistry have traditionally utilized test solutions (buffers) at low pH[95-97] or in acetate[98-100] or nitrate rich buffers[101-103]. While such solutions allow electrochemical characterizations, they are not ideal for environmental characterizations. Second, in our prior work, we established a Cu specific electrochemical FSCV waveform[94] but here we discovered that this waveform was not suitable for Pb detection. In this paper, we describe methods to overcome both challenges.

We employed PHREEQCi software to develop a model test solution that mimics stormwater runoff, which we then optimized for electrochemical analysis.

We subsequently optimized a Pb-specific FSCV waveform with high sensitivity and temporal resolution. Finally, we analyzed real stormwater samples spiked with Pb and were able to detect rapidly fluctuating Pb concentrations with the same voltammetric profile as our model solution.

We therefore present a novel experimental method for rapid Pb analysis. We created this system to best mimic stormwater runoff, while retaining sufficient ionic composition required for FSCV analysis. Our novel system will allow researchers to investigate Pb chemistry, kinetics and transport in model and real environmental systems.

3.2 Materials and Methods

3.2.1 Solutions

Stock Pb^{2+} solutions were prepared by dissolving $Pb(NO_3)_2$ (Mallinckrodt Baker Inc, Japan) into different buffer solutions. Tris-buffer ingredients (15 mM $H_2NC(CH_2)OH)_3 \cdot HCl$, 140 mM NaCl, 3.25 mM KCl,1.2 mM $CaCl_2$, 1.25 mM $NaH_2PO_4 \cdot H2O$, 1.2 mM $MgCl_2$ and 2.0 mM Na_2SO_4 with the pH adjusted to 7.4) were purchased from EMD Chemicals Inc, USA. The composition of our model solutions were based on the geometric mean concentration of major ions observed in stormwaters, as described in the International Stormwater BMP Database [104]: 1.2mM HCO_3^-, 230mM Ca^{2+}, 33mM Mg^{2+}, 20mM K^+, 25mM NO_3^-, and 80mM SO_4^{2-}. Final solutions were further optimized based on the PHREEQCi modeling results. The Version 1 (V1) model surface water solution was 0.23 mM $NaHCO_3$, 0.16 mM $CaSO_4$, 2.2 mM $MgCl_2$, 0.062 mM KCl, 0.036 mM KNO_3, and 0.013 mM Na_2HPO_4 at pH 7.0. The Version 2 (V2) model surface

water solution was 0.0012 mM $NaHCO_3$, 0.23 mM $CaCl_2$, 0.033 mM $MgCl_2$, 0.020 mM KCl, 0.025 mM KNO_3, 4.0mM NaCl, and 0.080mM Na_2SO_4 at pH 6.5. All aqueous solutions were made with deionized water.

3.2.2 Stormwater Collection

We collected stormwater samples during a 30 minute runoff event on Dec. 4, 2012 that deposited 0.2 inches of rain over a 45 acre paved parking area in southeast Michigan. Samples were collected in pre-cleaned 1L bottles using a Sigma SD9000 All Weather-Refrigerated Sampler. Sample bottles were cleaned with soap - phosphate free detergent (e.g., Liqui-Nox® soap) – and water, rinsed nanopure water (>18MΩ), rinsed with 37% trace-metal grade HCl and triple rinsed with nanopure water. Samples were refrigerated (4 ± 1°C) until they were transported in a dark cooler on ice to the laboratory where they were filtered through a 0.45μm pore size AquaPrep™ filter within 6 hours. After filtering no additional alterations where made to the sample and they were stored refrigerated (4 ± 1°C) in the dark. From these discrete samples, one of the samples collected at approximately peak flow of the runoff event was selected for voltammetric experiments.

3.2.3 Carbon-Fiber Microelectrodes

Carbon-fiber microelectrodes were fabricated using 7μm radius carbon-fibers (Goodfellow Corporation, USA) vacuum-aspirated into a glass capillary (0.6 mm external diameter, 0.4 mm internal diameter, A-M Systems, Inc., Sequim, WA) and pulled with a vertical micropipette puller (Narishige, Tokyo, Japan) to form a

carbon-glass seal. The exposed length of the carbon fiber was trimmed to 150 μm under an optical microscope.

3.2.4 Data Acquisition

All electrochemical experiments employed a custom-built instrument for potential application to the electrochemical cell and current transduction (University of North Carolina at Chapel Hill, Department of Chemistry Electronics Facility). Output of waveform, data acquisition, and signal processing (background subtraction, signal averaging, and digital filtering) were achieved using a customized version of TH-1 software (ESA, Chelmsford, MA) written in LabVIEW (National Instruments, Austin, TX). All potential values are quoted with respect to Ag/AgCl, which was constructed by electroplating Cl^- onto silver wire (A-M systems, WA, USA) (Ag wire was immersed in 1 M HCl and held at + 13 V vs. W for 5 seconds).

3.2.5 Data Analysis

Custom-built software, written in LabVIEW 2009, was used for background subtraction, data analysis and signal processing. Pooled data is presented with errors signified by the standard error of the mean (SEM). Student's t-tests were performed on paired data sets, $p < 0.05$ was taken as significant and signified with a star.

3.2.6 Flow Injection Analysis

The carbon-fiber microelectrode was inserted into a flangeless short 1/8 nut (PEEK P-335, IDEX, Middleboro, MA), and fastened to a modified HPLC union (Elbow, PEEK 3432, IDEX, Middleboro, MA) in the output of the flow injection

apparatus. The apparatus consisted of a six-port HPLC loop injector affixed to a two-position actuator (Rheodyne model 7010 valve and 5701 actuator) and a syringe infusion pump (kd Scientific, model KDS-410, Holliston, MA). A rectangular pulse of analyte was introduced to the carbon-fiber microelectrode surface at a flow rate of 2 mL min^{-1}. For calibrations and waveform optimization, standards were injected randomly instead of sequentially to avoid carry-over effects.

3.2.7 PHREEQCi

Solution chemistry was modeled in PHREEQCi (available for free download at http://wwwbrr.cr.usgs.gov/projects/GWC_coupled/phreeqci/). PHREEQCi is a geochemical modeling software capable of determining speciation based on thermodynamic equilibrium.[105] Chemical reactions used for this determination were supplied by the MINTEQ.v4 database developed by the U.S. Environmental Protection Agency.[106] Solutions were modeled in equilibrium with $CO_{2(g)}$ ($10^{-4.8}$ atm) and $O_{2(g)}$ ($10^{-0.67}$ atm). The pH of our solutions was within 0.05 pH units of that predicted by the PHREEQCi model.

3.3 Results and Disscusion

3.3.1 Fast Voltammetric Detection of Metals

Electrochemistry has been employed as an important tool for metals detection since Heyrovsky brought polarography to popularity in the 1920s.[107] The most popular polarographic method for metals analysis is anodic stripping voltammetry (ASV). The fundamental principle here is that the potential on a Hg droplet is held at a negative value so that metal ions in solution electrodeposit within the Hg

matrix, creating an amalgam. If this process is given enough time, it can serve as a powerful preconcentrator of the metal ions on the electrode surface. Thus, when the potential is ramped in the positive direction, the deposited metal is 'stripped' off the electrode surface, providing high currents relative to the metal concentration. ASV is an important method for laboratory analysis, however, concerns about Hg toxicity and the portability of the polarographic set-up has severely limited the application of ASV for environmental analyses. As such, researchers have explored a variety of safe materials, along with modifications to voltammetric methods in order to create devices more suited to monitor the environment. Amongst these, the bismuth film electrode (BFE) is particularly popular.[108-110] The BFE forms "fused alloys" with metal ions, analogous to the formation of an amalgam. Negligible toxicity is its main advantage, however, the BFE is limited by a narrow anodic range that makes it impossible to detect metal ions with oxidation potentials more positive than Bi (e.g., Cu, Sn and Sb).[111]

New materials can improve the applicability of stripping methods for environmental studies, however another ongoing challenge is to improve temporal resolution. This challenge is particularly pertinent during stormwater runoff events where is it important to understand the fate and transport of Pb (e.g., kinetics of metal-organic interactions).[112] Ion-selective electrodes, measuring potential changes due to partition of Pb ions into a selective membrane, have improved temporal resolution.[113-115] However, their response time is still > 20 seconds, and issues with stability and sensitivity create additional challenges for environmental analyses.

We recently described a fast method for Cu detection on carbon fiber microelectrodes (CFM).[94] Our method utilizes the adsorptive capacities of carbon fiber surfaces to rapidly preconcentrate metal ions onto the electrode surface prior to a fast cyclic voltammetric scan. For Cu, a preconcentration time of 100 ms resulted in ppb (parts per billion) sensitivity.[94] This method is fast, selective and Hg-free, critical ingredients for a potential environmental analytical tool. Using flow injection analysis (FIA), we studied the response of our method to Pb^{2+} with our previously established Cu specific waveform.[94] FIA provides reproducible and rapid pulses of analytes to the electrode surface, making it an ideal tool to probe dynamic metal chemistry. The potential was initially ramped in the negative direction from 0 to -1.4 V and then in the positive direction to 1.3 V and finally back to 0 V resting potential. **Figure 3.1.A** shows an injection of Cu^{2+} (10 μM $Cu(NO_3)_2$) onto a CFM. The color plot is constructed by stacking background-subtracted cyclic voltammograms (CVs) (y-axis) with time (x-axis) and assigning false color to current changes (z-axis). The start and end of the injection are denoted by the dashed black lines. As we previously found, the voltammetric signature during the injection identifies Cu^{2+} based on the position of the initial reduction and subsequent oxidation peak taken from a cyclic voltammogram (CV) (inset) during the injection indicated by the white dashed line. In **Figure 3.1.B**, we performed the identical experiment for an injection of Pb^{2+} (10 μM $Pb(NO_3)_2$). Here we encountered two problems. First, Pb^{2+} has limited solubility in Tris buffer and, as such, our standard solutions visibly displayed high levels of precipitation. Second, the $Pb^{2+}_{(aq)}$ in this solution did not give rise to a

redox-recognizable process as evidenced by the lack of an oxidation peak (inset CV). This observation was not surprising since Pb^{2+} is larger than Cu^{2+} and necessarily has different absorption and reaction kinetics. This experiment shows that different metals demand unique FSCV waveforms, optimized for their kinetic characteristics. We can employ different FSCV waveforms to provide enhanced selectivity for individual metals. Selectivity can be further improved by using ionophores to preconcentrate metals on the electrode surface prior to the voltammetric scan. This is currently one of our research objectives.

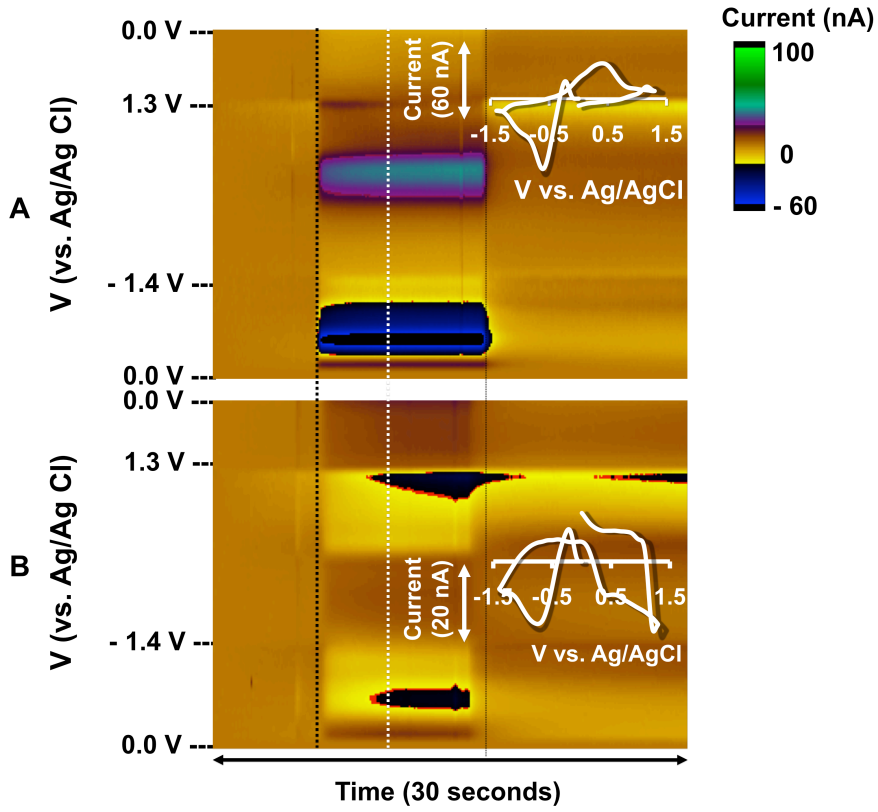

Figure 3.1. Color plots with potential on the y-axis plotted against time on the x-axis and the current response represented in false color. In **A**, Cu^{2+} (10 µM) was flow injected onto a carbon fiber microelectrode and in **B**, Pb^{2+} (10 µM) was injected. Insets show cyclic voltammograms taken at the vertical white dashed line.

In the following sections, we optimize the test solution to create stability for Pb and create an FSCV waveform for discrete Pb detection.

3.3.2 Model Surface Water Solution for Pb Electrochemistry

Previously, when establishing a Cu^{2+} specific waveform, we utilized a Tris buffer test solution because the majority of FSCV characterizations are carried out in this buffer system.[77,116] However metals in natural waters exhibit considerably different speciation than under laboratory conditions. Pb has limited solubility and readily forms carbonate and hydroxy complexes with common buffers.[117] This reactivity makes it difficult to utilize standard laboratory buffer systems for Pb analysis. As such, researchers have traditionally used test solutions at low pH[95-97] and with compositions that are not environmentally relevant.[99-103,118]. Furthermore, it is difficult to compare data between different test solutions because the concentration of free Pb^{2+} can vary due to differences in complexation. Therefore it is important to establish an environmentally relevant model test solution for Pb analysis that can also facilitate electrochemical measurements.

We first created a solution based on the ionic composition of stormwater typical of northern climates where road salt is used.[119]. This solution, V1, was at pH 7 with an ionic strength of 4.0×10^{-3} M. When Pb^{2+} was added to this solution to make a standard concentration of 100 μM, we found that the solution was unstable (**Figure 3.2**). With a relevant waveform (we describe full optimization in the next section), the Pb^{2+} standard was successively flow injected onto a CFM. In **Figure 3.2,** the maximum reduction current response to the injection was

plotted with injection number in the blue trace. It is clear that the electrode response decreases with increasing injection number. We have previously shown that FSCV responses to metals are stable with repeated injections,[94] therefore this decrease in signal is indicative of solution instability. To further validate this hypothesis, test solutions were left overnight, resulting in formation of a white precipitate. After filtering out the precipitate, the FSCV response was no longer detectable, suggesting that the concentration of free Pb^{2+} was dramatically reduced in solution due to precipitate formation. This speculation was confirmed with a PHREEQCi model. The thermodynamic equilibrium described by PHREEQCi predicted that Pb would precipitate as cerrusite ($PbCO_3$) for solutions with this composition and pH until it reached a concentration of 2.6 μM, currently below our detection limit.

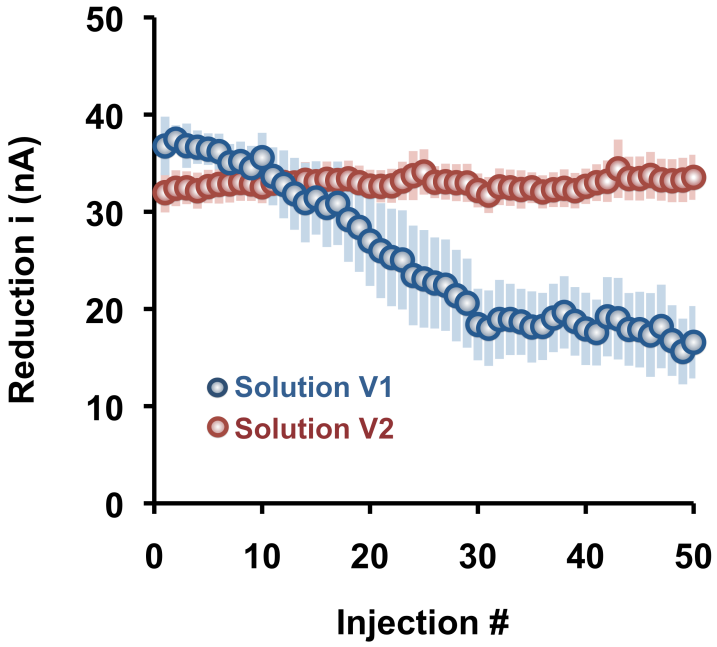

Figure 3.2. Maximum reduction current to successive flow injections of Pb^{2+} in solutions V1 (blue) and V2 (red). Error bars are ± SEM (standard error the mean).

To minimize cerrusite formation, we reduced the concentration of bicarbonate, decreased the pH to 6.5, and eliminated phosphate from solution. The ionic strength was similar at 5.3 x 10^{-3} M (compared to 4.0 x 10^{-3} M). This solution, V2, displayed increased stability. The red trace in **Figure 3.2** shows successive injections of Pb^{2+} onto the CFM with no loss in response. When this solution was left overnight, no precipitates formed. This result was further verified in PHREEQCi, which predicted that this solution should be at equilibrium.

Taken together, these results constitute the first report of a stable solution closely mimicking stormwater composition suitable for Pb electrochemical analysis. Importantly, this solution resembles the reported make-up of authentic stormwater samples submitted to the International Stormwater BMP database,[104] making it an ideal test solution for environmental analyses. Moreover, the solution has sufficient ionic and buffer capacity to enable accurate fundamental electrochemical characterizations with FSCV.

3.3.3 Optimization of a Voltammetric Waveform for Pb Detection

In **Figure 3.1**, we showed that our Cu^{2+} specific FSCV waveform was not suitable for Pb^{2+} detection. Because the ionic radius of Pb^{2+} is larger than that of Cu^{2+}, we expect differences in the FSCV kinetics between the two, thus we expected Pb^{2+} to require different electrochemical detection parameters. To create a unique waveform for Pb^{2+} detection with a robust redox signature, we systematically altered the electrochemical potential limits, the resting potential, and the scan rate. **Figure 3.3** shows the results of this optimization (100 µM Pb^{2+}). The initial cathodic scan induces Pb^{2+} reduction, therefore we increased

the reduction potential window by increasing the resting potential, as shown in **Figure 3.3.A**. We found that, as we increased the potential window, the peak reduction current increased, and we were able to capture redox processes on both cathodic and anodic scans. When we increased the positive potential above 0.2 V, we found increased peak separation between the oxidation and reduction peaks. We therefore chose 0.2 V as the ideal resting potential. Here the reduction current was 34.4 ± 2.6 nA (n = 4 ± SEM).

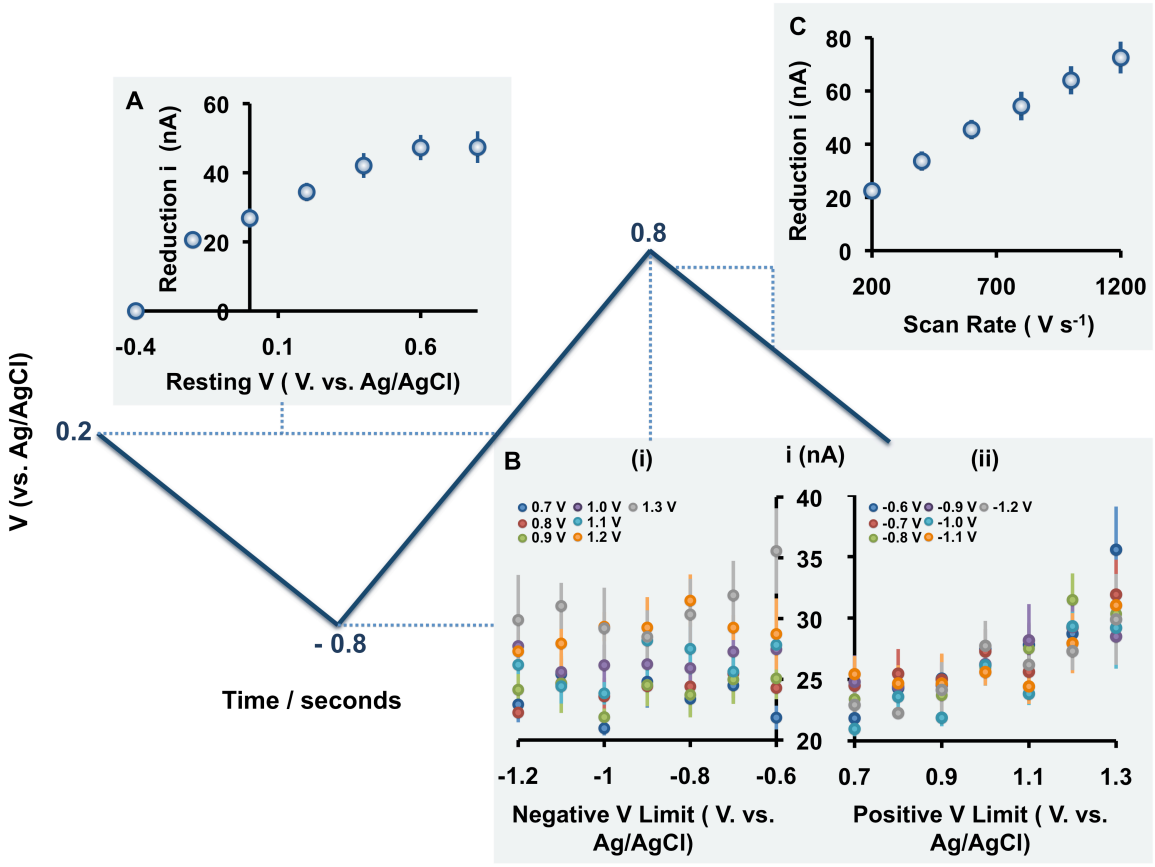

Figure 3.3. Results of waveform optimization. The optimized waveform is shown in blue. **A** shows resting potential dependence on i at - 0.8 – +0.8 V, with a scan rate of 400 V s^{-1}. B shows potential limit dependence. **B(i)** shows values of i for combinations of positive and negative potential limit when the negative potential limit is plotted on the x-axis. **B(ii)** shows values of i for combinations of positive and negative potential limit when the positive potential limit is plotted on the x-axis. **C** shows scan rate dependence on i at - 0.8 – +0.8 V, with a rest potential of 0.2 V.

Figure 3.3.B illustrates the effects of varying positive and negative potential limits. **Figure 3.3.B(i)** displays values of peak reduction current for combinations of positive and negative potential limit when the negative potential limit is plotted on the x-axis while **Figure 3.3.B(ii)** shows the same when the positive potential limit is plotted on the x-axis. There was not a strong trend when we increased the negative potential window. In **Figure S3.1.A** in **Appendix A** the current at -0.6 V was statistically compared to the current at -1.2 V for every positive potential studied. Only one of the series showed a significant trend. At very low negative potentials (< -1.0 V), O_2 reduction can be observed on CFMs;[120,121] given that O_2 levels are likely to fluctuate in environmental systems, we chose -0.8 V as our negative potential limit. As the positive potential was increased, there was a significant increase in the signal.

In **Figure S3.1.B** in **Appendix A**, the current at 0.7 V was statistically compared to the current at 1.3 V for every negative potential studied. All but one of the series showed a significant trend due to over-oxidation of the carbon fiber microelectrode surface as described previously.[116,122] Although the response increased with increasing positive potential limit, at high positive potential limits, oxidation and reduction peaks were undefined and indicated kinetic limitations. We therefore determined that a positive potential limit of +0.8 V would yield high sensitivity and discrete redox peaks.

Finally, we confirmed scan rate dependence on current by varying the scan rate from 200 – 1200 V s^{-1}. We found a positive correlation with increasing scan

rate, however, the IR drop created by high scan rates increased peak separation and distorted the CVs. We therefore chose 400 Vs^{-1} as the optimal scan rate.

Our optimal waveform, shown in **Figure 3.3**, is -0.8 – +0.8 V, resting at 0.2 V, and with a scan rate of 400 Vs^{-1}. With this waveform sensitivity to Pb^{2+} is 0.17 nA μM^{-1} or 0.84 nA ppm^{-1}, the limit of detection (LOD) is 10 μM or 2.1 ppm and the linear calibration range is up to 350 μM or 73 ppm.

3.3.4 Optimized Pb Detection Model

We combined our model test solution with our Pb-optimized waveform in order to create a novel Pb analysis method. **Figure 3.4** shows an FIA experiment where our test solution was used as the flow injection solvent and Pb^{2+} (100 μM) was injected into the flow stream onto a CFM. The color plot (middle panel) shows electrochemical events after injection and the CV (top panel, extracted from the vertical dashed line) verifies a robust redox process with defined reduction and oxidation peaks at -0.35 and +0.2 V respectively. Pb^{2+} perturbations on an environmentally relevant temporal scale can be established by extracting i vs. t at the peak reduction current (horizontal white dashed line). When compared to calibrations, these data can be turned into [Pb] vs. time as previously described;[94] shown in the bottom panel. The entirety of this event lasts 30 seconds.

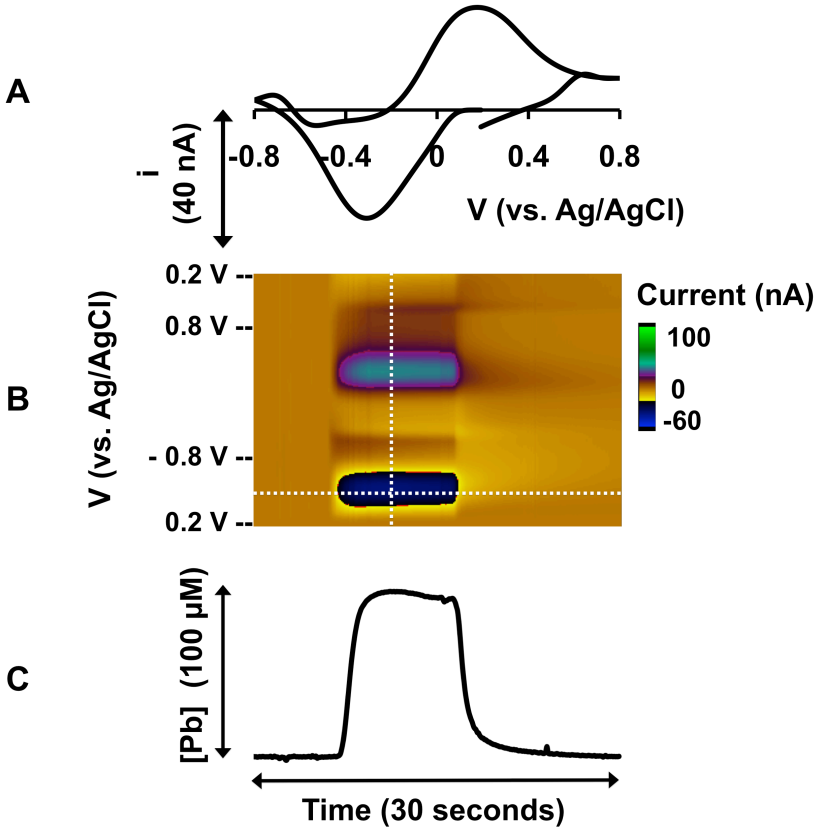

Figure 3.4. A flow injection analysis response to Pb^{2+} with optimized test solution and waveform. **A** shows a CV taken at the vertical white dashed line from the color plot in **B**. **C** shows a plot of [Pb^{2+}] vs. time, which was determined by taking i vs. t from the horizontal white dashed line in the color plot. The i vs. t trace was reversed to create a positive value (as described in ref [94]) and represents 100 µM Pb^{2+}.

Standard Pb calibrations are shown in **Figure 3.5**. Typically calibrations for electrochemical analyses utilize acidified solutions, which maximize free Pb^{2+}.[98,123] In acidic solutions, the [Pb^{2+}] can be considered the same as the total [Pb]. However in natural systems, complexation with ligands can reduce [Pb^{2+}]. If not taken into account, this will result in inaccurate concentration measurements.

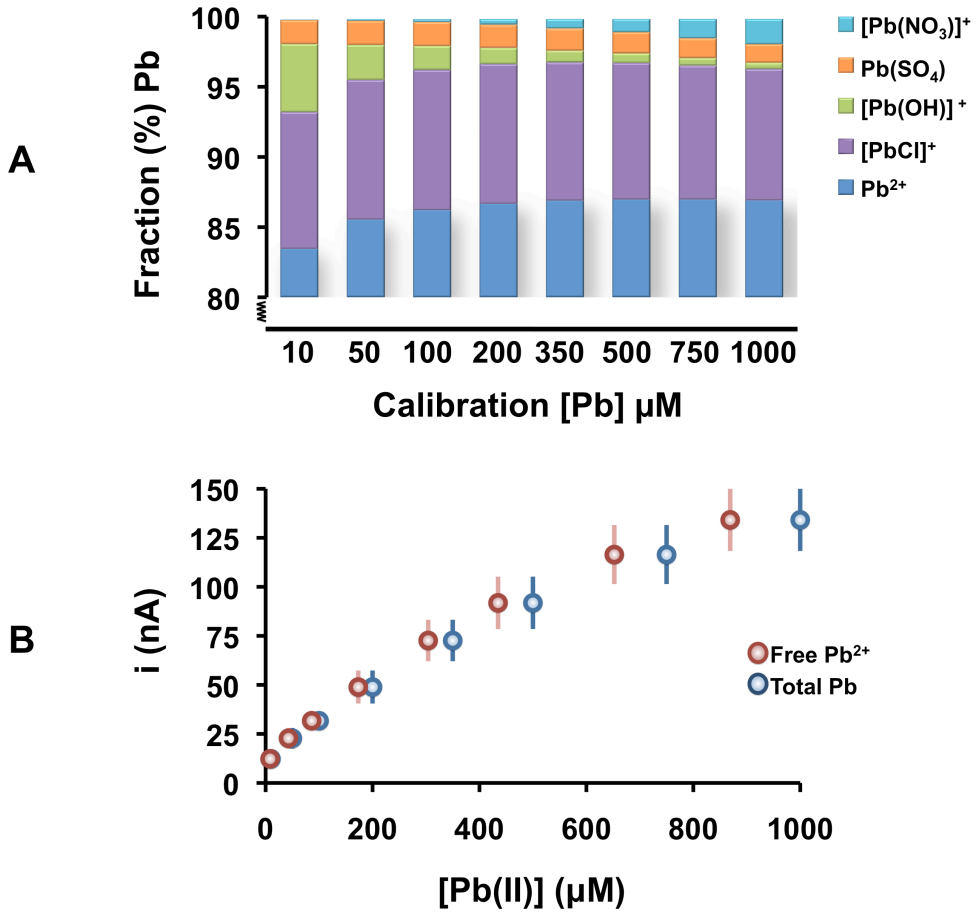

Figure 3.5. A shows the PHREEQCi models predicting the speciation of Pb in terms of the % fraction of Pb in various forms. This speciation information is for Pb in the calibration standards used to construct the calibration curves in **B**. The blue calibration trace shows total [Pb] in solution while the red trace shows the free Pb^{2+} in solution.

Figure 3.5.A shows the speciation of Pb in each of the calibration standards modeled with PHREEQCi. Our calibration standards ranged in concentration from 10 to 1000 µM Pb. Due to solution composition, the pH of our standards decreased with increasing total [Pb]. When considering speciation, this ΔpH impacts complexation, in particular with respect to Pb-OH complexes. As a result, the relative fraction of Pb associated with hydroxides decreased with increased

total Pb, a trend that can be seen by the reduction in the green section of the histogram. Therefore, not only is there a difference between added Pb and Pb^{2+} in solution, this difference is not linear with increasing concentration and needs to be accounted for. Because our sensor responds to Pb^{2+} it is important to know the concentration of free Pb^{2+} in solution for accurate calibration.

In **Figure 3.5.B**, the responses to the total solution Pb are plotted in blue and free Pb^{2+} concentrations are plotted in red. When taking speciation into account, the sensitivity of our method to Pb^{2+} is improved: above, we reported a sensitivity of 0.17 nA μM^{-1} or 0.84 nA ppm^{-1} and an LOD of 10 μM or 2.1 ppm; in actuality the sensitivity is 0.20 nA μM^{-1} or 1.0 nA ppm^{-1} and the LOD is 8.4 μM or 1.7 ppm.

3.3.5 Pb Detection in Real Environmental Samples

We have designed and characterized a robust experimental model for quantifying Pb fluctuations in real-time. While invaluable for studying metals in solutions of known composition, it is important to establish our method's feasibility for studying real environmental samples of unknown composition.

In **Figure 3.6**, we used real stormwater samples as our flow injection analysis solvent. We spiked the samples with three different Pb^{2+} concentrations (A: 20 μM, B: 50 μM, C: 100 μM) and injected these onto our CFM. The top panel of **Figure 3.6** displays the corresponding color plots, where rapid, concentration dependent Pb responses can be observed. CVs collected from the vertical white dashed lines are displayed in the bottom panel. These CVs resemble those collected with our model solution (**Figure 3.4**); however, the peaks are more separated on the potential axis. This increased separation is to be expected

since the solution resistance, which determines the IR drop across the electrode, is different. We therefore show proof of principle that our method can be applied in real environmental systems to measure rapidly fluctuating Pb.

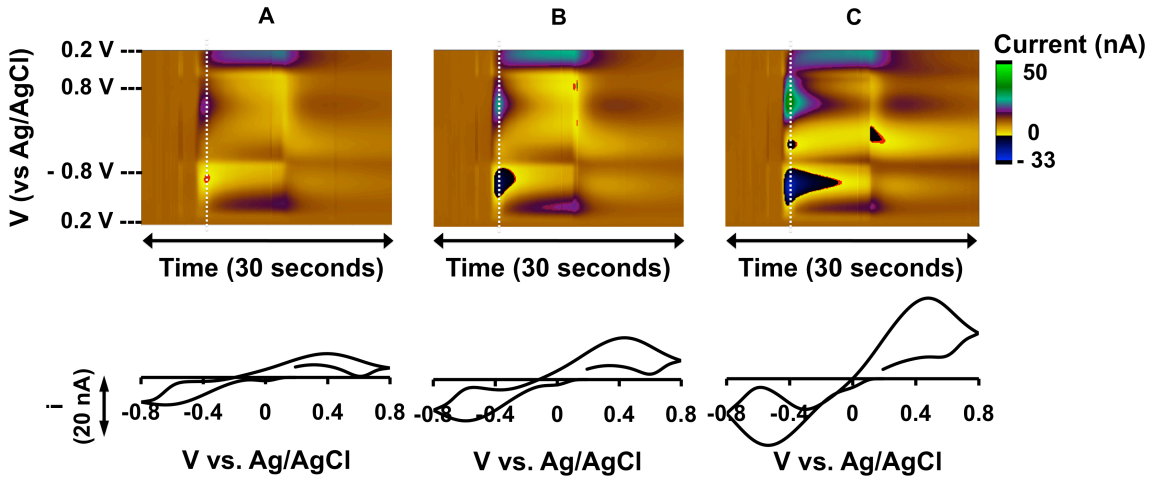

Figure 3.6. Flow injection analysis of real samples spiked with Pb. The top panel shows color plots during the injection and the bottom panel displays CVs taken from the vertical white dashed lines. Plots **A – C** represent responses to different Pb concentrations (20, 50 and 100 µM, respectively).

3.4 Conclusions

It is important to mitigate the impact of Pb on the environment since it is a pressing public health issue. In order to design effective mitigation strategies, it is essential that Pb can be analyzed in dynamic environmental systems. Electrochemical Pb analysis has traditionally been limited by its temporal resolution, Hg toxicity and stability concerns. In this paper we described safe, stable and fast analysis of Pb with FSCV. Additionally, we modeled test solutions to mimic environmental stormwater runoff. When coupled to our analysis approach, we showed that our novel method can characterize Pb in model and

environmental systems. Our technology heralds a new wave of electrochemical sensors that can ultimately be developed for effective on-site metals analysis.

CHAPTER 4. A DENSITY-CONTROLLED SCAFFOLDING STRATEGY FOR COVALENT FUNCTIONALIZATION OF CARBON-FIBER MICROELECTRODES

Trace metal detection is of great importance in environmental and biological systems. Recently, we described a method for ultrafast and sensitive detection of Cu(II) and Pb(II) in aqueous environmental samples using fast scan cyclic voltammetry (FSCV) at carbon-fiber microelectrodes (CFMs). In this chapter, we describe a scaffolding strategy for covalent modification of CFMs as a platform for creating selective adsorption sites. We create a monolayer of acetylene-terminated scaffolds on CFMs through the electrochemical reduction of alkynyl aryl diazonium salts bearing sterically differentiated silyl groups, which control the density of the scaffolds. Desilylation reveals the alkyne for further functionalization via Cu(I)-catalyzed azide-alkyne cycloaddition (CuAAC). As a proof of principle, we optimized the conditions for azidomethyl ferrocene to be grafted with the alkynes. The generalized approach offers the potential to attach azide-appended recognition groups to different electrodes in a high throughput manner. This technology will ultimately allow real-time ultra-selective FSCV analysis of metals in complex ecological and biological systems.

Yang, Y., Ibrahim, A. A., Stockdill, J. L. and Hashemi, P. *Analytical Methods*, **2015**, 7: 7352-7357.

4.1 Introduction

Detection of trace metals in real-time has important applications in environmental and biological processes. Trace metal contamination of aquatic environments is highly toxic to plants and animals with humans at a particularly high risk because of trace metals' ability to bioaccumulate.[124,125] Biologically, there is significant evidence that metals play dynamic physiological roles, specifically as neurotransmitters.[126,127] Therefore, sensitive, qualitative, and rapid detection of trace metals would greatly aid investigations into environmental pollution and physiological disease.

There are few analytical methods that can report trace metal levels in such harsh, complex environments in real time. We recently described a method applying fast scan cyclic voltammetry (FSCV) at carbon-fiber microelectrodes (CFMs) for real-time measurement of Cu(II)[44] and Pb(II).[45] We showed that CFMs have a unique ability to adsorb metals, allowing for ultra rapid electrochemical detection.[35] Metals adsorb to carbon surfaces with differing affinities;[128] however, adsorption affinities are pre-defined (via mode of surface activation) and do not allow sufficient selectivity for analysis in multi-component systems. To address this issue, different modifications have been made on CFMs to improve analytical selectivity. The most popular method for modifying CFMs is surface activation via over-oxidation.[129-131] Other approaches include modification with charge-exchange polymers (e.g., Nafion)[77,132,133] and carbon nanotubes.[133-135] These modifications significantly enhance selectivity[77,132,133]

and sensitivity;[129-131,133-135] however, they do not provide selective adsorption for analytes of similar charge (i.e., metals).

In this paper, we describe a robust strategy to utilize CFMs as a platform for creating selective adsorption sites by modifying and applying a protocol for electrochemical reduction of alkynyl aryl diazonium salts to CFMs. Our covalent modification displays a layer of density-controlled scaffolds ready for grafting of a variety of functional molecules. We first synthesized a series of aryl diazonium salts bearing sterically-differentiated silyl groups. We then optimized a protocol for reductive coupling of these species to the CFM surface. Next, we deprotected the silyl functionality to reveal the reactive alkynes. Finally, we optimized the conditions for copper(I)-catalyzed azide-alkyne cycloaddition (CuAAC) of azidomethylferrocene with these alkynes. Each step was verified electrochemically. Ultimately, the CuAAC reaction can be conducted with a variety of azide-appended ligands selective for analytes of interest. This novel strategy represents a general approach to producing analyte-selective CFMs in a high throughput manner, which will eventually enable ultra-selective FSCV analysis of metals in complex ecological and biological systems.

4.2 Materials and Methods

4.2.1 Chemicals

Tetrabutylammonium hexafluorophosphate ($TBAPF_6$), tetrabutylammonium fluoride (TBAF), ferrocene, $CuSO_4 \cdot 5H_2O$ and ascorbic acid were of analytical grade from Sigma-Aldrich, St. Louis, MO. Diazonium reagents and azidomethylferrocene were synthesized according to the procedures in

Appendix B. Abbreviations are as follows: trimethylsilyl (TMS), *t*-butyldimenthylsilyl (TBS), triisopropylsilyl (TIPS).

4.2.2 Carbon-fiber microelectrodes

CFMs were fabricated by vacuum aspirating a 5 μm radius carbon-fiber (T-650, Goodfellow Corporation, PA) into a glass capillary (1.0 mm external diameter, 0.5 mm internal diameter, A-M Systems, Inc., Sequim, WA). The carbon-fiber filled capillary was pulled with a vertical micropipette puller (Narishige, Tokyo, Japan) to form a carbon-glass seal. The carbon-fiber end was trimmed to have an exposed length of 150 μm out of the capillary under an optical microscope.

4.2.3 Instrumentation and data acquisition

All electrochemical measurements were performed with Dagan ChemClamp potentiostat (Dagan, Minneapolis, MN) and customized software, CV (Knowmad Technologies, AZ), written in LAB-VIEW 2012 (National Instruments, Austin, TX). A two-electrode system was employed. The working electrode was a CFM. The reference Ag/AgCl electrode was fabricated by electroplating Cl^- ions onto silver wire (A-M systems, WA) for 5 s. All cyclic voltammograms (CVs) were collected and averaged out from 4 different electrodes. Data were smoothed with a 3-point moving average filter. Student's T-tests were performed on unpaired data sets.

4.2.4 Reductive Coupling of Diazonium Salts to the CFM surface

A bare CFM (**CFM1**) was cycled between +0.80 and -0.55 V vs. Ag/AgCl at scan rate 0.05 V s^{-1} in ACN containing 0.01 M silylated diazonium salt (**4a-c**) as reactant and 0.1 M $TBAPF_6$ as electrolyte to generate a silylated CFM (**CFM2**).

CFM2 was carefully rinsed with ACN and acetone for three times. Desilylation was achieved by dipping **CFM2** in a solution of 0.1 M TBAF in THF for 5 min. The desilylated CFM (**CFM3**) was cleaned with a copious amount of THF and acetone. Electrochemistry of ferrocene was accessed for differently silylated CFMs (**4a-c**) at three stages (**CFM1**, **CFM2**, **CFM3**). The CFM was cycled between 0 and +0.8 V vs. Ag/AgCl at scan rate 0.1 V s^{-1} in a solution of 1 x 10^{-3} M ferrocene in ACN (+0.1 M $TBAPF_6$).

4.2.5 Copper(I)-catalyzed azide-alkyne cycloaddition (CuAAC) at CFM

In the presence of 0.05 M $CuSO_4 \cdot 5H_2O$ and 0.1 M L (+)-ascorbic acid as catalysts, **CFM3** was stirred in 0.05 M azidomethylferrocene in DMF for at least 2 hours to produce ferrocene-appended CFM (**CFM4**). **CFM4** was rinsed with acetone for 1min, stirred 10 min in 1 M HCl, 10 min in saturated EDTA, and 10 min in deionized water to remove any residue if presented.[136] **CFM4** was ready to be immediately used after drying in an oven at 70 ºC for 30 min.

4.3 Results and Discussion

4.3.1 Prior Electrode Modifications

One of the most effective approaches to impart selectivity is to introduce selective modifiers to electrodes. For example, in solid-contact ion-selective electrodes, ionophores are normally incorporated in transducer membranes (e.g., polymers,[137-139] nano-materials[140-142]) and then deposited onto electrode surfaces. Ionophores selectively bind to metal ions of a particular size and charge. Electrodes coated with these membranes often have delayed response times because of restricted diffusion caused by membrane thickness. Additionally, the

lifetime and stability of these electrodes is compromised due to water layer formation.[139,143]

Covalent modification of electrode surfaces largely circumvents issues of lag time and stability. Carbon based electrodes have rich surface chemistry that lends itself to forming various types of covalent bonds. Oxidation of carbon surfaces results in the formation of hydroxyl groups or carboxylates. This modification in itself increases sensitivity and selectivity to cations because of increased adsorption to the electrode surface. Additionally, surface groups that arise after carbon activation can be reacted with molecules bearing selective recognition groups. For example, surface hydroxyl groups can be reacted with molecules bearing activated carboxylic acid moieties to generate ester linkages[58] and surface carboxylate groups can be reacted with amines to form amide bonds.[144-146] These methods enable covalent attachment of recognition molecules to electrode surfaces; however, these processes involve harsh reagents, produce unwanted side reactions, and result in inconsistent and limited electrode surface coverage.[56]

More recently, Rosenthal and Watson employed electro-grafted aryl groups to functionalize carbon paper.[147] Both of these approaches allowed the reaction of alkyne-appended aryl diazonium species with carbon surfaces. In the latter work, three strategies were reported to subsequently attach recognition motifs: Hüisgen cycloaddition (copper-mediated azide-alkyne cycloaddition), Sonogashira coupling, and Glaser reactions.[147]

For CFMs, strategies are limited. Wightman and Anderson also utilized the diazonium reduction approach to attach moieties to CFMs.[67] This work described attachment of a nitroaryl diazonium, followed by reduction to the amine, and amide bond formation. While reductive coupling of diazonium salts is among the mildest and most reproducible methods for functionalizing CFMs,[56] it is currently limited by the need to design and synthesize a new aryl diazonium salt for each desired modification. The incompatibility of diazonium species with many organic reaction conditions, in addition to the conflict of many organic functional groups with the conditions required for generating the diazoniums limits the potential to apply this approach in a general way. Furthermore, the electrochemical coupling protocol (applied potential, solvent, reaction time, etc.) for each of these aryl diazonium salts must be individually optimized. We therefore sought to develop a general, high-throughput strategy to facilitate CFMs selective for a variety of analytes. Theoretically, a large number of identical electrodes could be rapidly generated, and then a variety of recognition molecules could be attached in a diversifying approach (*vide infra*).

4.3.2 Toward A General Approach to Covalent CFM Modification

Scheme 4.1. Planned general strategy for CFM modification.

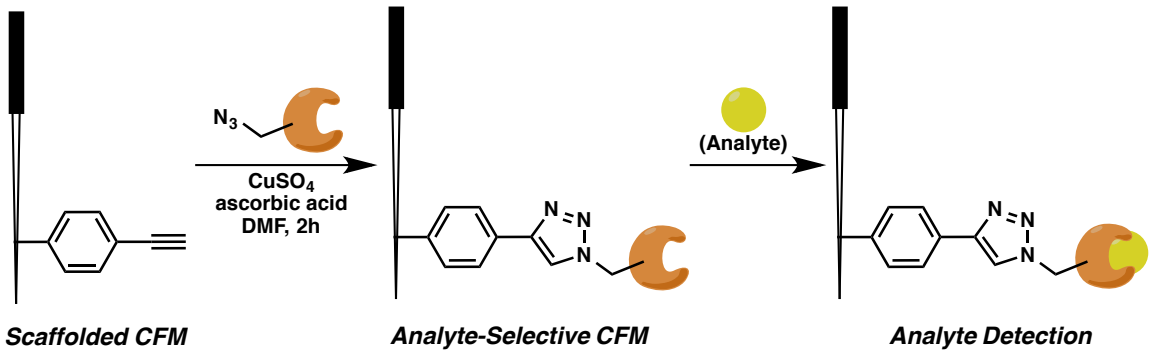

We envisioned a modular strategy for covalent CFM modification, wherein a single molecular entity could be used to conduct an initial surface functionalization to form a surface presenting a monolayer of molecular scaffolds for further functionalization. These scaffolds could then be reacted with a wide range of ligands bearing a functional group of complimentary reactivity, which would allow for the generation of a diverse set of analyte-selective CFMs. We favored a strategy similar to those reported by Hapiot and Rosenthal and Watson, namely, self-inhibiting reduction of an aryl diazonium salt bearing a functional group handle for further manipulation (i.e., an alkyne)[64,65,147]. We anticipated that application of this approach to a CFM would afford alkyne-scaffolded CFMs poised for further reaction with a diverse set of azides, linking analyte-selective ligands to the CFM via a triazole moiety (**Scheme 4.1**).

Each resulting electrode would exhibit enhanced detection of its particular analyte by biasing the adsorption (pre-concentration) equilibrium in favor of the target analyte.[35] Once optimized, this protocol should enable systematic generation of seective devices for the real-time detection of important metal analytes in complex biological and environmental systems via FSCV.

4.3.3 Synthesis of Aryl Diazonium Salts Bearing Sterically-Differentiated Silyl Groups

A series of alkynyl aryl diazonium salts protected by silyl groups of varying sizes were synthesized via a straightforward 2-step protocol (**Scheme 4.2**). 4-Iodoaniline (**1**) was subjected to Sonogashira cross coupling conditions with different alkynyl silanes, from the relatively compact TMS (**2a**) to the moderately

sized TBS (**2b**) to the quite bulky TIPS (**2c**). The product aryl amines (**3a-c**) were treated with sodium nitrite in HBF_4 to afford the corresponding diazonium tetrafluoroborate salts (**4a-c**) in good yields. (see **Appendix B**).

Scheme 4.2. Alkynyl diazonium salts synthesis

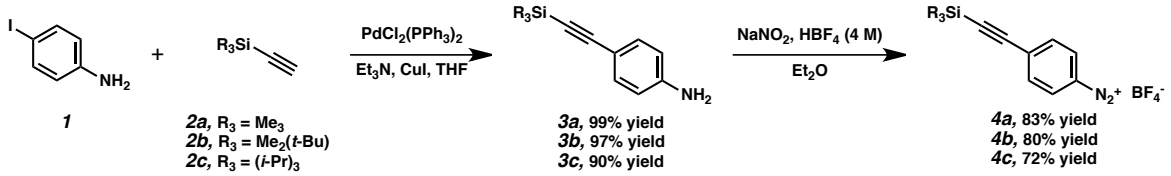

4.3.4 Protocol for Reductive Coupling of Diazonium Salts to the CFM surface

Scheme 4.3 illustrates the creation of the scaffolds. A reduction potential was applied to the bare CFM (**CFM1**), resulting in electron transfer to the silylated diazonium salt (**4a-c**). The resulting diazenyl radical fragmented to release N_2 and an aryl radical. Recombination of the aryl radical with the CFM surface resulted in C–C bond formation and afforded a silylated CFM (**CFM2**).[148] Deprotection of the silyl moieties was accomplished in only 5 minutes by exposure to TBAF, unveiling alkyne-terminated scaffolds (**CFM3**). These reactions were followed electrochemically as described below. First, the process of grafting the TMS-substituted diazoarylalkyne (**4a**, **Figure 4.1.A(i)**) onto the CFM was monitored via collection of a CV during the electroreduction process (**Figure 4.1.A(ii)**).

Scheme 4.3. CFM functionalization by reductive coupling.

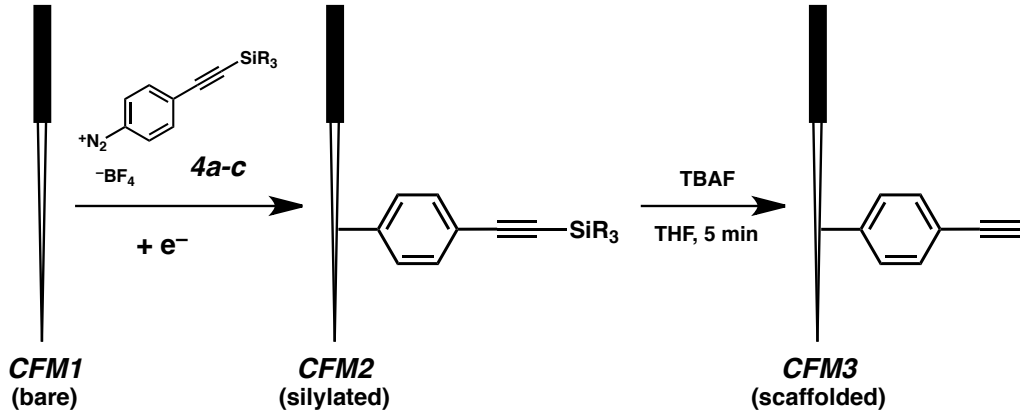

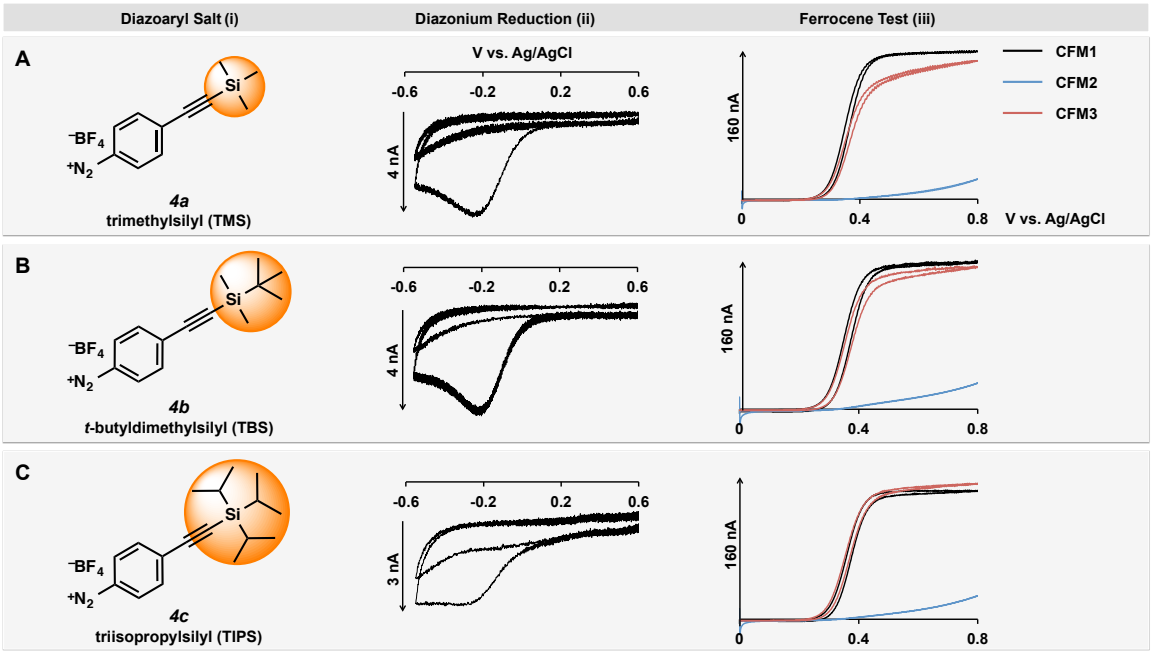

Figure 4.1. (**i**) Aryldiazonium salts employed for each electrode, (**ii**) CVs of self-inhibiting attachment of diazonium salts to the electrodes, (**iii**) ferrocene tests confirm attachment and deprotection of the silyl groups.

We applied a cyclic voltage to the CFM (+0.80 to -0.55 V at 50 mV s^{-1}) and diazonium electroreduction proceeded to completion during the first cycle, as evidenced by the pronounced reduction peak, and further confirmed by a lack of peaks in subsequent scans (**Figure 4.1.A(ii)**). Second, a ferrocene redox probe

confirmed the conversion of **CFM1** (black trace) to **CFM2** (blue trace) due to the loss of the ferrocene redox couple (**Figure 4.1.A(iii)**). Upon desilylation to generate **CFM3**, the redox couple re-appears (red trace), establishing the availability of the surface for redox chemistry.

The same steps were executed for the larger TBS (**4b**) and TIPS (**4c**) groups. The same electrochemical trends were apparent for these salts with two notable differences (**Figure 4.1.B-C**). First, as expected, the reduction peaks occurred at progressively more negative potentials for each diazonium salt (from **4a**, **4b** to **4c**). As the electron withdrawing nature of the silyl groups decreases from TMS (**4a**) to TBS (**4b**) to TIPS (**4c**), the diazonium salt becomes less electrophilic, and a higher reductive potential is required for the reaction.[149] Second, the silylation is auto-inhibitory which creates monolayer structures on CFMs. An important advantage of our method is that the packing density on the CFMs' surface is controlled by and correlates to the size of the silyl groups. Notably, CVs collected after deprotection showed an increased response to ferrocene as the size of the templating silyl group increased. This effect is consistent with the observations of Hapiot and co-workers.[65]

4.3.5 Optimization of Conditions for Azide-Alkyne Cycloaddition

We envision the use of "click" chemistry as a general method to graft many different recognition groups onto our scaffolds. To establish the feasibility of this approach, we attached ferrocene onto the scaffolds through copper(I)-catalyzed azide-alkyne cycloaddition (CuAAC). Ferrocene is a well-established probe to assess the integrity of modification strategies.[150] As shown in **Scheme 4.4**,

alkyne-substituted electrodes (**CFM3**) were reacted with azidomethyl ferrocene, linking ferrocene to the electrode via a triazole moiety (**CFM4**).

Scheme 4.4. CuAAC of azidomethylferrocene (5) and the alkyne scaffolds.

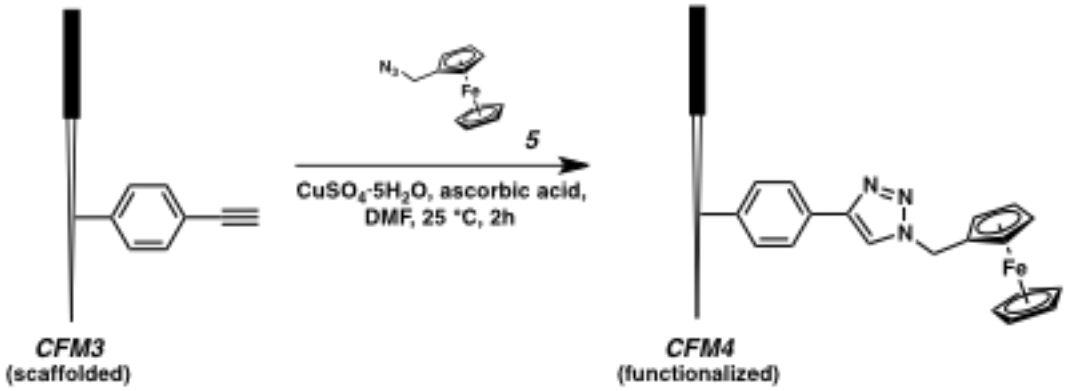

Hapiot and co-workers use either a 1:1 mixture of THF and water or a 1:1 mixture of ethanol and water. Aqueous and ethanolic solutions are typically most effective in CuAAC chemistry.[63] Unfortunately, the low solubility of azidomethylferrocene (**5**) limits the utility of these conditions on the much smaller microelectrode surface. Watson and co-workers used DMF, which offers improved solubility of the azide, but their reactions were conducted in a glovebox.[147] We sought to identify conditions that would be robust across a range of potential azides, and ultimately could be adopted with facility by the broader community. We focused on simplifying the DMF reaction, given the exceptional solubilizing ability of DMF, by removing the need for a glove box. Further, we conducted these studies on the benchtop because we wanted a protocol that would not require specialized equipment for inert atmosphere. A thorough and systematic optimization of the reaction parameters was performed to achieve this simplification. For operational simplicity and cost, we used a solution of

$CuSO_4 \cdot 5H_2O$ and ascorbic acid to generate Cu(I) *in situ*.[62] A slight excess of ascorbic acid to prevent formation of oxidative coupling products of Cu(I).

We electrochemically verified the attachment to **CFM4**. **Figure 4.2** shows the precursor diazonium salts (**4a-c, A-Ci**) used to create the scaffolds and the CVs obtained after ferrocene attachment (**CFM4, A-Cii**). These CVs were obtained in a solution of acetonitrile using $TBAPF_6$ as the supporting electrolyte. The ferrocene/ferrocenium redox couple was identified at +0.6/+0.4 V vs. Ag/AgCl at scan rate of 10 V s^{-1}. This ferrocene signal established the successful reaction of our alkyne scaffolds with the azide via CuAAC. We optimized the reaction conditions by measuring the change in oxidation current of the CVs as each parameter was adjusted. Specifically, we varied the concentrations and equivalents of ascorbic acid, copper sulfate, and azide **2** as well as the reaction time. Ultimately, we found that immersion of **CFM3** in a DMF solution of 0.05 M $CuSO_4 \cdot 5H_2O$, 0.1 M (+)-ascorbic acid, and 0.05 M azidomethyl ferrocene (**5**) was optimal. The current intensity decreases as the size of silyl groups increases from TMS (***4a***) to TBS (***4b***) to TIPS (***4c***), indicating that fewer ferrocene molecules are linked to the electrode. This observation validates the hypothesis that the density of the scaffolds can be tuned by adjusting the steric bulk of the silyl groups.

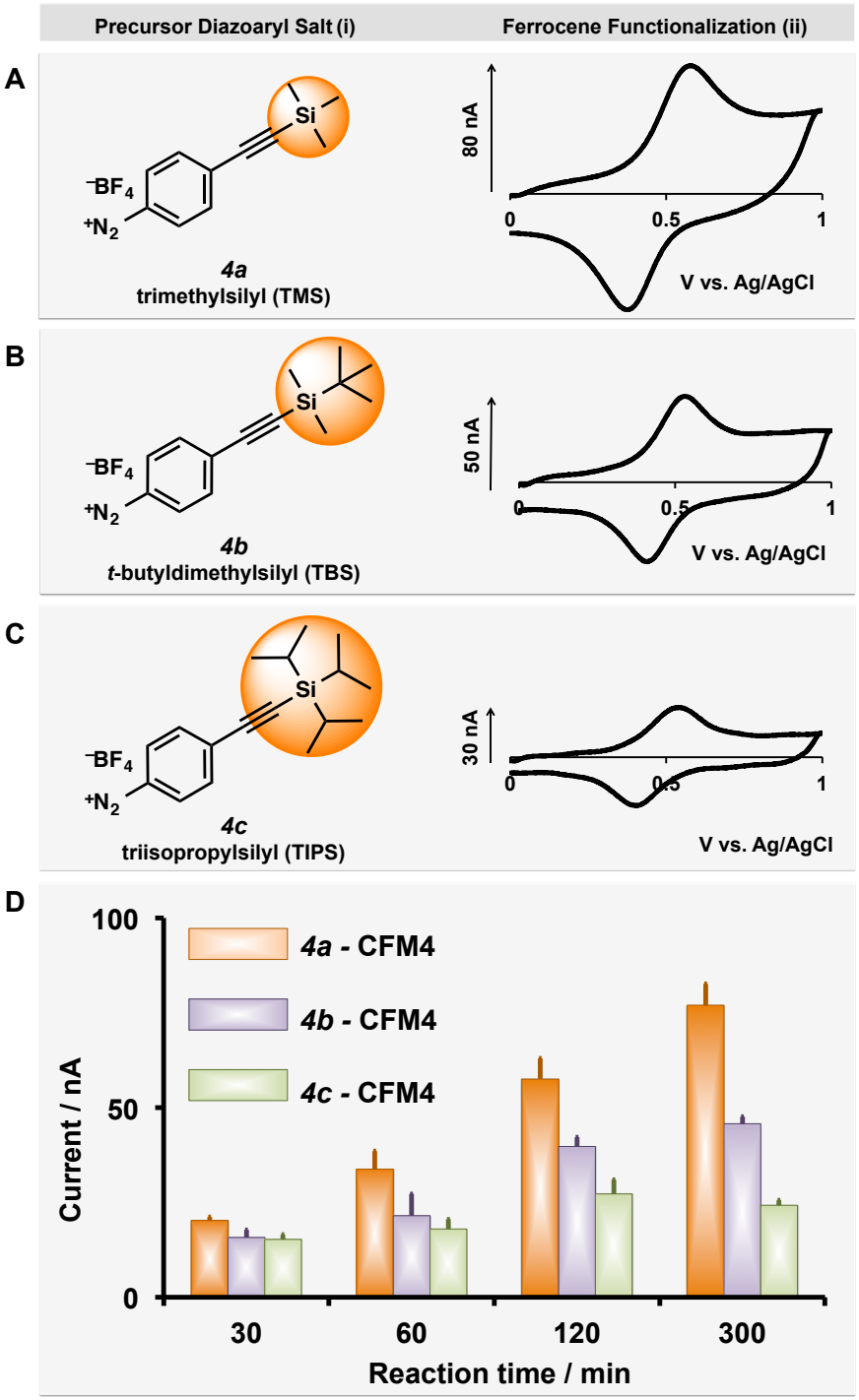

Figure 4.2. (**A**-**Ci**) Aryldiazonium salts employed for each electrode, (**A-Cii**) CVs of ferrocene-appended electrodes, (**D**) Optimization of CuAAC attachment time.

To optimize the coupling time for ferrocene-appended CFMs (**CFM4**s) generated from **4a-c**, we investigated the influence of reaction time on the ferrocene signal intensity. As shown in **Figure 4.2.D**, we varied the reaction time from 10 to 300 min and found that as reaction time increased, there was an overall signal increment for all the **CFM4**s until they reached their maximum coverage in a sequence of t_{TMS} (orange) > t_{TBS} (purple) > t_{TIPS} (green). By 120 min, the TBS (**4b-CFM4**) and TIPS (**4c-CFM4**) had reached a maximum current intensity.

The TMS signal was not measured beyond 300 min. However, at this time point, the signals from the 3 types of electrodes were well differentiated. At earlier time points, the reaction is incomplete, and the effect of the changes in surface functionalization density cannot be detected. These qualitative observations were statistically confirmed. After 2 h, the density difference was significant ($p = 0.042$ (TMS/TBS), 0.016 (TMS/TIPS), and 0.049 (TBS/TIPS)).

4.4 Conclusions

Real-time trace metal determination is of great importance in environmental and biological systems. A highly promising technique is FSCV at CFMs, which we have previously utilized for ultrafast and sensitive detection of Cu(II) and Pb(II). Because metals of similar size and charge adsorb strongly to CFM surfaces, the selectivity of FSCV towards metals in complex media is limited. In this paper, we developed an efficient, robust, and tunable covalent modification method for CFM functionalization. We electrochemically generated a monolayer of acetylene-terminated scaffolds on CFMs at different densities. We also

established mild reaction conditions for the attachment of azides to the alkyne scaffolding groups. This work provides the foundation for the development of a broadly applicable, systematic approach to creating a variety of functionalized electrodes. Our technology will ultimately provide selective carbon fiber based sensors that will facilitate real-time detection of important analytes in complex biological and environmental systems.

CHAPTER 5. REAL-TIME, ULTRA-SELECTIVE DETECTION OF COPPER(II) USING IONOPHORE-GRAFTED CARBON-FIBER MICROELECTRODES

Rapid detection of Cu(II) is analytically valuable. We recently described a real-time Cu(II) electroanalysis method based on fast-scan cyclic voltammetry (FSCV) at carbon-fiber microelectrodes (CFMs). To enhance the sensitivity of our method, we previously designed a generalized covalent functionalization strategy for CFMs. In this chapter, we report the first effective application of this technique by modifying CFMs with a Cu(II) ionophores. We describe our 3-step modification method with simultaneous blocking of coordination sites of other ions. In a chemically complex medium, we were able to make ultra-selective and fast Cu(II) measurements This strategy represents a transformative innovation in development of a robust on-line detection device for metal analysis.

Yang, Y., Ibrahim, A. A., Hashemi, P. and Stockdill, J. L. “Real-Time, Ultra-Selective Detection of Copper(II) using Ionophore-Grafted Carbon-Fiber Microelectrodes’’, *In preparation*

5.1 Introduction

Electrochemical micro-sensors for rapid, selective and sensitive Cu(II) detection is highly desirable in a number situations including analysis in biological, environmental and industrial systems.[10,151-154] While ion selective electrodes have shown promise for electrochemical Cu(II) analysis, they suffer from low stability and their response time (5-20 minutes) does not afford information on a rapid enough timescale to investigate fast processes.[23]

As explained in Chapter 2, we recently pioneered fast-scan cyclic voltammetry (FSCV) at carbon-fiber microelectrodes (CFMs) for ultra-fast Cu(II) detection.[35,44,45] The ultra-micron dimensions of the CFM are minimally disturbing to their analysis medium, and their chemically rich, striated surface promotes sufficient pre-concentration of cations for highly sensitive Cu(II) analysis every 100 miliseconds.[35] A fundamental technical aspect that has hindered application of our method to real samples, which we address in this communication, is analytical selectivity.

We have studied Cu(II) adsorption onto CFMs in detail.[35] The ambient oxygen moieties on CFMs responsible for cation preconcentration do not provide a high level of discrimination between metal ions. This non-selective adsorption makes it significantly challenging to apply voltammetry, albeit a selective method, to samples containing multiple metal ions.

We postulate that creating a mechanism for selective adsorption will enable an ultra-selective FSCV sensor. In Chapter 4, as a first step towards addressing this postulation, we recently reported a general strategy to covalently

functionalize CFMs.[155] A monolayer of acetylene-terminated scaffolds were grafted onto CFMs via electrochemical reduction of diazonium salts, and the backbone was appended with ferrocene through Cu(I)-catalyzed azide-alkyne cycloaddition as proof of principle of the modification.[155]

In this chapter, we extend this work by modifying CFMs with a Cu(II) ionophore which facilitates selective Cu(II) adsorption onto CFMs. We use this sensor to selectively detect Cu(II) as the minor component of a mixed metal solution. This essential bringing together of two powerful analytical methods (ISEs and voltammetry) represents a crucial advancement for rapid and selective trace metal electroanalysis because it capitalizes on the unparalleled temporal capabilities of FSCV while imparting selectivity via covalent attachment of a Cu(II)-ionophore.

5.2 Materials and Methods

5.2.1 Chemicals

Tetrabutylammonium hexafluorophosphate ($TBAPF_6$), tetrabutylammonium fluoride (TBAF), ferrocene, $CuSO_4 \cdot 5H_2O$ and ascorbic acid were of analytical grade from Sigma-Aldrich, St. Louis, MO. Diazonium reagents and azidomethylferrocene were synthesized according to the procedures in **Appendix C**. Abbreviations are as follows: trimethylsilyl (TMS), *t*-butyldimenthylsilyl (TBS), triisopropylsilyl (TIPS).

5.2.2 Carbon-fiber Microelectrodes

CFMs were fabricated by vacuum aspirating a 5 μm radius carbon-fiber (T-650, Goodfellow Corporation, PA) into a glass capillary (1.0 mm external diameter, 0.5

mm internal diameter, A-M Systems, Inc., Sequim, WA). The carbon-fiber filled capillary was pulled with a vertical micropipette puller (Narishige, Tokyo, Japan) to form a carbon-glass seal. The carbon-fiber end was trimmed to have an exposed length of 150 μm (or 200 μm, 300 μm) out of the capillary under an optical microscope.

5.2.3 Diazonium Electrochemical Reduction At CFMs

The covalent modification route for CFM is shown in **Scheme 5.1**. A bare CFM (**CFM 1**) was cycled between +0.80 and -0.8 V vs. Ag/AgCl at scan rate 0.05 V s^{-1} in ACN containing 0.01 M silylated diazonium salt as reactant and 0.1 M $TBAPF_6$ as electrolyte to generate a **CFM 2**. The **CFM 2** was carefully rinsed with ACN and acetone three times. Deprotection was achieved by dipping **CFM 2** in a solution of 0.1 M TBAF in THF for 20 min. The deprotected CFM (**CFM3**) was cleaned with a copious amount of THF and acetone.

5.2.4 Copper(I)-Catalyzed Azide-Alkyne Cycloaddition

CuAAC was accomplished by treatment of **CFM 3 or 3'** with a stirred solution of 0.05 M azido-ionophore, 0.05 M $CuSO_4 \cdot 5H_2O$, and 0.1 M L (+)-ascorbic acid in DMF for 4 h to produce ionophore-grafted **CFM 4 or 4'**. The resulting electrode was then rinsed with acetone, stirred in saturated EDTA for 10 min, then in deionized water for 10 min to remove any residue from the electrode surface.

5.2.5 Silylation Of Surface Oxygen Groups

CFM 3 was inserted into an Ar-purged air-tight vial containing a 10.00 mL CH_2Cl_2 solution of 0.10 M TMSCl, 0.11 M Imidazole, and 0.01 M 4-

dimethylaminopyridine. A reductive potential of –1.9 V was then applied for 4 h to generate **CFM 3'**.

5.2.6 Electrochemical Characterization

All electrochemical measurements were performed with a Dagan ChemClamp potentiostat (Dagan, Minneapolis, MN) and customized softwares, CV and FSCV (Knowmad Technologies, AZ), written in LAB-VIEW 2012 (National Instruments, Austin, TX). A two-electrode system was employed. The working electrode was a CFM. The reference Ag/AgCl electrode was fabricated by electroplating Cl^- ions onto silver wire (A-M systems, WA) for 5 s. All cyclic voltammograms (CVs) are the averaged data collected from 4 different electrodes. Student's T-tests were performed on unpaired data sets.

5.3 Results and Discussion

5.3.1 Organic Synthesis Strategy

At the outset of our work, we identified Cu(II) ionophore I (Selectophore **1**), a commercially available ionophore, as an excellent candidate structure for rendering Cu(II) selectivity to CFMs (**Scheme 5.1**).[156] However, to accomplish a covalent modification, we required a chemically modified version of Selectophore possessing an azide functional group handle. Thus, azido-ionophore **7** was synthesized from commercially available 3-nitrophthalic acid (**2**). Selective borane reduction of the carboxylic acids was accomplished in quantitative yield, generating diol **3**. Hydrogenolysis of the nitro group then yielded aniline derivative **4**, which was converted to the corresponding azide (**5**) in the presence of TMS azide and *t*-butyl nitrite. Bromination of the benzylic alcohols afforded

dibromide **6**, which was then treated with a pre-stirred solution of CS_2, diisobutylamine, and K_2CO_3 in MeOH to provide the desired azide-appended ionophore **7**.

Scheme 5.1. Synthesis of azido-ionophore (compound **7**)

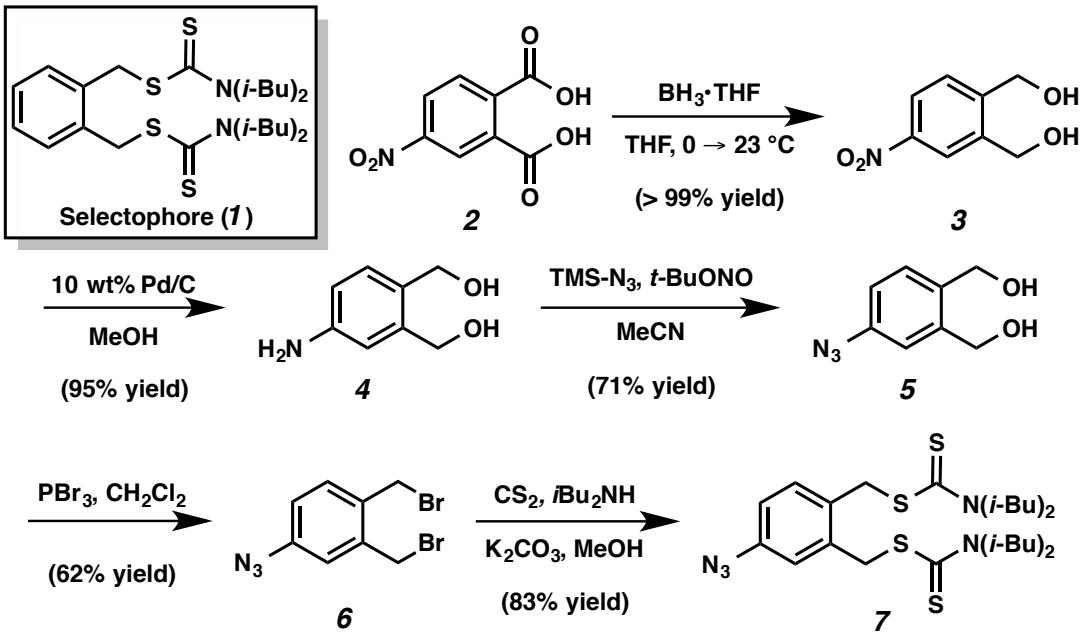

As outlined in **Scheme 5.2**, a potential was applied to a bare CFM (**CFM 1**) in the presence of diazonium salt **8** to produce **CFM 2**. Desilylation of **CFM 2** was accomplished in the presence of TBAF to generate a scaffolded electrode (**CFM 3**). Subsequent azide-alkyne cycloaddition with azido-ionophore derivative **7** completed the functionalization process, affording **CFM 4**. Each step of the CFM functionalization process was monitored electrochemically with FSCV (see **Appendix D** for details)

Scheme 5.2. Covalent modification strategy towards Cu(II) selective CFM.

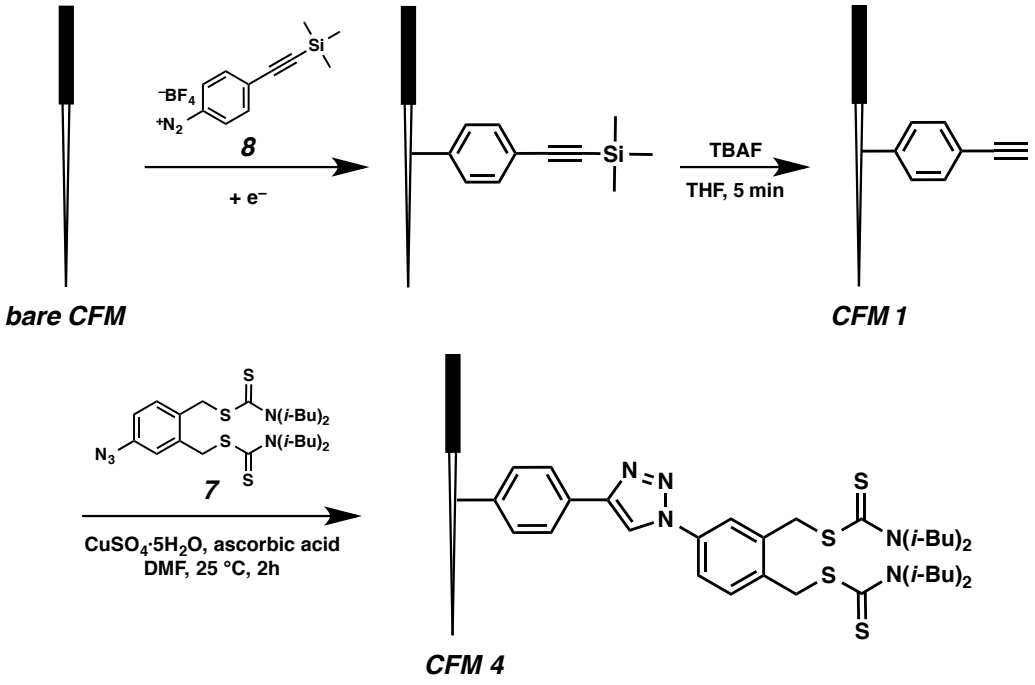

5.3.2 Characterization of Modified CFM

Using an FSCV waveform we previously developed for Cu(II), we compared the responses of bare electrodes (**CFM 1**, **Column I**) to ionophore-grafted electrodes (**CFM 4**, **Column II**) to a flow injection of a solution of Cu(II) in NaCl (**Figure 5.1.A**) and to a flow injection of a solution consisting of 8 other divalent metal ions (**Figure 5.1.B**). Interpretation of the color plots in this figure is described elsewhere in detail.[157] Briefly, background subtracted cyclic voltammograms (CVs) taken every 100 ms are displayed as potential on the y-xis, time on the x-axis, and current in false color. A representative cyclic voltammogram (CV) shown below each color plot was taken from the color plot at the white dotted lines.

The CVs taken for both electrodes resemble those we have previously seen.[35] The CV taken with **CFM 4** had two reduction peaks, likely because of two

types of adsorption sites (oxygen moieties and ionophore) now available. While it is difficult to attribute the peaks to specific adsorption sites, a later experiments imply that the peak at -0.9 V arises from the Cu(II) adsorbed onto ionophore sites. This more negative potential is consistent with the higher equilibrium constant (10) for Cu(II) adsorption to Selectophore (approx.10^{10}) vs. bare CFMs (approx. 10^{7}) requiring more energy for Cu(II) reduction.

In **Figure 5.1.B**, a mixture of 1 μM $Cu(NO_3)_2$ and 10 μM each of $Zn(NO_3)_2$, $Cd(NO_3)_2$, $Ni(NO_3)_2$, $Co(NO_3)_2$, $Ca(NO_3)_2$, $Mg(NO_3)_2$, $Pb(NO_3)_2$, and $Mn(NO_3)_2$ was flow injected onto bare electrodes (**CFM 1**, **Column I**) and the ionophore-grafted electrodes (**CFM 4**, **Column II**). In both cases, it is impossible to distinguish any recognizable Faradaic features in the CVs. We hypothesized that because our modification occurs via a C-C bond, it has little effect on the ambient oxygen functionalities on the CFM surface, thus the other divalent metal ions remain free to adsorb onto the CFM.

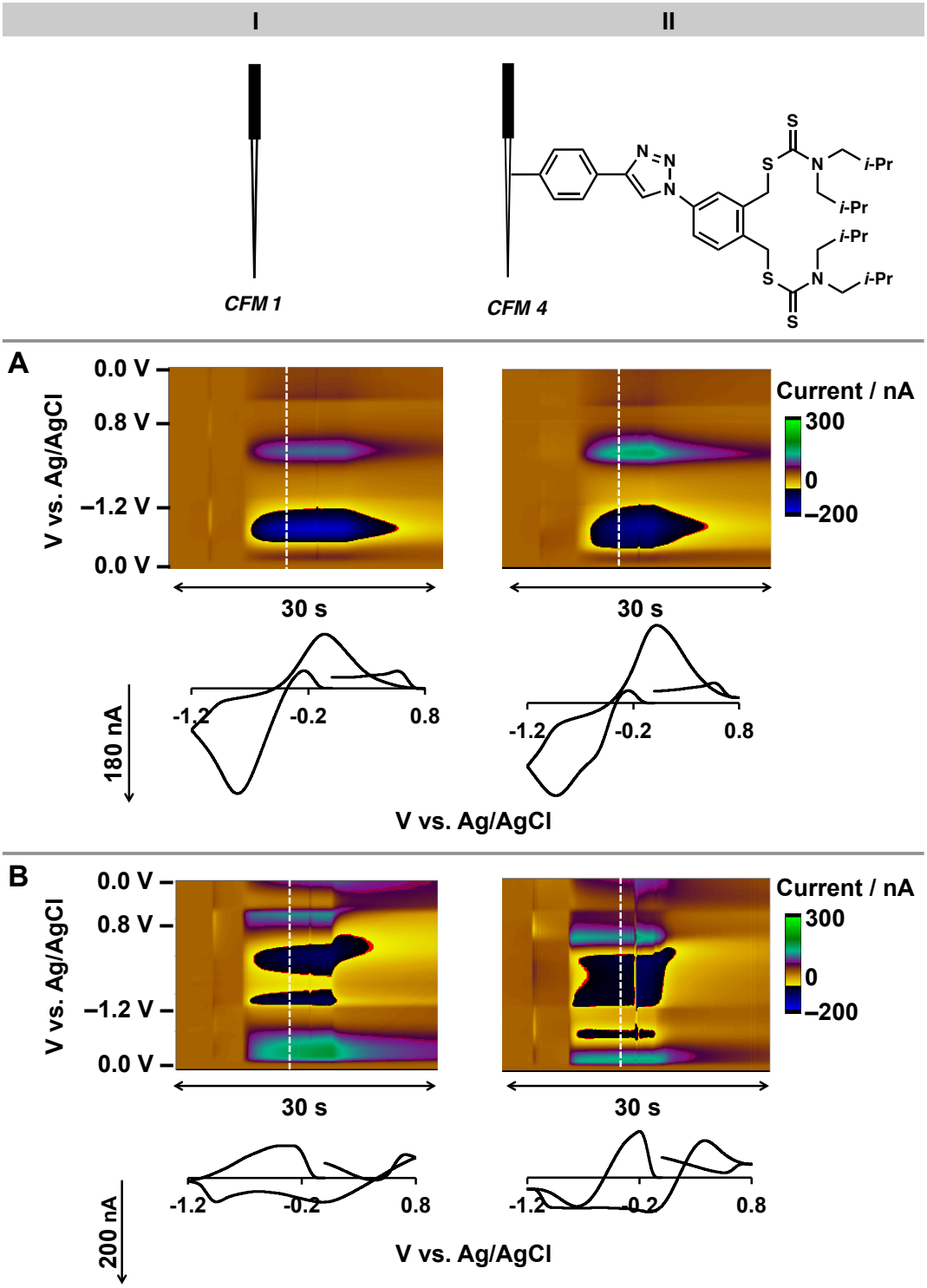

Figure 5.1. Comparison of (**I**) unfunctionalized and (**II**) Cu(II)-ionophore-functionalized electrodes in (**A**) 1 µM Cu(II) and (**B**) mixed metal (1.0 µM Cu(II), 10 µM each: Zn(II), Cd(II), Ni(II), Co(II), Ca(II), Mg(II), Pb(II), Mn(II)) solutions. All counterions are NO_3^-. Waveform: –1.2/+0.8 V, Exposed carbon fiber length: 150 µm.

5.3.3 Syilation of Surface Oxygen Groups

These oxygen-containing functional groups are primarily hydroxyl groups.[80] Thus to hinder adsorption of interfering analytes, we modified the electrode fabrication process to include a blocking step that would mask the majority of these sites. As shown in **Scheme 5.3**, the scaffolded **CFM 3** was exposed to a solution of *t*-butyldimethylsilyl chloride in the presence of triethylamine to convert any hydroxyl groups present to the corresponding silyl ethers, which are known to be poor chelators to metal ions. This process was conducted while applying a negative potential to the electrode with the aim of reducing any carbonyl groups that might be present to the corresponding alcohols *in situ*. These alcohols would then be blocked by the silyl groups, ultimately affording **CFM 3'**. Azide-alkyne cycloaddition was executed as above to access ionophore-grafted electrode **CFM 4'** with blocked surface oxygenation.

Scheme 5.3. Inhibition of surface oxygen groups on CFM 3.

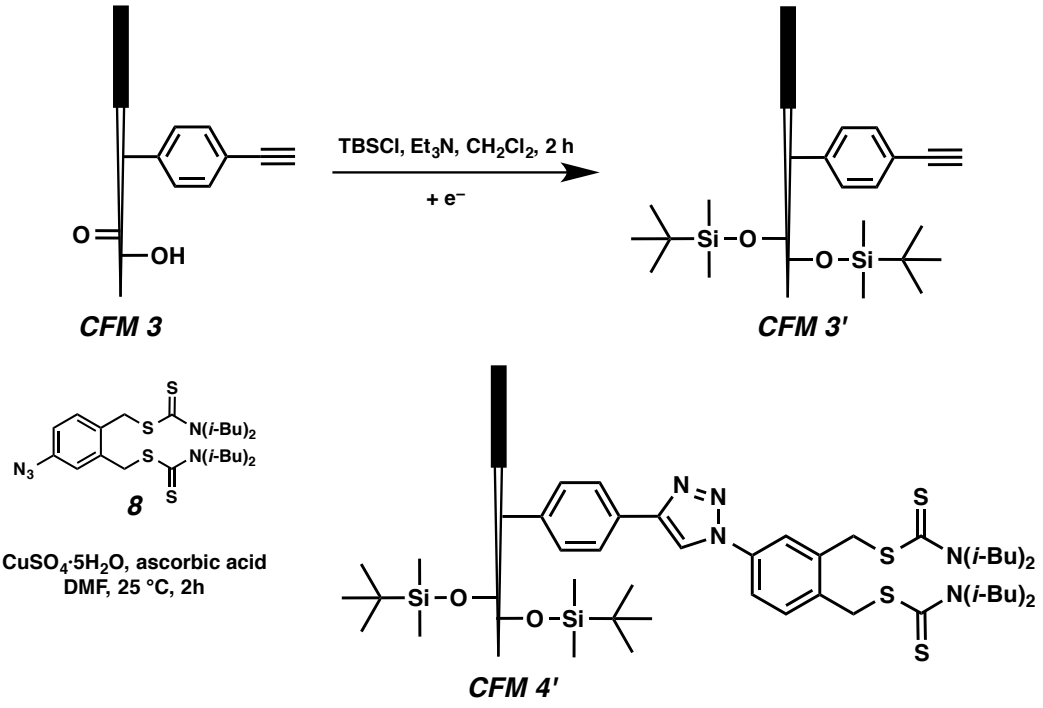

To validate the efficacy of this blocking protocol, **CFM 3'** was characterized by its response to a 1.0 μM $Cu(NO_3)_2$ solution (**Figure 5.2**).

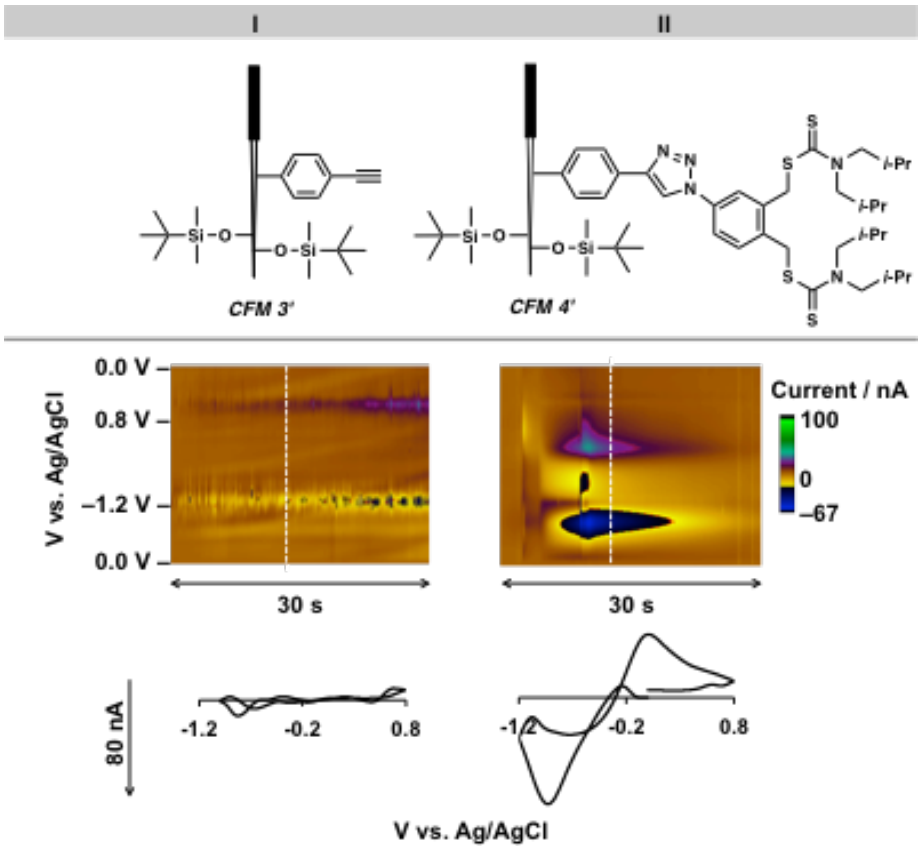

Figure 5.2. In 1 μM Cu(II) solution, (**I**) Scaffolded, *O*-blocked electrodes show no signal and (**II**) Cu(II)-ionophore-functionalized, *O*-blocked electrodes show expected color plot and CV for Cu(II). Waveform: –1.2V/+0.8 V, Exposed carbon fiber length: (**I**) 150 μm, (**II**) 300 μm.

As we anticipated, **CFM 3'** (**Column I**) shows no significant electrochemical signal, indicating successful blocking of the oxygen adsorption sites on the electrode. Initially, when the exposed carbon fiber of **CFM 4'** was 150 μM in length, minimal signal was observed. We reasoned that because of the spacing between the aryl alkyne scaffolding groups, there should be a significant decrease in adsorption sites for Cu(II) in **CFM 4'** relative to **CFM 4**, which has adsorption sites derived from both the ionophore and surface oxygen groups. To

increase the number of adsorption sites available to Cu(II), we increased the length of the electrode to 300 μM and repeated the functionalization process in **Scheme 5.3**. After this alteration, **CFM 4'** showed a very clear reduction peak at –0.9 V upon exposure to 1.0 μM Cu(II) (**Figure 5.2**, **Column II**).

5.3.4 Cu(II)Selective CFM

We next returned our attention to selective detection of Cu(II) in a mixed metal solution. **CFM 4'** was exposed to the mixed metal solution (*vide supra*) via flow injection (**Figure 5.3**, **Column II**). **CFM 4'** clearly showed reversible Faradaic behavior with a strong reduction peak at –0.9 V. Importantly, there was no apparent signal arising from any of the other metals in the solution. Thus, our ionophore-grafted, *O*-blocked electrodes are able to detect Cu(II) as the minor component of a mixture of metal ions. The streaking behavior in the color plot for this electrode (**CFM 4'**) indicates a prolonged clearance time for Cu(II) relative to the bare electrode (**CFM 1**). This observation is unsurprising considering the higher K_{ads} of Selectophore vs. the bare CFM. Electrochemical optimizations of the waveform can be created to circumvent this, which is the focus of our future studies. This is the first time that FSCV has given a purely selective response to one analyte, and to our knowledge the first time that Cu(II) has been measured selectively with sub-second temporal resolution at a micro-sensor.

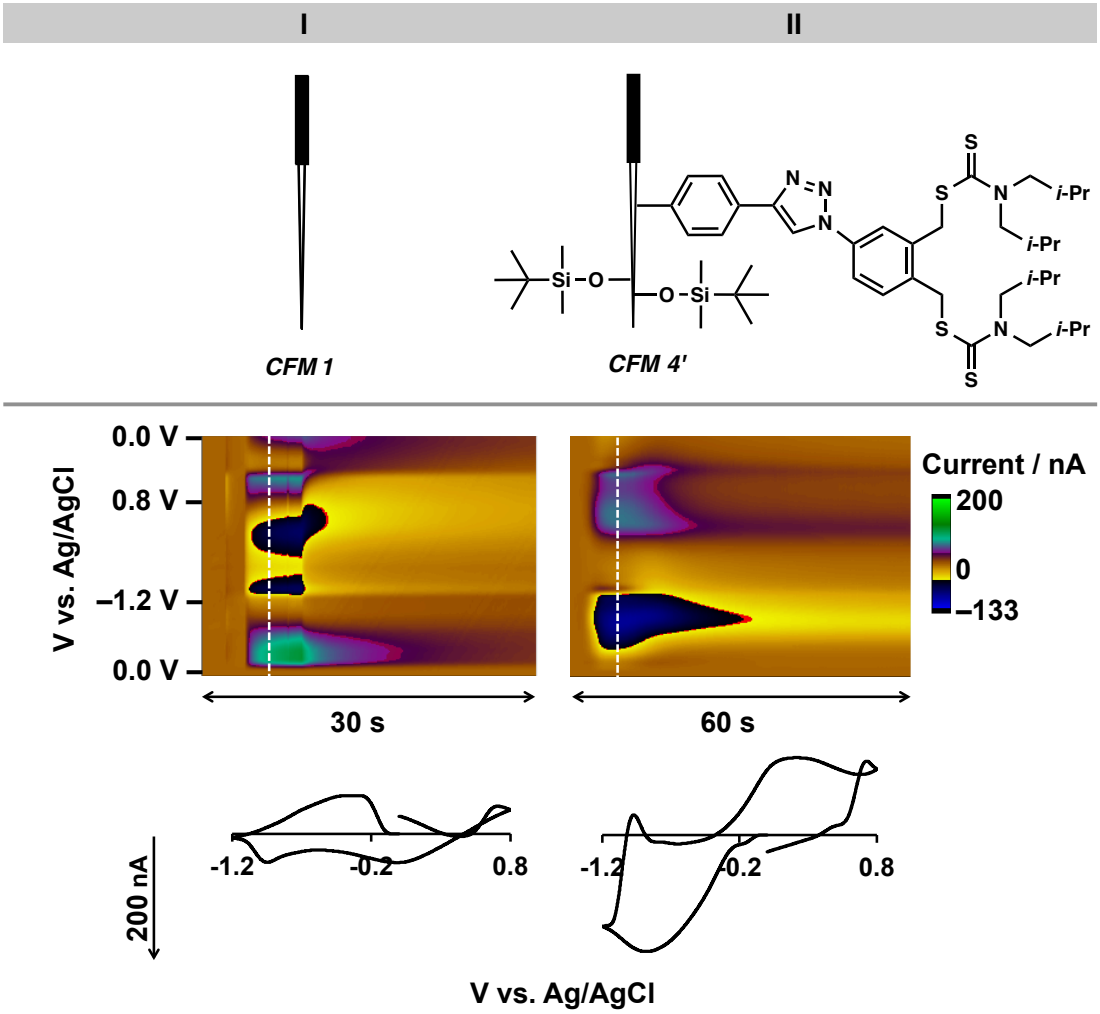

Figure 5.3. In mixed metal solution, (**I**) unfunctionalized electrodes cannot detect Cu(II) (data repeated from Figure 5.2.B for convenience), and (**II**) Cu(II)-ionophore-functionalized, *O*-blocked electrodes show Cu(II) redox signal. Waveform: –1.2V/+0.8 V, Exposed carbon fiber length: (**I**) 150 µm, (**II**) 300 µm.

The stability of this modification is a critical parameter to address. Thus, we exposed 4 ionophore-grafted, *O*-blocked electrodes (**CFM 4'**) to 50 successive injections of Cu(II). **Figure 5.4.A** shows the averaged, normalized current for these 4 electrodes with each injection. The electrodes show excellent stability over this short-term experiment. In **Figure 5.4.B**, electrodes shelf life was assessed whereby electrodes were stored for 16 weeks. Measurements were

taken weekly for the first 4 weeks, and monthly after that. The averaged, normalized current at these specific time points was again excellent showing that the ionophore does not undergo any decomposition upon storage over this time period.

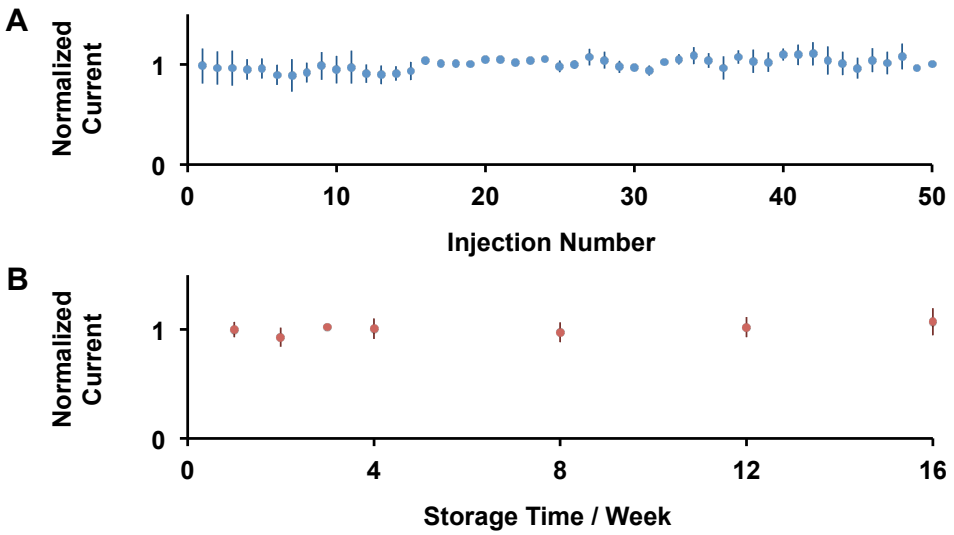

Figure 5.4. Stability tests of ionophore-grafted electrodes with blocked surface oxygenated groups. (**A**) Response of CFM 4' to 50 successive injections of 1.0 μM Cu(II). (**B**) Response of CFM 4' to injections of 1.0 μM Cu(II) over 16 weeks.

5.4 Conclusions

In summary, we designed an efficient synthesis of an azido-ionophore selective for Cu(II) and electrochemically validated our general covalent functionalization approach.[155] By strategically blocking the surface oxygen groups, we were able to prevent coordination of interfering analytes. The resulting electrode was found to be highly selective for Cu(II) in a solution of many, more-concentrated divalent metal ions. We have thus successfully developed the first effective strategy for covalent modification of CFMs with

ionophores, enabling real-time ultra-selective detection of Cu(II). This sensor heralds a transformative step for electroanalysis in providing unparalleled selectivity and temporal resolution.

CHAPTER 6. A NOVEL CARBON NANOFIBER PYROLYZED PHOTORESIST MICROELECTRODE ARRAY FOR FAST SCAN CYCLIC VOLTAMMETRY ANALYSIS

Pyrolyzed photoresist film (PPF) microelectrode arrays (MEAs) show a great deal of promise for multi-dimensional electrochemical recordings. In this paper, as a first step towards achieving our ultimate goal of simultaneous, selective detection of multiple different targets, we fabricate MEAs with a highly reproducible and rich chemical surface area for fast scan cyclic voltammetry (FSCV) analysis. We manipulate electrode surface area without compromising electrode dimensions via creation of nanofibers from negative pyrolyzed photoresist. Nanofibers are created by employing a two-step pyrolysis process and applying a dual O_2 plasma. We illustrate how our novel approach improves film adhesion and increases surface reactivity. We finally showcase the electrodes' suitability for FSCV analysis by demonstrating a highly sensitive and stable FSCV dopamine measurement on a prototype 4-channel array.

Yang, Y.,* Yi, W.,* Hashemi, P., Cheng, M. "A Novel Carbon Nanofiber Pyrolyzed Photoresist Microelectrode Array for Fast Scan Cyclic Voltammetry Analysis" *In preparation,* *Contributed equally.

6.1 Introduction

Carbon materials are widely employed in microsensor fabrication because they are versatile, low cost and display excellent electrochemical properties and biocompatibility.[158,159] Traditional manufacturing processes for carbon-based microelectrodes include encapsulation of carbon fibers with insulation materials,[160-162] deposition of carbon materials directly on micro-pipets[163,164] and formation of carbon from pyrolysis of polymer or photoresist coated on micro-pipets.[165,166] The application of these single-unit configurations is limited in integrative environments where spatial resolution and multiple targets are of great significance. Therefore recently, micro-fabricated carbon electrodes with multiple sensing elements are gaining popularity.

Carbon films have been sputtered[167] or vacuum-deposited onto various substrates.[168] However, these microfabrication processes suffer from poor adhesion.[169] A robust microfabrication process involving pyrolysis of a patterned photoresist has recently been developed to form carbonaceous microelectrode arrays (MEAs).[47,158,169-180] The photoresist, as a starting material for microelectrode fabrication, is especially advantageous because it is finely and reproducibly patterned by lithography techniques.[181] Pyrolyzed photoresist film (PPF) electrodes can sense molecules such as neurotransmitters,[47,172,174-176] O_2,[176] glucose,[179,180] H_2O_2,[177] DNA,[182] oncoprotein,[178] Hg,[183] and Ni.[173] For analysis in real systems, researchers strive to augment sensitivity and decrease the limit of detection (LOD) of their sensors and it is well accepted that increasing the reactive surface area of a sensing device is an effective way to achieve these

goals.[170] Because it is desirable to maintain the miniaturized geometry of sensing surfaces (minimal impact on surroundings), a number of approaches have been used to increase the physical reaction sites, including 3D architecture,[170,172,179] coatings of nanomaterials,[177,180] flame etching,[161] laser activation,[184] and electrochemical treatments.[81,185-187] These methods either generate new surface area or refresh the surface by removing adsorbed, interfering reactants.

Different analysis methods including high speed chronoamperometry,[172,176-180] cyclic voltammetry (CV),[172,173] and fast scan cyclic voltammetry (FSCV)[47,174-176] have been coupled with MEAs. Our research focuses on pairing FSCV to MEAs for real-time, sub-second measurements of multiple analytes with high selectivity and sensitivity.[188,189] Our interests lie in applying FSCV to electrochemically detect neurotransmitters and trace metal ions.[189-192] In Chapter 4, we described a generalized covalent modification strategy to functionalize carbon fiber microelectrodes (CFMs) with controllable densities.[191] This procedure will ultimately create ultra-selective CFM surfaces via specific recognition adsorption sites. Our ultimate goal is to utilize this novel chemistry for simultaneous, selective detection of multiple different targets. To achieve this goal, we fabricated MEAs with a highly reproducible and easy to functionalize surface area, as described in this chapter.

We extend on pioneering work by Wightman and McCarty who developed FSCV compatible PPF arrays and applied an extended electrochemical waveform[81] to over-oxidize the resulting carbon surfaces for improved sensitivity towards dopamine.[47,176] Here, to orient Wightman and McCarty's work towards

our own goals, we concentrate on improving manipulation of physical electrode surface area without compromising the miniature electrode dimension. We achieve this by a novel method to fabricate nanofiber structured MEAs from negative pyrolyzed photoresist, which carries fundamental advantages over positive photoresist for our electrochemical applications. We employ a two-step pyrolysis process and apply a dual O_2 plasma treatment including a primary plasma before and a secondary plasma after pyrolysis. We found that the two-step pyrolysis improved film adhesion and by optimizing O_2 plasma treatment parameters, we found high surface reactivity. We characterized the electrodes' performance to assess their suitability for FSCV analysis and showed highly sensitive and stable FSCV measurements on prototype 4-channel arrays.

The advanced strategy that we illustrate here is a robust approach for fabricating highly sensitive PPF MEAs with reproducible surface area, which will ultimately facilitate simultaneous multi-target FSCV detection.

6.2 Materials and Methods

6.2.1 Chemicals

Dopamine solutions were prepared by dissolving dopamine HClO into Tris-buffer prior to each experiment. Tris-buffer constituents (15 mM $H_2NC(CH2)OH)_3 \cdot HCl$, 140 mM NaCl, 3.25 mM KCl,1.2 mM $CaCl_2$, 1.25 mM $NaH_2PO_4 \cdot H_2O$, 1.2 mM $MgCl_2$ and 2.0 mM Na_2SO_4 with the pH adjusted to 7.4) were purchased from EMD Chemicals Inc, USA. All aqueous solutions were made with deionized water.

6.2.2 Electrode Fabrication

The process flow of the electrode fabrication is shown in **Figure 6.1**. After standard cleaning, 1 μm silicon nitride was grown on a silicon substrate by low-pressure chemical vapor deposition (LPCVD). Ti/Pt (20 nm/200 nm) was deposited by e-beam evaporation and patterned by lift-off to serve as electrode pads and interconnections. 1~2 μm silicon dioxide was deposited by plasma enhanced chemical vapor deposition (PECVD) and then patterned by wet etching to expose the electrodes and contact pads. SU-8 photoresist was then patterned onto the electrode area. Next, the sample was treated by a primary O_2 plasma (8min, 300W, 30 sccm O_2, 160 mTorr), in order to create the fiber structure of the SU-8. A two-step pyrolysis process was performed to convert the SU-8 polymer to carbon. The samples were first heated in a nitrogen environment at 300°C for about 30min. Then the temperature was raised to 900 °C over about 20 min. The nitrogen gas was shut off and H_2(2%)/Ar were introduced for 1h. Finally the furnace was slowly cooled down to room temperature. Then the backside of the wafer was coated with aluminum and patterned. The wafers were then diced to release the electrodes. The secondary O_2 plasma step was then applied to the obtained electrodes (30 s, 100 W, 30 sccm O_2, 160 mTorr) for sensitivity enhancement. For easier reference in the following discussion, the samples with different fabrication and treatment conditions are labeled in **Table 6.1**.

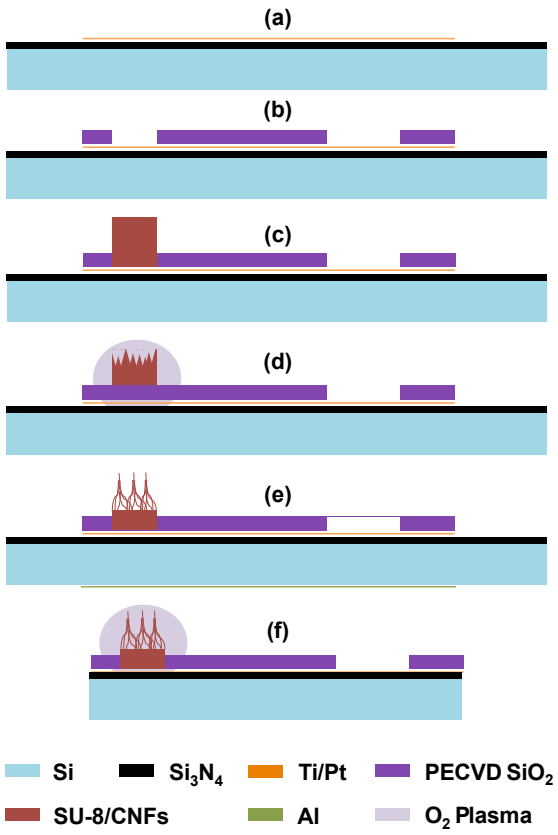

Figure 6.1. Process flow for the fabrication and treatment of PPF MEAs.

Table 6.1. Parameters for dual O_2 plasma treatment in the device fabrication.

	0 s secondary O_2 plasma	10 s secondary O_2 plasma	20 s secondary O_2 plasma	30 s secondary O_2 plasma
No primary O_2 plasma No pyrolysis	CMEA 001	N/A	N/A	N/A
Primary O_2 plasma No pyrolysis	CMEA 002	N/A	N/A	N/A
No primary O_2 plasma With pyrolysis	CMEA 100	CMEA 101	CMEA 102	CMEA 103
Primary O_2 plasma With pyrolysis	CMEA 200	CMEA 201	CMEA 202	CMEA 203

6.2.3 Electrode Characterization

The morphologies of the produced electrodes were observed by scanning electron microscopy (SEM). The images were taken using a TUSCAN GAIA dual beam focused ion beam system. The surface roughness of the electrodes was assessed using a NanoScope AFM with silicon TESP probe tips (Nanosensors). The degree of graphitization was measured using the E-Z Raman spectroscopy system at 532 nm excitation. X-Ray photoelectron spectroscopy (XPS) measurements were performed on a Kratos Axis Ultra spectrometer that was equipped with a monochromatic Al X-ray source (hv = 1486.6 eV). The measurements were carried out at 150 W power (15 KV, 10 mA) in an analysis chamber at a pressure of $< 5 \times 10^{-9}$ mbar.

6.2.4 Electrochemical Instrumentation and Data Acquisition

All electrochemical experiments were performed using a Dagan ChemClamp potentiostat (Dagan, Minneapolis, MN). Custom-built software, WCCV (Knowmad Technologies, AZ), written in LABVIEW 2012 (National Instruments, Austin, TX), was used for background subtraction, data analysis and signal processing. A two-electrode system was employed. The working electrode was a 4-channel PPF MEA. An Ag/AgCl reference electrode was fabricated by electroplating Cl^- ions onto a silver wire (A-M systems, WA) for 5 s. All color plots and cyclic voltammograms (CVs) were collected and averaged across 12 different electrodes of 3 devices. Pooled data is presented with error bars signifying the standard error of the mean (SEM). Student's t tests were performed on paired data sets; $p < 0.05$ was taken as significant.

6.2.5 Flow Injection Analysis

A MEA was fixed in a modified HPLC union (Elbow, PEEK 3432, IDEX, Middleboro, MA), and connected by the output of a flow injection apparatus. The apparatus consisted of a six-port HPLC loop injector affixed to a two-position actuator (Rheodyne model 7010 valve and 5701 actuator) and a syringe infusion pump (kd Scientific, model KDS-410, Holliston, MA). A rectangular pulse of analyte was introduced to the MEA surface at a flow rate of 2 mL min^{-1}.

6.3 Results and Discussion

6.3.1 Electrode Design and Fabrication

Spin coating with subsequent photoresist photolithographic patterning is a well-developed technique in the semiconductor industry. Pyrolysis of the photoresist material in an oxygen-free atmosphere is known to form carbon structures via depletion of volatile materials. Therefore, we employed the photoresist as a structural material to create carbon electrodes in an array formation that is integratable into microdevices. The novelty in our work is incorporation of a two-step pyrolysis procedure (two temperatures) and a dual O_2 plasma treatment (different power and duration) into the fabrication procedure.

In our electrode design and fabrication, there are three aspects to address:

a) Electrode geometry and dimensions: Our interests lie in biological and environmental analysis, thus electrode dimensions should be minimized; as a starting point, we chose an active geometric surface area ranging from 3000 to 5000 μm^2 which is comparable to the surface area of cylindrical CFMs used in previous studies.[190,191] As shown in the optical images in **Figure 6.2.a** and **b**, four

electrodes were fashioned in parallel as an array to form the tip of a single device with a spacing of 30 μm. We aimed to keep our device under 30 μm to maintain negligible tissue damage[193] and to prevent cross-talk [176].

b) Adherence to functionalization strategy: It is important to produce an active carbon surface with sufficient reaction sites over a fixed geometric area. Our O_2 plasma pretreatment creates a forest of highly reactive carbon nanofibers, with abundant edge planes, as evident in **Figure 6.2.c**. These carbon nanofibers are responsible for greatly augmenting surface area compared with flat carbon film electrodes. This phenomenon can be seen in the SEM images of the PPF electrodes with and without O_2 plasma in **Figure 6.1.c** and **d** respectively where untreated PPF resembles a flat plane while the pretreated PPF consists of carbon nanofiber structures. The mechanisms of nanofiber formation are well described;[192] in brief, the SU-8 polymer chain is composed of both aromatic and linear sections, thus the etching rates of these two sections are different. This phenomenon, which results in a higher vertical than parallel growth rate, promotes the formation of nano-filaments, which are predecessors for nanofibers. In addition, SU-8's high number of aliphatic chains means that the crystallization temperature for SU-8 is generally higher than for positive photoresist which already tend to contain high numbers of ringed hexagons. This means that at the same pyrolysis temperature, more defect sites will be formed on SU-8 than on positive photoresists;[194] an auspicious surface effect for electrochemical applications.[187]

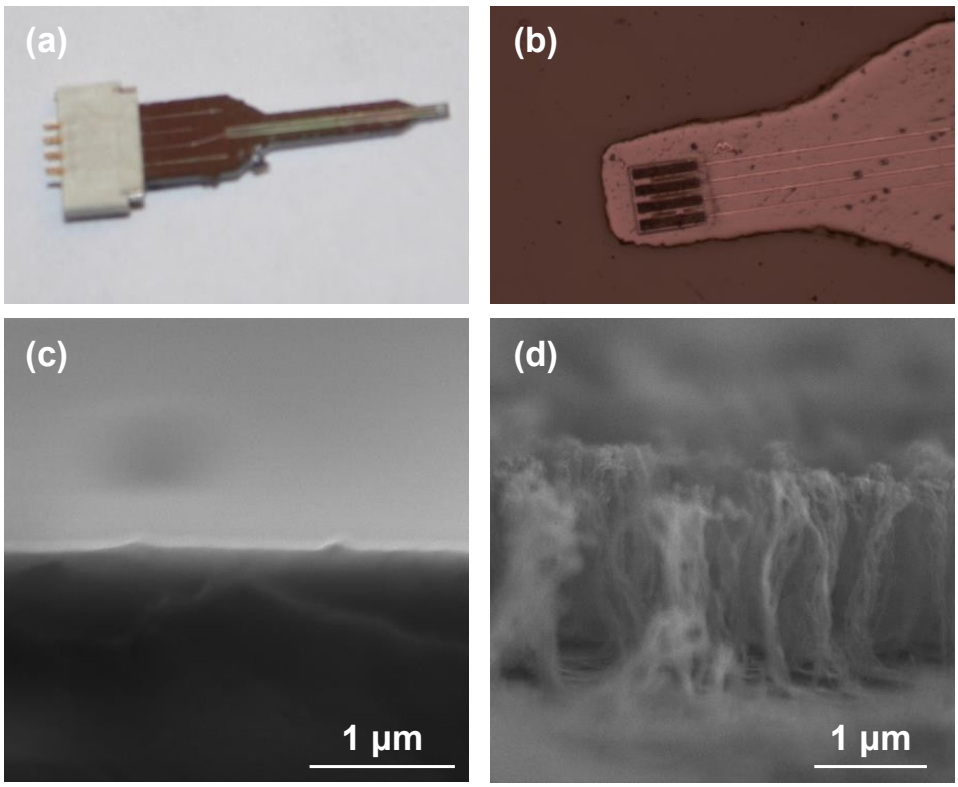

Figure 6.2. (**a**, **b**) Optical images of PPF MEAs. SEM images show the microstructure of the pyrolyzed photoresist (**c**) without and (**d**) with oxygen plasma pre-treatment.

c) Stability: Here we define stability as adhesion of carbon structures to the substrate. SU-8 is known to provide better adhesion after pyrolysis compared with positive photoresists.[159,194] A likely reason is that negative photoresists have low glass transition temperatures and low molecular weights, which means that the photoresist flows once melted during pyrolysis. The result of this effect is fewer pores and cracks that arise due to evolution.[159,194] Because pores and cracks are usually the cause of poor adhesion, negative photoresists tend to display better stability. However, we and others still experienced instability via peeling of carbon patterns from the insulated substrate when using a traditional one step pyrolysis.[192,194] (data not shown) We addressed this problem by employing a two-step heating process, as previously described.[192] The

measuring process involves employing a lower temperature (300 °C) as an initial step before utilizing 1000 °C. The additional lower temperature lead to better adhesion and allowed us to form devices stable in aqueous environments. This is likely because compared to a one-step process, the two-step process will reach the pyrolysis temperature less dramatically. This more gradual meander towards 1000 °C more readily releases tensile stress near the interface between the photoresist and the substrate, that exists because of the thermal expansion coefficient. Additionally, for the same reason, less dramatic degassing reduces the odds of micro-crack formation. Both of these effects improve the adhesion of the film. Finally, we postulated that the primary O_2 plasma step itself contributed to improving adhesion, and tested this notion in section **6.3.3** (*vide infra*).

6.3.2 Characterization of PPF MEAs

Having designed our electrodes to be of the correct dimensions, and to have a suitable surface area and stability for our applications, we next characterize our electrodes by employing a host of surface analysis methods.

AFM

To ensure that a dual O_2 plasma treatment (vs. a one-step treatment) does not negatively influence PPF electrode surface structure, we employed atomic force microscopy (AFM). The surface topography of the PPF MEAs was evaluated by tapping mode AFM. Images (5 x 5 μm) are presented in **Figure 6.3**. Cross-sectional plots accompany each image. The surface features on PPF MEAs after primary O_2 plasma are greatly enhanced (**c**, **d**) compared to PPF MEAs with no plasma treatment (as see in the SEM imagine, *vide supra*). For

both PPF MEAs with and without primary O_2 plasma, there is no significant structural change after the secondary plasma, showing that a dual plasma process does not unfavorably impact the PPF surface.

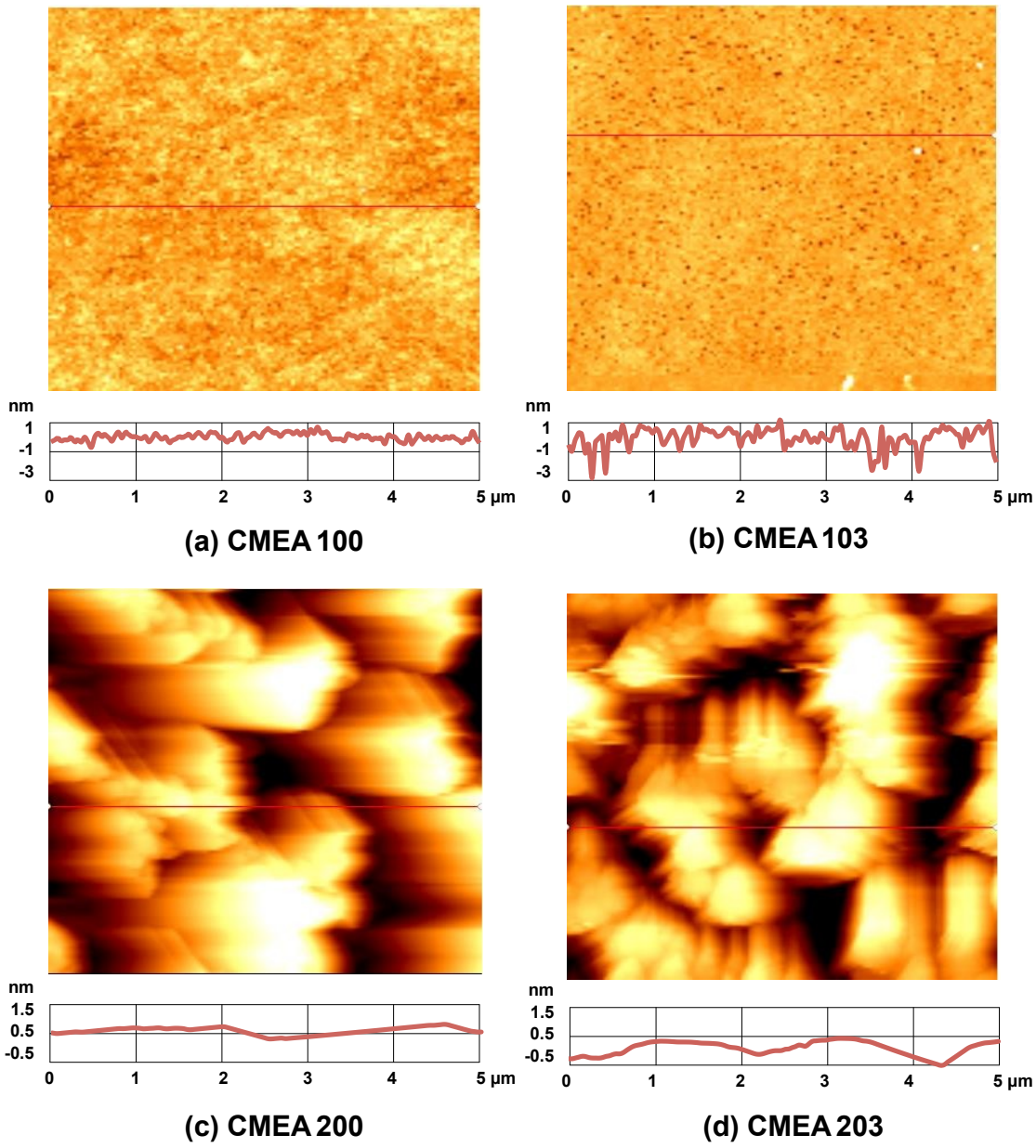

Figure 6.3. AFM images with associated line plot collect at (**a**) CMEA 100, (**b**) CMEA 103, (**c**) CMEA 200, and (**d**) CMEA 203.

Raman

To verify that the surface of the nanofibers formed after the dual O_2 plasma treatment is suitable for electrochemistry, we took advantage of the ability of Micro-Raman spectroscopy to indicate the presence of edge planes, regions with more reaction sites for electrochemical reactions, on our carbon nanofiber surfaces. **Figure 6.4** shows Raman spectra of SU-8 before pyrolysis (CMEA 001/002), after pyrolysis and no O_2 plasma (CMEA 100), after pyrolysis and the secondary plasma (CMEA 103), after pyrolysis and the primary plasma (CMEA 200) and after pyrolysis and dual plasma (CMEA 203). Before pyrolysis, no characteristic peak was observed, however after pyrolysis, two broad peaks centered at around 1350 (D band) and 1590 (G band) cm^{-1} were present. The band at around 1350 cm^{-1} is consistent with disordered carbon, while the band at around 1590 cm^{-1} can be assigned to crystallized graphitic structure.[195] The integrated intensity ratio of D/G is frequently used as an indicator of the fraction of disordered SP_2 C-C bonding present in the graphitic structure, therefore higher I_D/I_G is indicative of presence of more edge planes.[196] We display these ratios for the pyrolyzed materials in **Table 6.2**. The primary plasma treated samples presents a higher I_D/I_G ratio (~ 1.1) compared to the untreated sample (I_D/I_G ~ 0.9) showing presence of more edge planes. It also can be seen that the primary plasma treated sample has lower peak intensity than the untreated one, possibly due to the formed nano structure.[197]

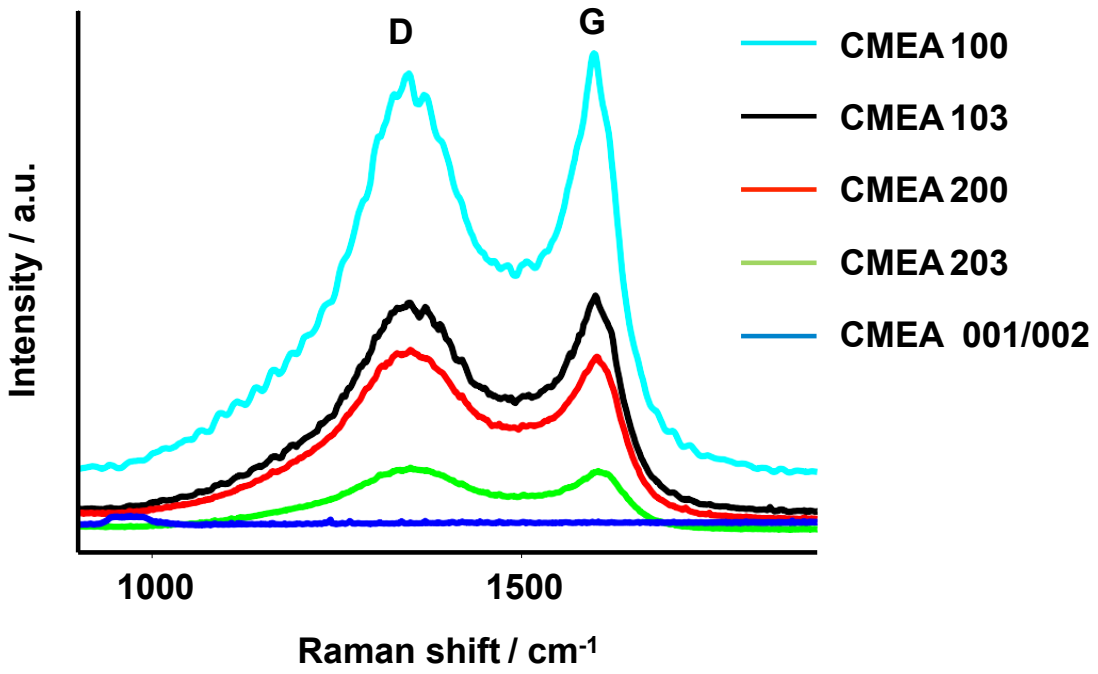

Figure 6.4 Raman spectra of photoresist derived carbon electrode with different treatments. Before pyrolysis, both pre-treated and un-pretreated samples (CMEA001/002) exhibit no characteristic peaks because of high fluorescence of SU8. After pyrolysis, pre-treated samples (CMEA 200) show a bigger ID/IG ratio than un-pretreated ones (CMEA 100), indicating more defects and more edge planes. The later application of oxygen plasma post-treatment results in no significant change of ID/IG on both pre-treated (CMEA 203) and un-pretreated samples (CMEA 103).

Table 6.2. Comparison of ID/IG and O/C ratio of electrodes under different treatments.

	CMEA 001	CMEA 002	CMEA 100	CMEA 103	CMEA 200	CMEA 203
Raman ID/IG	No peak	No peak	0.90	0.91	1.10	1.11
O/C ratio from XPS	1.01	10.02	0.13	1.06	0.13	3.5

XPS

We aim to apply these electrodes to FSCV measurements. On CFMs, the electrochemical signal is inherently regulated by analytes' adsorption, which itself is controlled by the presence of oxygen moieties on the carbon surface. Thus to verify that our electrodes contain sufficient surface oxygen, we utilized x-ray photoelectron spectroscopy (XPS) to analyze surface groups. Samples were vacuum-sealed immediately upon removal from pyrolysis furnaces or other process steps for later XPS spectra. Although this short-time exposure to air may result in some oxidation of the surface, it is thought that oxidation of pyrolyzed photoresist in air is slow enough to be negligible within the time frame of our experiment.[198] Despite this, as a cautionary measure, we kept the exposure time in air for all our samples consistent. The changes in the XPS spectra, therefore, are considered to be primarily caused by our different fabrication conditions and treatments. Atomic concentration ratio, O/C, (see **Table 6.2**) was determined from the C_{1s} and O_{1s} spectra (**Figure 6.5**). Primary O_2 plasma introduced more O_2 to the surface as expected. After pyrolysis, the O_{1s} peak diminished drastically for both O_2 plasma treated and untreated samples. Previous studies on the pyrolysis of photoresist have indicated that oxygen and nitrogen are removed at 300~500^{o}C.[196] In our case, the pyrolysis was carried out at 900 °C, which explains the O_{1s} peak reduction. In fact, the reductive atmosphere used for pyrolysis is expected to generate a hydrogen terminated surface,[159] which may interfere with electrochemical behavior of carbon surfaces. The increase in O/C after plasma treatment elicits the elimination of hydrogen and subsequent

surface occupation of oxygen groups, consistent with prior work showing that plasma treatments can form surface carboxyl functional groups.[199] It is worth noting that the increase of O/C in primary plasma treated samples is greater than the one without primary plasma which may be attributable to more reactions sites for binding oxygen groups on the nanostructured surface originating from the primary plasma treatment. These data imply that primary O_2 plasma is responsible for creating more reaction sites; while the secondary O_2 plasma accounts for bringing O_2 containing groups to the surface.

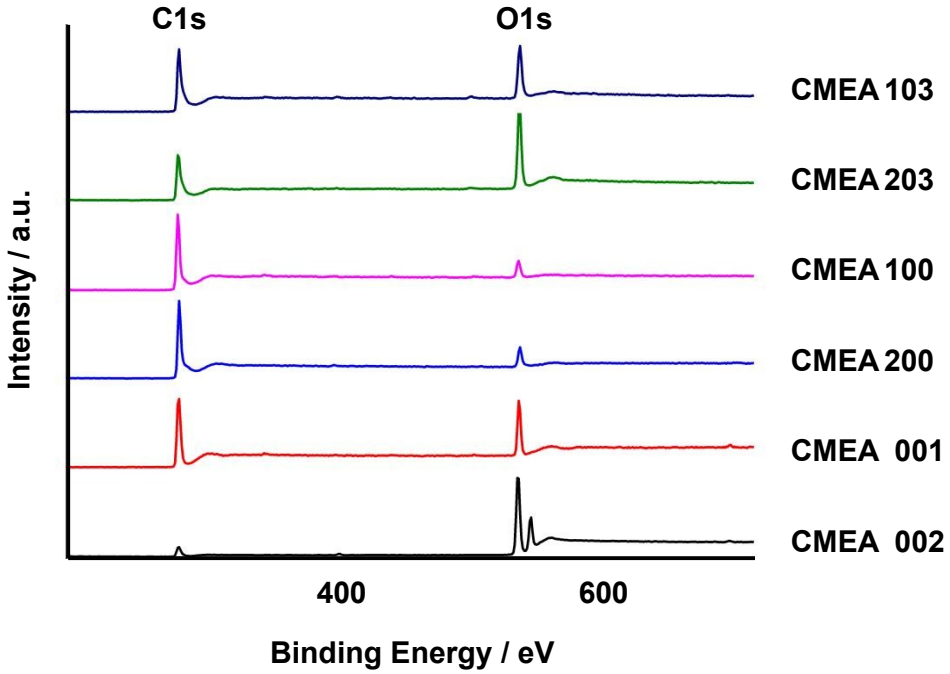

Figure 6.5. XPS comparison of photoresist derived carbon electrode with different treatments. Before pyrolysis, oxygen plasma pre-treatment caused higher O/C ratio (CMEA 002) compared to un-pretreated sample (CMEA 001). After pyrolysis in a reductive environment, the O/C ratio decreased to similar level for both pre-treated (CMEA 200) and un-pretreated samples (CMEA 100). Then oxygen plasma post-pyrolysis treatment was applied and led to the increased O/C ratio. Pre-treated samples (CMEA 203) showed bigger increase of O/C compared to un-pretreated samples (CMEA 103), due to larger surface area thus more oxygen binding sites.

These surface analyses illustrate that two-step pyrolysis and dual O_2 plasma treatment (CMEA 202) create a rich carbon surface for electrochemistry, we next explore the suitability of this surface for FSCV analysis.

6.3.3 FSCV Characterizations

Electrochemical effects of dual O_2 plasma treatments on MEAs

FSCV utilizes scan rates typically between 400 and 1000 V s^{-1} and acquires one cyclic voltammogram in approximately 2 ms every 100 ms. The fast scan rate renders the method highly selective but also generates a large charging current. Background subtraction eliminates the charging current, resulting in cyclic voltammograms characteristic of redox active species that can be used as a "fingerprint" for identification. Dopamine, as a biologically important and well-characterized molecule, was chosen as a standard analyte herein to compare with related studies. A typical FSCV characterization for the 4-electrode array is shown in **Figure 6.6**. Cyclic voltammograms were collected for 30 s during a flow injection analysis (FIA) of 1.0 μM dopamine onto CMEA 202. The traditional triangular waveform for dopamine detection was employed where the potential ramps from –0.4 V to +1.3 V and back at a scan rate of 400 V s^{-1} and application frequency of 10 Hz. A color plots illustrates this 30 s FIA event with injections of dopamine between 5 and 15 s (interpretation of a color plot can be found in Hashemi *et al.*[200]). **Figure 6.6.a** shows cyclic voltammograms taken during the dopamine injections at 4 channels of CMEA 202, indicated by the vertical white dashed line in the color plots from **Figure 6.6.b**. The redox peaks of dopamine are in accord with values reported for conventional CFMs under the same

experimental conditions.[139] **Figure 6.6.c** displays the current vs. time profiles at the maximum oxidation potential taken from the horizontal white dashed line in the color plots. Our optimized electrodes are highly sensitive, yielding 76.6 ± 4.9 nA (n = 12 ± SEM) for a 1.0 μM dopamine injection, (compared with prior studies showing 10 nA for conventional CFMs with surface areas ~ 1000 μm^2).[176]

We attribute the vast sensitivity improvements to the O_2 plasma treatments for three reasons:

a) Our pre-treatment leads to formation of fine structures on the MEAs and increased physical surface areas within equivalent geometric surfaces. The result is increased FSCV response because mass-transport is less hindered thus analyte flux is increased.

b) An additional advantage of O_2 plasma treatment is the creation of edge planes (indicated by the Raman spectra, *vide supra*). Prior studies on pyrolytic graphite have shown that edge planes are the primary reaction site.[201,202]

c) Previous studies on conventional CFMs have shown that the dopamine FSCV response is adsorption-controlled at physiological pH,[162,175] thus over oxidation (to induce oxygen moieties on the carbon surface)[175,176] and a negative resting potential between scans[175,176] are used to promote this adsorption. Our O_2 plasma treatment induces many oxygen containing functional groups to the reactive sites (XPS data, *vide supra*). As a result, dopamine adsorption, and hence sensitivity, on the electrode surface is greatly enhanced.

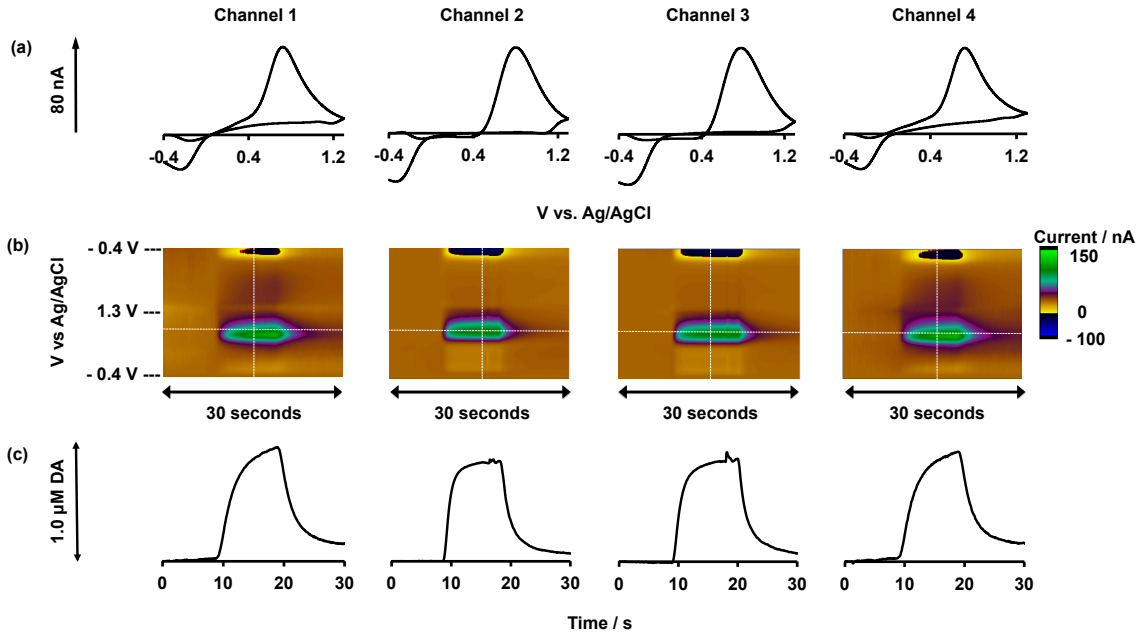

Figure 6.6. (**a**) A FIA response of electrode CMEA 202 to injection of 1.0 µM dopamine solution. (**a**) shows CVs taken at the vertical white dashed line in the corresponding color plots (**b**). (**c**) shows plots of current vs time, which was determined by taking *i* vs *t* from the horizontal white dashed line in the corresponding color plots (**b**).

We next optimized the dual O_2 plasma treatment conditions to establish the optimal electrode performance. 12 electrodes (3 devices) were selected for primary plasma treated (green) and untreated (purple) group. **Figure 6.7** compares the average current responses at the maximum dopamine oxidation potential for both groups under secondary O_2 plasma for 0, 10, 20, and 30 s. In general, the green group showed more current response than the purple group. When the secondary plasma treatment time increased, the current response for both groups showed an overall increasing trend and reached plateau at 20 s. The plateaued response of the green group (~ 80 nA) was almost 3 times that of the purple group (~ 27 nA). At 30 s, both groups reached saturation state, likely due to a damaged surface via extended secondary plasma.[203,204] Because there was no significant difference between the current responses at 20 s and 30 s for both

groups (p = 0.8015), the duration of secondary O_2 plasma treatment was set at 20 s.

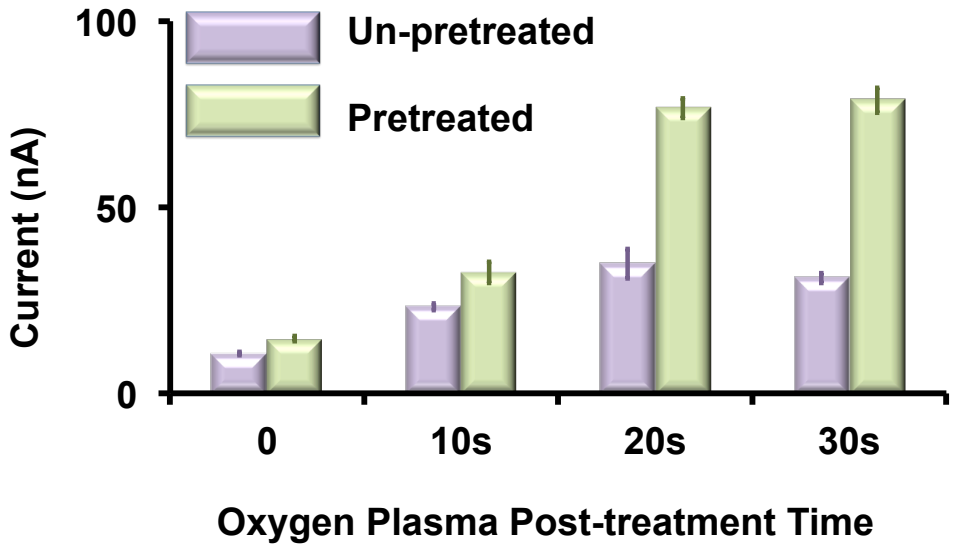

Figure 6.7. Effect of pre- and post- treatment on the sensitivity. The pre-treated samples show greater response current than non-pretreated ones. 20 s post-pyrolysis treatment saturates the surfaces with oxygen containing functional group.

Calibration and limit of detection

A standard calibration of the optimized MEAs for dopamine is presented in **Figure 6.8** (n = 12 ± SEM). The calibration was conducted within a concentration range from 0.10 µM to 10 µM. The limit of detection (LOD) was 0.10 µM, which is significantly lower than reported values for PPF electrodes.[176] A linear calibration range up to 5.0 µM is appropriate for biological analyses. The sensitivity (slope) in this range is 80 nA/µM as shown in the inset.

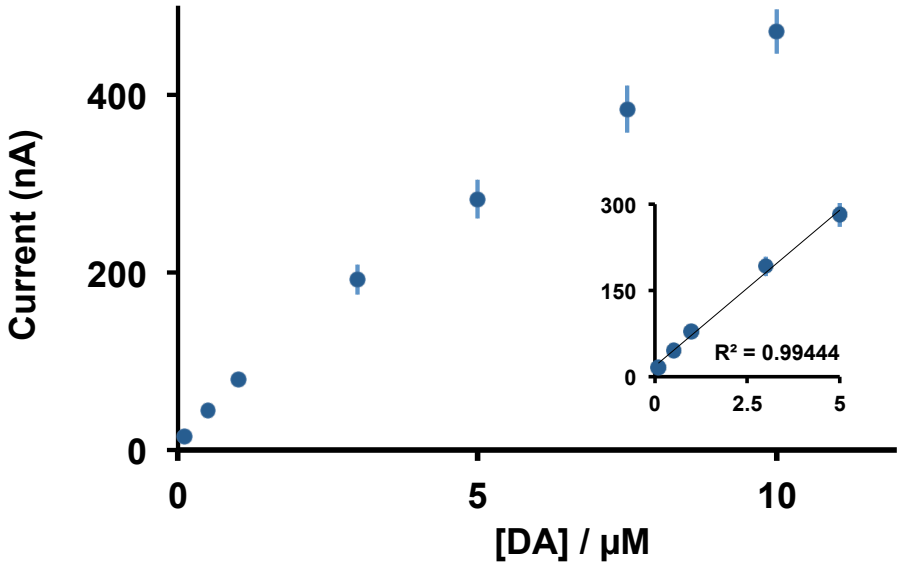

Figure 6.8. Detection limit (Sensitivity) of the optimized electrodes. The plot shows voltammetric peak current as a function of dopamine concentration. The error bars are the standard deviation (n = 12 ± SEM). Inset: Linear range of dopamine on pyrolyzed photoresist MEAs. All measurements were done at 400 V s^{-1}, 10 Hz in Tris buffer, pH 7.4.

Stability

As previously discussed, the primary reason for conventional PPF electrodes stability failure is peeling of the carbon film off the substrate and we addressed this by employing negative photoresist instead of positive photoresist. Successive injection tests were performed for both primary O_2 plasma treated and untreated groups. We successively injected 1.0 µM dopamine onto the electrode for 50 times, and we recorded the peak oxidation peak currents each time (n = 12 ± SEM). The normalized currents (observed current / average current) are plotted versus injection number in **Figure 6.9**. Both groups showed consistent responses with 50 successive injections, yet the untreated PPF electrodes displayed a greater standard deviation, likely because the primary O_2

plasma can cause certain compressive stress that further enhances the adhesion of the generated carbon films.

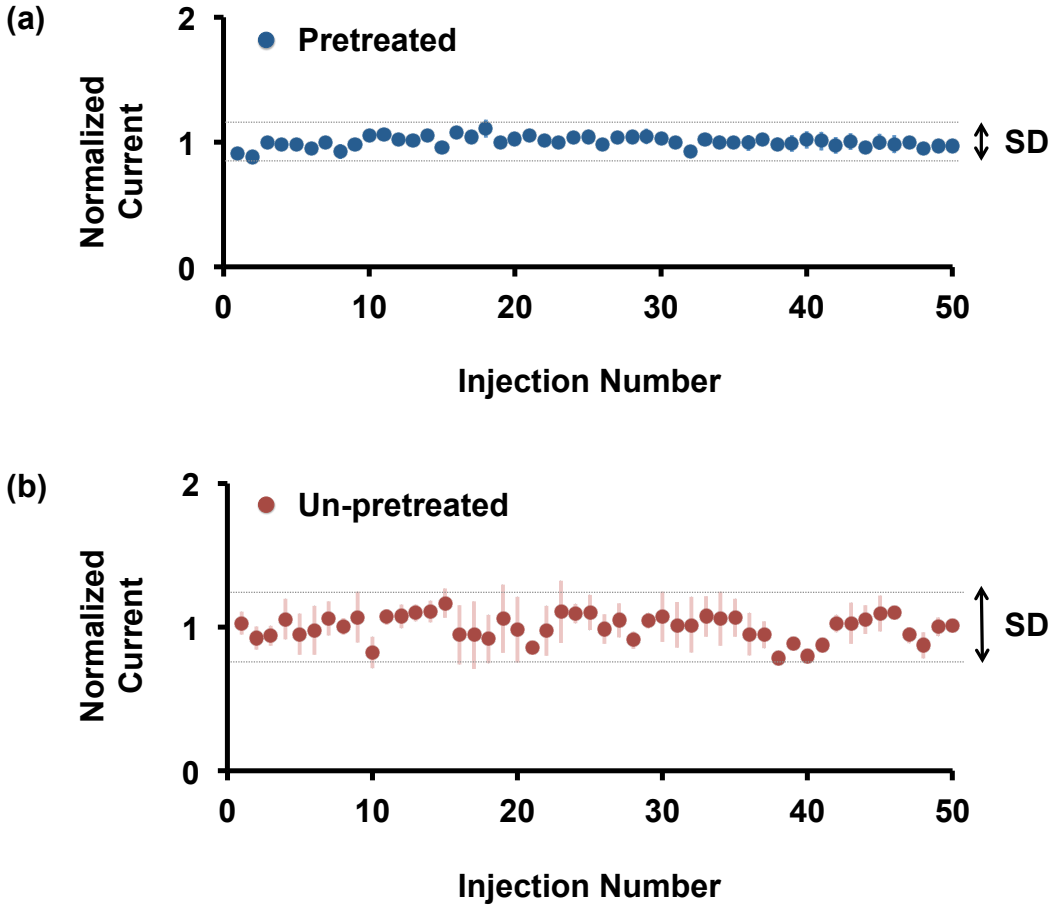

Figure 6.9. Effect of oxygen plasma pre-treatment on device stability. (a) Blue dots show the normalized current of dopamine oxidation at pre-treated MEAs for 50 times. (b) Red dots show the normalized current of dopamine oxidation at un-pretreated MEAs for 50 times. Horizontal lines indicate SD limits.

The minimal standard deviation of pretreated MEAs also implies good reproducibility. Highly reproducible batch microfabrication processes are advantageous in decreasing electrode surface area deviations, thus improving the capability of reproducible electrochemical detection. In contrast, the traditional manually cut carbon fiber microelectrodes are less precisely controlled,

and are not suitable for accurate multi-site and multi-analyte detection, even though they can be bundled up to create a compact unit.

6.4 Conclusions

PPF MEAs are an important tool for providing multiple measurement platforms with versatile spatial geometry. In this paper, we described the development of PPF MEAs that give highly reproducible, sensitive and stable responses when coupled to FSCV. These desirable characteristics are due to nanofiber formation via a novel strategy, application of a two-step pyrolysis process and dual O_2 plasma. We utilized a host of analytical methods to show that our strategy greatly improves film adhesion and surface reactivity. These devices represent an important first step towards dynamic, simultaneous and selective multi-analyte FSCV detection.

CHAPTER 7. CONCLUSION AND FUTURE PROSPECTUS

Development of novel analytical methods for trace metal detection is important for understanding metals' roles in environmental and biological systems. Our technique, fast-scan cyclic voltammetry (FSCV) at carbon-fiber microelectrodes (CFMs), is a powerful tool that can rapidly detect metal ions with high sensitivity and selectivity. Enormous efforts have been made to optimize this newly developed method from different angles to achieve its ultimate goal of application in complex natural systems.

While electrochemical techniques have traditionally been limited by their temporal resolution, Hg toxicity and stability concerns, we presented the use of FSCV towards fast, safe, and robust analysis of metals. Effective advancements were also made in model solution creation and waveform optimization. This method showed powerful strengths for not only real-time monitoring of fluctuating metal ions in real environmental samples, but also in fast metal speciation studies. This research built concrete theoretical and experimental foundations for expanding FSCV to analyzing other metal species.

Selectivity was improved through electrode modification on CFMs. We utilized and redesigned previously reported methods to develop an efficient, robust, and tunable covalent functionalization strategy. Diazonium electrochemical reduction followed by click chemistry was applied for the attachment of selective molecules to CFMs. This universal modification approach was initially characterized through grafted ferrocene as an in-situ redox label with different densities. Using optimized conditions, we attached Cu(II) ionophores covalently to fabricate Cu(II)

selective CFMs. An additional elevated level of selectivity was achieved by blocking the surface oxygen groups to prevent the adsorption of other species. This covalent modification method provided the groundwork for creating a variety of functionalized CFMs with improved selectivity while maintaining good sensitivity, response, stability, and lifetime.

In parallel work, we developed pyrolyzed photoresist film (PPF) microelectrode arrays (MEAs) as another sensor platform to be coupled with FSCV. PPF MEAs have multiple sensing channels and can be fabricated in bulk. We employed a two-step pyrolysis process and a dual O2 plasma for the carbon nanofiber formation on the novel FSCV compatible MEAs. Our strategy greatly improved film adhesion, surface reactivity, and spatial geometry. These devices represent an important first step towards dynamic, simultaneous and selective multi-analyte FSCV detection.

Future research will be focused on integrating the covalent modification strategy into the development of multiple analyte selective MEAs. In Chapter 5, we covalently attached Cu(II) ionophores to CFMs. The real power of this approach is apparent in modification for MEAs fabricated in Chapter 6. We purposefully designed the reaction scheme to be dependent on electrochemical manipulation. For example, modification of bulk carbon fibers would be less challenging (fibers, reagents and ionophores could be reacted in one vessel). However, while this approach is useful for producing microelectrodes from a stock of modified fibers, if we wish to address a single channel on a MEA, it would fail. Here, the ability to modify individual electrodes by applying potential to

one channel is invaluable. In our covalent modification strategy, a negative potential will be applied to only one channel of the 4-channel device at a time to electrochemically reduce alkynyl aryl diazonium salts. The click reaction will be followed for attaching azide-appended Cu(II)-ionophores to the alkyne-scaffolded channel. As in Chapter 4 and Chapter 5, we will test combinations of organic compounds' concentrations, potentials, reaction time and solvents in order to find optimum parameters to be used in the modification of MEAs.

Individually addressable microelectrode arrays can be modified to give selective and simultaneous multi-analyte readouts. One promising direction is to graft different ionophores, which are selective to different metal ions and other analytes of interest. Upon completion of this objective, we will have sufficient fundamental understanding of the method to impact future water detection technologies. Moreover, the completed method is very low cost and portable. Our finished device composed of simple carbon and silicon chips that can be integrated into water streams or immersed into aqueous systems. Real-time selective trace metal detection technologies can aid trace metal mitigation by providing diagnostic chemical information. Fundamentally our studies will pave the way for ultra-fast, simultaneous measurements of any electroactive molecule; this has transformative analytical implications in countless fundamental, health, biological and environmental arenas.

APPENDIX A. OPTIMIZATION OF PB(II) FSCV WAVEFORM UTILIZED IN CHAPTER 3

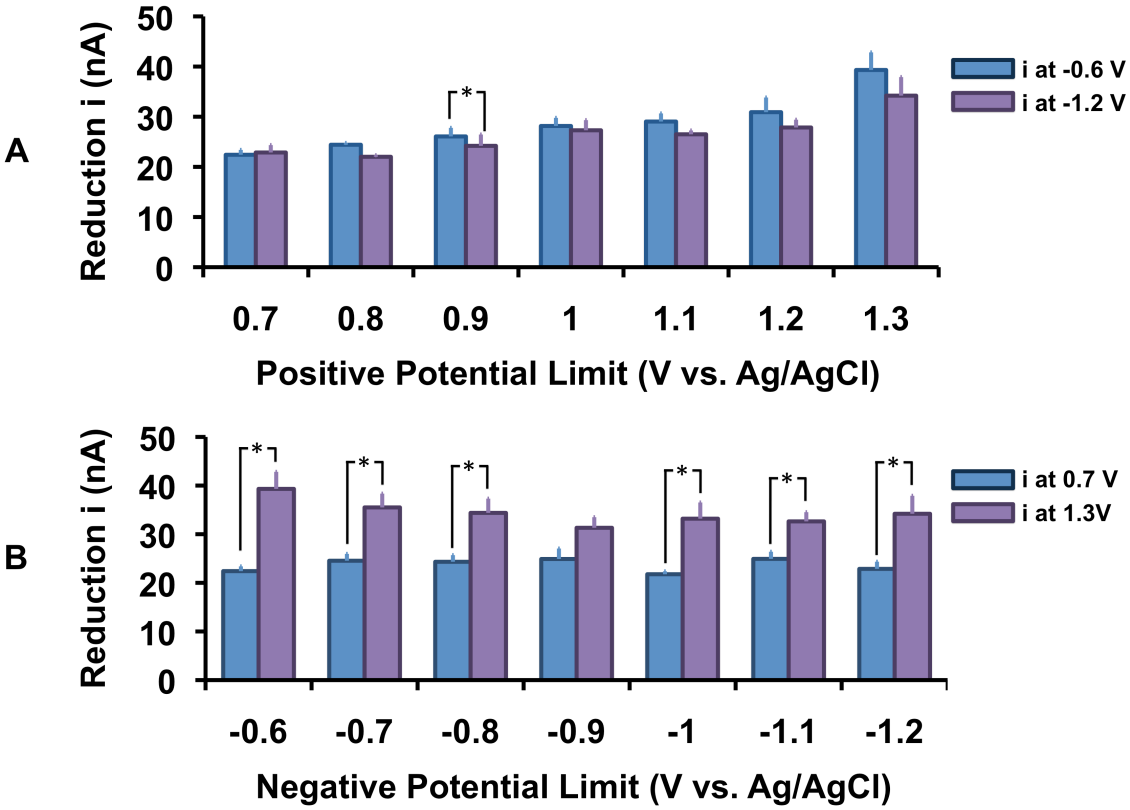

Figure S3.1. A. The maximum reduction current at -0.6 V (blue) compared to the current at -1.2 V (purple) for every positive potential studied. **B.** The maximum reduction current at 1.3 V (purple) compared to the current at 0.7 V (blue) for every negative potential studied. Stars signify statistically different values.

APPENDIX B. SYNTHESIS OF ORGANIC COMPOUNDS IN CHAPTER 4

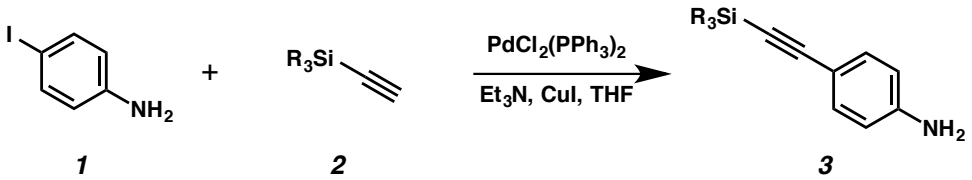

1 *2* *3*

4-((trimethylsilyl)ethynyl)aniline (3a):

4-Iodoaniline (426 mg, 1.94 mmol), copper(I) iodide (37 mg, 0.0.195 mmol), triphenylphosphine (51 mg, 0.195 mmol), and $Pd(PPh_3)_2Cl_2$ (68 mg, 0.097 mmol) were dissolved in dry THF (4.3 mL) and triethylamine (2.4 mL) was added at room temperature with exclusion of light, then the solution was degassed by 3 freeze pump and thaw cycles. After 10 min stirring, trimethylsilylacetylene (220 mg, 316 µL, 2.24 mmol) was added dropwise to this solution. After 16 h, the reaction mixture was filtered through celite and precipitates were washed with ethyl acetate (20 mL). Then the filtrate was washed with distilled water and the layer were separated, the aqueous layer was extracted with EtOAc (3 x 20 mL), then the combined organic extracts were washed with brine, dried over anhydrous $MgSO_4$ and the solvent was removed under reduced pressure and the crude was purified by column chromatography with 0-20% EtOAc/Hexane gradient isolated as a slight yellow solid (367 mg, >99% yield). NMR data matched literature.[64,65]

4-((tert-butyldimethylsilyl)ethynyl)aniline (3b):

4-Iodoaniline (500 mg, 2.283 mmol), copper(I) iodide (43 mg, 0.228 mmol), triphenylphosphine (60 mg, 0.228 mmol), and $Pd(PPh_3)_2Cl_2$ (80 mg, 0.114 mmol)

were dissolved in dry THF (5.1 mL) and triethylamine (2.8 mL) was added at room temperature with exclusion of light, then the solution was degassed by 3 freeze pump and thaw cycles. After 10 min stirring, *t*-butyldimethylsilylacetylene (368 mg, 453 µL, 2.63 mmol) was added dropwise to this solution. After 16 h, the reaction mixture was filtered through celite and precipitates were washed with ethyl acetate (20 mL). Then the filtrate was washed with distilled water and the layer were separated, the aqueous layer was extracted with EtOAc (3 x 20 mL), then the combined organic extracts were washed with brine, dried over anhydrous $MgSO_4$ and the solvent was removed under reduced pressure and the crude was purified by column chromatography with 0-20% EtOAc/Hexane gradient isolated as a slight white solid (513 mg, 97% yield); ^{1}H NMR (400 MHz, $CDCl_3$) δ 7.29 – 7.26 (m, *J* = 8.6 Hz, 2H), 6.58 (d, *J* = 8.6 Hz, 2H), 0.98 (s, 9H), 0.16 (s, 5H); ^{13}C NMR (101 MHz, $CDCL_3$) δ 146.7, 133.4, 114.5, 112.7, 106.6, 89.6, 77.3, 77.0, 76.7, 26.2, 16.8, -4.5; IR

4-((triisopropylsilyl)ethynyl)aniline (3c):

4-Iodoaniline (500 mg, 2.283 mmol), copper(I) iodide (43 mg, 0.228 mmol), triphenylphosphine (60 mg, 0.228 mmol), and $Pd(PPh_3)_2Cl_2$ (80 mg, 0.114 mmol) were dissolved in dry THF (5.1 mL) and triethylamine (2.8 mL) was added at room temperature with exclusion of light, then the solution was degassed by 3 freeze pump and thaw cycles. After 10 min stirring, triisoprpylsilylacetylene (478 mg, 589 µL, 2.63 mmol) was added dropwise to this solution. After 16 h, the reaction mixture was filtered through celite and precipitates were washed with ethyl acetate (20 mL). Then the filtrate was washed with distilled water and the

layer were separated, the aqueous layer was extracted with EtOAc (3 x 20 mL), then the combined organic extracts were washed with brine, dried over anhydrous $MgSO_4$ and the solvent was removed under reduced pressure and the crude was purified by column chromatography with 0-20% EtOAc/Hexane gradient isolated as a slight yellow oil (560 mg, 90% yield). NMR data matched literature.[64,65]

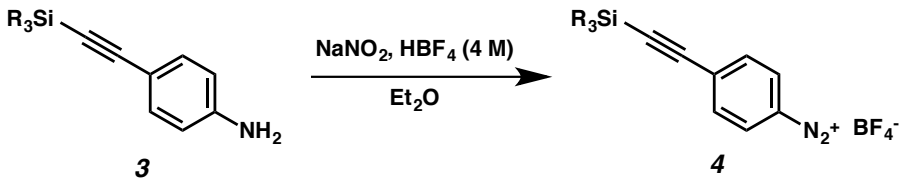

4-((trimethylsilyl)ethynyl)benzenediazonium tetrafluoroborate (4a):

The aniline (**3a**) (310 mg, 1.64 mmol) was dissolved in ether (1 mL) then water (0.9 mL) and 48w% aqueous HBF_4 (1 mL) were added the mixture was cooled to 0 °C then $NaNO_2$ was added slowly. The reaction was allowed to warm up to ambient temperature in melting ice bath and stirred over night with the flask opened to allow the ether to evaporate. The reaction was filtered through a Büchner funnel, the precipitate was washed with ice cold 5wt% aqueous $NaBF_4$ (5 mL), then ice cold water (5 mL), then ice cold methanol (5 mL), then ice cold ether (5 mL), affording beige solid (390 mg, 83% yield). NMR spectra matched literature.[64,65]

4-((tert-butyldimethylsilyl)ethynyl)benzenediazonium tetrafluoroborate (4b):

The aniline (**3b**) (195 mg, 0.843 mmol) was dissolved in ether (1 mL) then water (1.1 mL) and 48w% aqueous HBF_4 (1 mL) were added the mixture was cooled to 0 °C then $NaNO_2$ (290 mg, 4.213 mmol) was added slowly then allowed to warm up to ambient temperature in melting ice bath and stirred over night then with the flask opened to let the ether to evaporate. The reaction was filtered through a Büchner funnel, the precipitate was washed with ice cold 5wt% aqueous $NaBF_4$ (5 mL), then ice cold water (5 mL), then ice cold methanol (5 mL), then ice cold ether (5 mL), affording beige solid (222 mg, 80% yield); ^{1}H NMR (400 MHz, $CDCL_3$) δ 8.55 (d, *J* = 8.9 Hz, 2H), 7.73 (d, *J* = 8.9 Hz, 2H), 0.98 (s, 9H), 0.21 (s, 6H);^{13}C NMR (101 MHz, $CDCL_3$) δ 136.55, 134.11, 132.75, 112.47, 108.06, 102.47, 77.32, 77.00, 76.68, 26.02, 16.70, -5.04; HRMS [M^+] m/z ES calc'd for $[C_{10}H_{14}O_2]^+$: 189.0886; observed: 189.1388; IR 2937, 2874, 1736, 1450 cm^{-1}.

4-((triisopropylsilyl)ethynyl)benzenediazonium tetrafluoroborate (4c)

The aniline (**3c**) (200 mg, 0.731 mmol) was dissolved in ether (1 mL) then water (0.9 mL) and 48w% aqueous HBF_4 (1 mL) were added the mixture was cooled to 0 °C then $NaNO_2$ (252 mg, 3.656 mmol) was added slowly then allowed to warm up to ambient temperature in melting ice bath and stirred over night with the flask opened to allow the ether to evaporate. The reaction was filtered through a Büchner funnel, the precipitate was washed with ice cold 5wt% aqueous $NaBF_4$ (5 mL), then ice cold water (5 mL), then ice cold methanol (5 mL) then ice cold ether (5 mL), affording beige solid (198 mg, 72% yield). NMR spectra matched literature.[64,65]

Azidomethylferrocene

Azidomethylferrocene was synthesized according to literature procedures.[205]

APPENDIX C. SYNTHESIS OF AZIDE APPENDED IONOPHORES IN CHAPTER 5

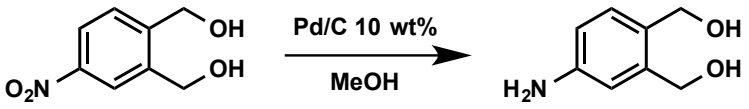

3 4

(4-amino-1,2-phenylene)dimethanol (4):

Pd/C 10 wt% (116.3 mg, 0.109 mmol) was added to a solution of **3** (2.00 g, 10.93 mmol) in methanol (109 mL) under an argon blanket, then the flask was sealed with a rubber septum and was subjected to 3 vacuum hydrogen cycles. The reaction was stirred under hydrogen balloon atmosphere for 1.5 h, and then was filtered through celite. The solvent was removed under reduced pressure and **4** was isolated as a yellow solid (1.67 g, >99%). ^{1}H NMR (400 MHz, CD_3OD) *δ* 7.08 (d, *J* = 8.0 Hz, 1H), 6.80 (d, *J* = 2.0 Hz, 1H), 6.61 (dt, *J* = 10.4, 5.2 Hz, 1H), 4.62 (s, 2H), 4.53 (d, *J* = 13.7 Hz, 2H); ^{13}C NMR (101 MHz, CD_3OD) δ 148.6, 141.7, 131.3, 129.6, 116.6, 115.2, 63.3, 63.1; HRMS [M+Na^+] m/z ESI calc'd for $[C_8H_{11}NO_2Na]^+$: 176.0687 observed: 176.0678; IR 3356, 3290, 3186, 2345.

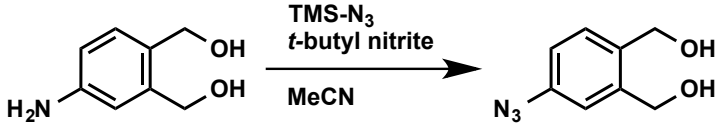

4 5

(4-azido-1,2-phenylene)dimethanol (5):

Azidotrimethylsilane (339 mg, 2.94 mmol) was added to a solution of **4** (375 mg, 2.45 mmol) in MeCN at 0 °C, then *t*-butyl nitrite (278 mg, 2.70 mmol) was added slowly over 15 min. The reaction was allowed to warm up to room

temperature and stirred until TLC showed complete conversion of starting material. The solvent was removed under reduced pressure and the crude product was purified by flash column chromatography 0-10% MeOH/DCM. The azide **5** was isolated as a yellow solid (313 mg, 71%). ^{1}H NMR (400 MHz, CD_3OD) δ 7.40 (d, *J* = 8.1 Hz, 1H), 7.15 (t, *J* = 8.8 Hz, 1H), 6.96 (dd, *J* = 8.1, 2.4 Hz, 1H), 4.70 (s, 2H), 4.64 (s, 2H); ^{13}C NMR (101 MHz, $CDCL_3$) δ 141.42, 140.26, 135.85, 131.30, 120.15, 118.65, 63.79, 63.54; HRMS [M+Na^+] m/z ESI calc'd for $[C_8H_9N_3O_2Na]^+$: 202.0592 observed: 202.0587; IR 3309, 2924, 2870.

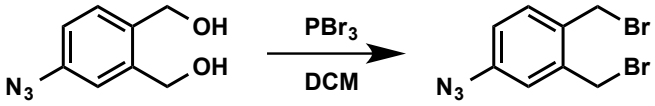

5 6

4-azido-1,2-bis(bromomethyl)benzene (6):

PBr_3 (1.46 g, 5.39 mmol) was added to a solution of **5** (322 mg, 1.797 mmol) in methylene chloride (6 mL) at 0 °C then was warmed up to rt and stirred until TLC showed complete consumption of starting materials about 4h. The reaction was diluted with methylene chloride (10 mL) and washed half saturated $NaHCO_3$ solution (10 mL) was added layers were separated and the aqueous layer was extracted with DCM (3 x 10 mL). The combined organics were dried over $MgSO_4$, the solvent was removed under reduced pressure, the dibromide **6** was isolated as a yellow oil (341 mg, 62%) and used without purification.

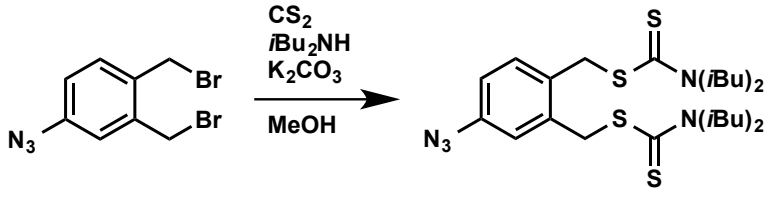

6 7

(4-azido-1,2-phenylene)bis(methylene) bis(diisobutylcarbamodithioate) (7):

Carbon disulfide (166 mg, 2.18 mmol), diisobutyl amine (282 mg, 2.18 mmol), and potassium carbonate (301 mg, 2.18 mmol) were added successively to a solution **6** (330 mg, 1.09 mmol) in methanol at 0 °C, then the reaction was warmed up to room temperature and stirred for 20 h. The reaction was concentrated under reduced pressure then water (10 mL) was added the aqueous layer was extracted with methylene chloride (4 x 10 mL) and the combined organics were dried over Na_2SO_4, The crude was purified by column chromatography eluted with 0-50% dichloromethane/hexanes, **7** was isolated as a yellow oil (531 mg, 88%). ^{1}H NMR (400 MHz, $CDCL_3$) δ 7.41 (d, *J* = 8.3 Hz, 1H), 7.11 (d, *J* = 2.3 Hz, 1H), 6.88 (dd, *J* = 8.2, 2.4 Hz, 1H), 4.61 (s, 2H), 4.60 (s, 2H), 3.96 – 3.75 (m, 4H), 3.63 – 3.43 (m, 4H), 2.53 – 2.38 (m, 2H), 2.36 – 2.17 (m, 2H), 0.98 – 0.84 (m, 24H); ^{13}C NMR (101 MHz, $CDCL_3$) δ 196.36, 196.09, 139.63, 137.18, 132.30, 131.58, 120.99, 118.55, 63.18, 63.06, 60.93, 39.44, 27.59, 26.23, 20.28; HRMS [M+H$^+$] m/z ESI calc'd for $[C_{26}H_{44}N_5S_4]^+$: 554.2480 observed: 554.2460; IR 2958, 2924, 2110, 1597, 1458.

APPENDIX D. DIAZONIUM ELECTROCHEMICAL REDUCTION ON CARBON FIBER MICROEELCTRODES IN CHAPTER 5

Figure S5.1.A illustrates the creation of the scaffolds. Upon a reduction potential, diazonium reagents were reduced on CFM and created a monolayer of TMS bearing scaffolds. The alkyne-terminated scaffolds were revealed by exposure to TBAF for deprotection of TMS moieties and afforded **CFM 3**. The surface variations caused by these reactions were followed electrochemically with FSCV of a 1.0 μM Cu(II) in 0.1 mM NaCl solution as shown in **Figure S5.1.A**. The amplitudes of reduction peaks of Cu(II) at three stages were collected and compared as shown in **Figure S5.1.B** for (180 ± 10) nA, (20 ± 7.0) nA, and (150 ± 14) nA respectively. After grafting a layer with bulky protection groups (diazonium reduction CV shown in the inset), the access of Cu(II) to the oxygenated groups are almost totally inhibited, therefore the signal was largely reduced. **Figure S5.1.C** shows the color plots collected under a waveform of -1.2V/ + 0.8 V for 30s and Cu(II) was injected during 5 to 15 s. **Figure S5.1.D** shows the CVs taken at the dashed lines and redox peaks are recognized at -0.7/0V.

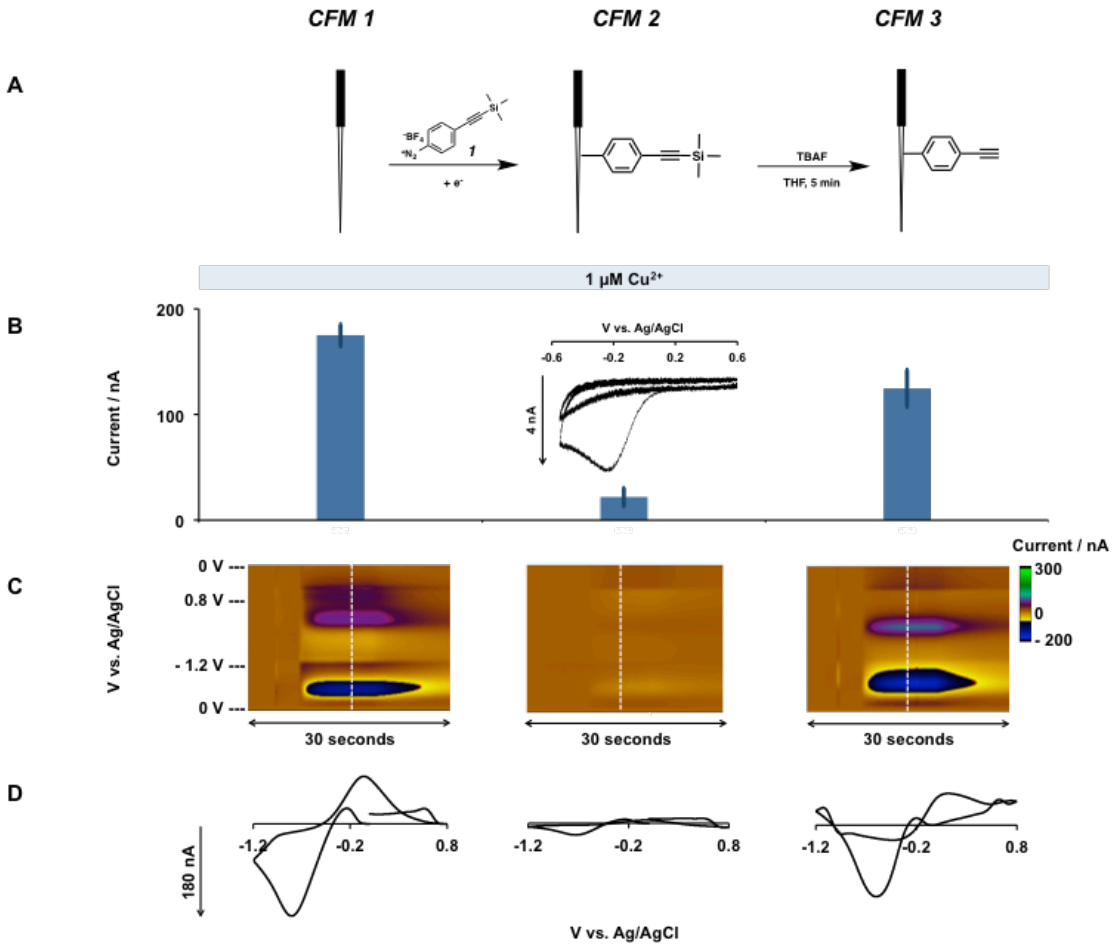

Figure S5.1 Electrochemical characterization of scaffolds created through diazonium electrochemical reduction.

BIBLIOGRAPHY

1. Rose, J. Trace elements in health: A review of current issues; Butterworth-Heinemann, 2013.
2. Bayen, S. Environment international 2012, 48, 84-101.
3. Naser, H. A. Marine pollution bulletin 2013, 72, 6-13.
4. Ritter, L.; Solomon, K.; Sibley, P.; Hall, K.; Keen, P.; Mattu, G.; Linton, B. Journal of Toxicology and Environmental Health-Part a-Current Issues 2002, 65, 1-142.
5. Ndlovu, T.; Arotiba, O. A.; Sampath, S.; Krause, R. W.; Mamba, B. B. Journal of Applied Electrochemistry 2011, 41, 1389-1396.
6. Buffle, J.; Tercier-Waeber, M. L. TrAC Trends in Analytical Chemistry 2005, 24, 172-191.
7. Korn, M. D. A.; de Andrade, J. B.; de Jesus, D. S.; Lemos, V. A.; Bandeira, M.; dos Santos, W. N. L.; Bezerra, M. A.; Amorim, F. A. C.; Souza, A. S.; Ferreira, S. L. C. Talanta 2006, 69, 16-24.
8. Hua, M.; Zhang, S.; Pan, B.; Zhang, W.; Lv, L.; Zhang, Q. Journal of Hazardous Materials 2012, 211, 317-331.
9. Aragay, G.; Merkoçi, A. Electrochimica Acta 2012, 84, 49-61.
10. Gumpu, M. B.; Sethuraman, S.; Krishnan, U. M.; Rayappan, J. B. B. Sensors and Actuators B: Chemical 2015, 213, 515-533.
11. Bersier, P. M.; Howell, J.; Bruntlett, C. Analyst 1994, 119, 219-232.

12. Economou, A.; Kokkinos, C. Advances Advances in Stripping Analysis of Metals. Electrochemical Strategies in Detection Science, The Royal Society of Chemistry 2016, 1-18.

13. Zbinden, C. Bull. Soc. Chim. Biol. 1931, 13.

14. Heyrovský, J.; Kůta, J. Principles of Polarography; Elsevier Science, 2013.

15. Paneli, M. G.; Voulgaropoulos, A. Electroanalysis 1993, 5, 355-373.

16. Arrigan, D. W. M. Analyst 1994, 119, 1953-1966.

17. Stozhko, N. Y.; Malakhova, N. A.; Fyodorov, M. V.; Brainina, K. Z. Journal of Solid State Electrochemistry 2008, 12, 1185-1204.

18. Li, M.; Li, Y.-T.; Li, D.-W.; Long, Y.-T. Analytica Chimica Acta 2012, 734, 31-44.

19. Yosypchuk, B.; Barek, J. Critical Reviews in Analytical Chemistry 2009, 39, 189-203.

20. Barón-Jaimez, J.; Joya, M. R.; Barba-Ortega, J. Journal of Physics: Conference Series 2013, 466, 012025.

21. Valerio, B.; Damien, W. M. A. Current Analytical Chemistry 2008, 4, 229-241.

22. Herzog, G.; Beni, V. Analytica Chimica Acta 2013, 769, 10-21.

23. Zuliani, C.; Diamond, D. Electrochimica Acta 2012, 84, 29-34.

24. Hines, W. G.; de Levie, R. Journal of Chemical Education 2010, 87, 1143-1153.

25. Bühlmann, P.; Chen, L. D. Supramolecular Chemistry: From Molecules to Nanomaterials.

26. Lindner, E.; Pendley, B. D. Analytica Chimica Acta 2013, 762, 1-13.

[27.] Pechenkina, I.; Mikhelson, K. Russian Journal of Electrochemistry 2015, 51, 93-102.

[28.] Steiner, R. A.; Oehme, M.; Ammann, D.; Simon, W. Anal Chem 1979, 51, 351-353.

[29.] Bakker, E.; Bühlmann, P.; Pretsch, E. Electroanalysis 1999, 11, 915-933.

[30.] Wipf, H. K.; Pioda, L. A. R.; Štefanac, Z.; Simon, W. Helvetica Chimica Acta 1968, 51, 377-381.

[31.] Mendecki, L.; Fayose, T.; Stockmal, K. A.; Wei, J.; Granados-Focil, S.; McGraw, C. M.; Radu, A. Anal Chem 2015, 87, 7515-7518.

[32.] Michalska, A. Electroanalysis 2012, 24, 1253-1265.

[33.] Armstrong-James, M.; Millar, J. Journal of Neuroscience Methods 1979, 1, 279-287.

[34.] Hermans, A.; Keithley, R. B.; Kita, J. M.; Sombers, L. A.; Wightman, R. M. Anal Chem 2008, 80, 4040-4048.

[35.] Pathirathna, P.; Samaranayake, S.; Atcherley, C. W.; Parent, K. L.; Heien, M. L.; McElmurry, S. P.; Hashemi, P. Analyst 2014, 139, 4673-4680.

[36.] Atcherley, C. W.; Laude, N. D.; Parent, K. L.; Heien, M. L. Langmuir 2013, 29, 14885-14892.

[37.] Bath, B. D.; Michael, D. J.; Trafton, B. J.; Joseph, J. D.; Runnels, P. L.; Wightman, R. M. Anal Chem 2000, 72, 5994-6002.

[38.] Lama, R. D.; Charlson, K.; Anantharam, A.; Hashemi, P. Anal Chem 2012, 84, 8096-8101.

[39.] Robinson, D. L.; Venton, B. J.; Heien, M. L. A. V.; Wightman, R. M. Clinical Chemistry 2003, 49, 1763-1773.

[40.] Hashemi, P.; Dankoski, E. C.; Wood, K. M.; Ambrose, R. E.; Wightman, R. M. Journal of Neurochemistry 2011, 118, 749-759.

[41.] Samaranayake, S.; Abdalla, A.; Robke, R.; Wood, K. M.; Zeqja, A.; Hashemi, P. Analyst 2015, 140, 3759-3765.

[42.] Ariansen, J. L.; Heien, M. L. A. V.; Hermans, A.; Phillips, P. E. M.; Hernadi, I.; Bermudez, M.; Schultz, W.; Wightman, R. M. Frontiers in Behavioral Neuroscience 2012, 6.

[43.] Huffman, M. L.; Venton, B. J. Analyst 2009, 134, 18-24.

[44.] Pathirathna, P.; Yang, Y. Y.; Forzley, K.; McElmurry, S. P.; Hashemi, P. Anal Chem 2012, 84, 6298-6302.

[45.] Yang, Y. Y.; Pathirathna, P.; Siriwardhane, T.; McElmurry, S. P.; Hashemi, P. Anal Chem 2013, 85, 7535-7541.

[46.] Swamy, B. E. K.; Venton, B. J. Analyst 2007, 132, 876-884.

[47.] Zachek, M. K.; Park, J.; Takmakov, P.; Wightman, R. M.; McCarty, G. S. Analyst 2010, 135, 1556-1563.

[48.] Gao, C.; Guo, Z.; Liu, J.-H.; Huang, X.-J. Nanoscale 2012, 4, 1948-1963.

[49.] Belanger, D.; Pinson, J. Chemical Society Reviews 2011, 40, 3995-4048.

[50.] Doyle, R. L.; Godwin, I. J.; Brandon, M. P.; Lyons, M. E. Physical Chemistry Chemical Physics 2013, 15, 13737-13783.

[51.] Yao, S. A.; Ruther, R. E.; Zhang, L.; Franking, R. A.; Hamers, R. J.; Berry, J. F. Journal of the American Chemical Society 2012, 134, 15632-15635.

52. Wang, L.; Su, B.; Cheng, C.; Ma, L.; Li, S.; Nie, S.; Zhao, C. Journal of Materials Chemistry B 2015, 3, 1391-1404.

53. Jesionowski, T.; Zdarta, J.; Krajewska, B. Adsorption 2014, 20, 801-821.

54. Ates, M.; Sarac, A. S. Progress in Organic Coatings 2009, 66, 337-358.

55. Le Floch, F.; Simonato, J. P.; Bidan, G. Electrochimica Acta 2009, 54, 3078-3085.

56. McCreery, R. L. Chem. Rev. 2008, 108, 2646-2687.

57. McCreery, R. L. Electroanalytical chemistry 1991, 17, 221-374.

58. Ray Iii, K. G.; McCreery, R. L. Journal of Electroanalytical Chemistry 1999, 469, 150-158.

59. Delamar, M.; Hitmi, R.; Pinson, J.; Saveant, J. M. Journal of the American Chemical Society 1992, 114, 5883-5884.

60. Coates, M.; Elamari, H.; Girard, C.; Griveau, S.; Nyokong, T.; Bedioui, F. Journal of Electroanalytical Chemistry 2012, 670, 79-84.

61. Tanaka, M.; Sawaguchi, T.; Sato, Y.; Yoshioka, K.; Niwa, O. Langmuir 2011, 27, 170-178.

62. Rostovtsev, V. V.; Green, L. G.; Fokin, V. V.; Sharpless, K. B. Angewandte Chemie-International Edition 2002, 41, 2596-+.

63. Himo, F.; Lovell, T.; Hilgraf, R.; Rostovtsev, V. V.; Noodleman, L.; Sharpless, K. B.; Fokin, V. V. Journal of the American Chemical Society 2005, 127, 210-216.

64. Leroux, Y. R.; Fei, H.; Noel, J. M.; Roux, C.; Hapiot, P. Journal of the American Chemical Society 2010, 132, 14039-14041.

65. Leroux, Y. R.; Hapiot, P. Chemistry of Materials 2013, 25, 489-495.

66. Feier, B.; Fizesan, I.; Mériadec, C.; Ababou Girard, S.; Cristea, C.; Sandulescu, R.; Geneste, F. Journal of Electroanalytical Chemistry 2015, 744, 1-7.

67. Bath, B. D.; Martin, H. B.; Wightman, R. M.; Anderson, M. R. Langmuir 2001, 17, 7032-7039.

68. Nasri, Z.; Shams, E. Electrochimica Acta 2013, 112, 640-647.

69. McElmurry, S. P.; Long, D. T.; Voice, T. C. Applied Geochemistry 2010, 25, 650-660.

70. Bigalke, M.; Weyer, S.; Wilcke, W. Environmental Science & Technology 2010, 44, 5496-5502.

71. Wang, J.; Marshall, W. D. Anal Chem 1994, 66, 3900-3907.

72. Harville, T. R.; Marcus, R. K. Anal Chem 1995, 67, 1271-1277.

73. Zhao, T.; Chen, T.; Qiu, Y.; Zou, X.; Li, X.; Su, M.; Yan, C.; Zhao, A.; Jia, W. Anal Chem 2009, 81, 3683-3692.

74. Mazloum Ardakani, M.; Salavati-Niasari, M.; Khayat Kashani, M.; Ghoreishi, S. M. Analytical and Bioanalytical Chemistry 2004, 378, 1659-1665.

75. Turyan, I.; Mandler, D. Anal Chem 1993, 65, 2089-2092.

76. Cahill, P. S.; Walker, Q. D.; Finnegan, J. M.; Mickelson, G. E.; Travis, E. R.; Wightman, R. M. Anal Chem 1996, 68, 3180-3186.

77. Hashemi, P.; Dankoski, E. C.; Petrovic, J.; Keithley, R. B.; Wightman, R. M. Analytical Chemistry 2009, 81, 9462-9471.

78. Millar, J.; Stamford, J. A.; Kruk, Z. L.; Wightman, R. M. European Journal of Pharmacology 1985, 109, 341-348.

79. Michael, D.; Travis, E. R.; Wightman, R. M. Anal Chem 1998, 70, 586A-592A.

80. Heien, M. L. A. V.; Phillips, P. E. M.; Stuber, G. D.; Seipel, A. T.; Wightman, R. M. Analyst 2003, 128, 1413-1419.

81. Takmakov, P.; Zachek, M. K.; Keithley, R. B.; Walsh, P. L.; Donley, C.; McCarty, G. S.; Wightman, R. M. Analytical chemistry 2010, 82, 2020-2028.

82. Laidlaw, M. A. S.; Filippelli, G. M. Applied Geochemistry 2008, 23, 2021-2039.

83. Nriagu, J. O. In The Biogeochemistry of lead in the environment, Nriagu, J. O., Ed.; Elsevier: Amsterda, 1978, pp 1-14.

84. Binns, H. J.; Campbell, C.; Brown, M. J. Pediatrics 2007, 120, E1285-E1298.

85. Zahran, S.; Laidlaw, M. A. S.; McElmurry, S. P.; Filippelli, G. M.; Taylor, M. Environmental Science & Technology 2013, 47, 2839-2845.

86. NRC. Urban Stormwater Management in the United States; National Academies Press: Washington, D.C., 2008.

87. EPA, National Water Quality Inventory: Report to Congress. 2004 Reporting Cycle; EPA 841-R-08-001; United State Environmental Protection Agency: Washington, DC, 2009.

88. Lee, H.; Lau, S.-L.; Kayhanian, M.; Stenstrom, M. K. Water Research 2004, 38, 4153-4163.

89. Strawn, D. G.; Sparks, D. L. Soil Science Society of America 2000, 64, 144-156.

90. Stumm, W.; Morgan, J. J. Aquatic Chemistry; Wiley: New York, 1996, p 1022.

91. Buffle, J.; Tercier-Waeber, M. L. Trac-Trends in Analytical Chemistry 2005, 24, 172-191.

92. Sigg, L.; Black, F.; Buffle, J.; Cao, J.; Cleven, R.; Davison, W.; Galceran, J.; Gunkel, P.; Kalis, E.; Kistler, D.; Martin, M.; Noel, S.; Nur, Y.; Odzak, N.; Puy, J.; Van Riemsdijk, W.; Temminghoff, E.; Tercier-Waeber, M. L.; Toepperwien, S.; Town, R. M.; Unsworth, E.; Warnken, K. W.; Weng, L.; Xue, H.; Zhang, H. Environ Sci Technol 2006, 40, 1934-1941.

93. Armstrong, K. C.; Tatum, C. E.; Dansby-Sparks, R. N.; Chambers, J. Q.; Xue, Z.-L. Talanta 2010, 82, 675-680.

94. Pathirathna, P.; Yang, Y.; Forzley, K.; McElmurry, S. P.; Hashemi, P. Anal Chem 2012, 84, 6298-6302.

95. Li, G.; Ji, Z.; Wu, K. Analytica Chimica Acta 2006, 577, 178-182.

96. Khun, N. W.; Liu, E. Electrochimica Acta 2009, 54, 2890-2898.

97. Bas, B.; Jakubowska, M.; Jez, M.; Ciepiela, F. Journal of Electroanalytical Chemistry 2010, 638, 3-8.

98. Sherigara, B. S.; Shivaraj, Y.; Mascarenhas, R. J.; Satpati, A. K. Electrochimica Acta 2007, 52, 3137-3142.

99. Kefala, G.; Economou, A.; Voulgaropoulos, A. Analyst 2004, 129, 1082-1090.

100. Guzsvany, V.; Nakajima, H.; Soh, N.; Nakano, K.; Svancara, I.; Vytras, K.; Bjelica, L.; Imato, T. Electroanalysis 2011, 23, 1593-1601.

101. Silva, P. R. M.; El Khakani, M. A.; Chaker, M.; Dufresne, A.; Courchesne, F. Sensors and Actuators B-Chemical 2001, 76, 250-257.

[102.] Prado, C.; Wilkins, S. J.; Marken, F.; Compton, R. G. Electroanalysis 2002, 14, 262-272.

[103.] dos Santos, A. C. V.; Masini, J. C. Analytical and Bioanalytical Chemistry 2006, 385, 1538-1544.

[104.] Wright Water Engineers; Geosyntec Consultants. Water Environment Research Foundation, American Society of Civil Engineers/Environmental and Water Resources Institute, American Public Works Association, Federal Highway Administration, U.S. Environmental Protection Agency: http://www.bmpdatabase.org/, 2007.

[105.] Charlton, S. R.; Macklin, C. L.; Parkhurst, D. L., Phreeqcl--A graphical user interface for the geochemical computer program PHREEQC: U.S. Geological Survey Water-Resources Investigations Report 97-4222; U.S. Geological Survey1997.

[106.] Allison, J. D.; Brown, D. S.; Novo-Gradae, K. J., MINTEQA2/PRODEFA2--A geochemical assessment model for environmental systems--version 3.0 user's manual.; Environmental Research Laboratory, Office of Research and Development, U.S. Environmental Protection Agency,: Athens, Georgia, 1990.

[107.] Heyrovsky, J.; Shikata, M. Recueil Des Travaux Chimiques Des Pays-Bas 1925, 44, 496-U497.

[108.] Economou, A. Trac-Trends in Analytical Chemistry 2005, 24, 334-340.

[109.] Kefala, G.; Economou, A. Analytica Chimica Acta 2006, 576, 283-289.

[110.] Ninwong, B.; Chuanuwatanakul, S.; Chailapakul, O.; Dungchai, W.; Motomizu, S. Talanta 2012, 96, 75-81.

[111.] Wang, J.; Lu, J. M.; Anik, U.; Hocevar, S. B.; Ogorevc, B. Analytica Chimica Acta 2001, 434, 29-34.

[112.] Dean, C. M.; Sansalone, J. J.; Cartledge, F. K.; Pardue, J. H. J. Environ. Eng.-ASCE 2005, 131, 632-642.

[113.] Aroua, M. K.; Leong, S. P. P.; Teo, L. Y.; Yin, C. Y.; Daud, W. M. A. W. Bioresource Technology 2008, 99, 5786-5792.

[114.] Puntener, M.; Vigassy, T.; Baier, E.; Ceresa, A.; Pretsch, E. Analytica Chimica Acta 2004, 503, 187-194.

[115.] Ganjali, M. R.; Motakef-Kazami, N.; Faridbod, F.; Khoee, S.; Norouzi, P. Journal of Hazardous Materials 2010, 173, 415-419.

[116.] Heien, M. L.; Phillips, P. E.; Stuber, G. D.; Seipel, A. T.; Wightman, R. M. Analyst 2003, 128, 1413-1419.

[117.] Stumm, W.; Morgan, J. J. Aquatic Chemistry, 3rd ed.; Wiley: New York, 1996.

[118.] Kokkinos, C.; Economou, A.; Raptis, I.; Speliotis, T. Electrochemistry Communications 2011, 13, 391-395.

[119.] Novotny, E. V.; Murphy, D.; Stefan, H. G. Sci. Total Environ. 2008, 406, 131-144.

[120.] Zimmerman, J. B.; Wightman, R. M. Anal Chem 1991, 63, 24-28.

[121.] Venton, B. J.; Michael, D. J.; Wightman, R. M. J Neurochem 2003, 84, 373-381.

[122.] Takmakov, P.; Zachek, M. K.; Keithley, R. B.; Walsh, P. L.; Donley, C.; McCarty, G. S.; Wightman, R. M. Anal Chem 2010, 82, 2020-2028.

[123.] Bonfil, Y.; Brand, M.; Kirowa-Eisner, E. Analytica Chimica Acta 2002, 464, 99-114.

[124.] Balshaw, S.; Edwards, J.; Daughtry, B.; Ross, K. Rev Environ Health 2007, 22, 91-113.

[125.] Ward, D. M.; Nislow, K. H.; Folt, C. L. Annals of the New York Academy of Sciences 2010, 1195, 62-83.

[126.] Gaier, E. D.; Eipper, B. A.; Mains, R. E. Journal of Neuroscience Research 2013, 91, 2-19.

[127.] Que, E. L.; Domaille, D. W.; Chang, C. J. Chem. Rev. 2008, 108, 1517-1549.

[128.] Corapcioglu, M. O.; Huang, C. P. Water Research 1987, 21, 1031-1044.

[129.] Heien, M.; Phillips, P. E. M.; Stuber, G. D.; Seipel, A. T.; Wightman, R. M. Analyst 2003, 128, 1413-1419.

[130.] Pihel, K.; Walker, Q. D.; Wightman, R. M. Anal Chem 1996, 68, 2084-2089.

[131.] Runnels, P. L.; Joseph, J. D.; Logman, M. J.; Wightman, R. M. Anal Chem 1999, 71, 2782-2789.

[132.] Weber, J.; Dunsch, L.; Neudeck, A. Electroanalysis 1995, 7, 255-259.

[133.] Ross, A. E.; Venton, B. J. Analyst 2012, 137, 3045-3051.

[134.] Jacobs, C. B.; Vickrey, T. L.; Venton, B. J. Analyst 2011, 136, 3557-3565.

[135.] Xiao, N.; Venton, B. J. Anal Chem 2012, 84, 7816-7822.

[136.] Mukherjee, S.; Sengupta, K.; Das, M. R.; Jana, S. S.; Dey, A. Journal of Biological Inorganic Chemistry 2012, 17, 1009-1023.

[137.] Bobacka, J. Electroanalysis 2006, 18, 7-18.

[138.] Michalska, A. Electroanalysis 2012, 24, 1253-1265.

[139.] Faridbod, F.; Ganjali, M. R.; Dinarvand, R.; Norouzi, P. Sensors 2008, 8, 2331-2412.

[140.] Zhu, J. W.; Qin, Y.; Zhang, Y. H. Electrochem. Commun. 2009, 11, 1684-1687.

[141.] Melzer, K.; Munzer, A. M.; Jaworska, E.; Maksymiuk, K.; Michalska, A.; Scarpa, G. Analyst 2014, 139, 4947-4954.

[142.] Guo, X. F.; Meyung, T.; Yun, Y. H.; Shanov, V. N.; Halsall, H. B.; Heineman, W. R. Electroanalysis 2012, 24, 2045-2048.

[143.] Ivanova, N. M.; Levin, M. B.; Mikhelson, K. N. Russian Chemical Bulletin 2012, 61, 926-936.

[144.] Guo, X. F.; Small, J. P.; Klare, J. E.; Wang, Y. L.; Purewal, M. S.; Tam, I. W.; Hong, B. H.; Caldwell, R.; Huang, L. M.; O'Brien, S.; Yan, J. M.; Breslow, R.; Wind, S. J.; Hone, J.; Kim, P.; Nuckolls, C. Science 2006, 311, 356-359.

[145.] Deinhammer, R. S.; Ho, M.; Anderegg, J. W.; Porter, M. D. Langmuir 1994, 10, 1306-1313.

[146.] Ramanathan, T.; Fisher, F. T.; Ruoff, R. S.; Brinson, L. C. Chemistry of Materials 2005, 17, 1290-1295.

[147.] Gietter, A. A. S.; Pupillo, R. C.; Yap, G. P. A.; Beebe, T. P.; Rosenthal, J.; Watson, D. A. Chemical Science 2013, 4, 437-443.

[148.] Allongue, P.; Delamar, M.; Desbat, B.; Fagebaume, O.; Hitmi, R.; Pinson, J.; Saveant, J. M. Journal of the American Chemical Society 1997, 119, 201-207.

[149.] Galli, C. Chem. Rev. 1988, 88, 765-792.

[150.] Evrard, D.; Lambert, F.; Policar, C.; Balland, V.; Limoges, B. Chemistry-a European Journal 2008, 14, 9286-9291.

[151.] Nurchi, V. M.; Villaescusa, I. Coordination Chemistry Reviews 2012, 256, 212-221.

[152.] Robert, A.; Liu, Y.; Nguyen, M.; Meunier, B. Accounts of Chemical Research 2015, 48, 1332-1339.

[153.] Burkhead, J. L.; Gogolin Reynolds, K. A.; Abdel-Ghany, S. E.; Cohu, C. M.; Pilon, M. New Phytologist 2009, 182, 799-816.

[154.] Valipour, A.; Hamnabard, N.; Woo, K.-S.; Ahn, Y.-H. Journal of Environmental Management 2014, 145, 1-8.

[155.] Yang, Y.; Ibrahim, A. A.; Stockdill, J. L.; Hashemi, P. Anal. Methods 2015, 7, 7352-7357.

[156.] Kamata, S.; Murata, H.; Kubo, Y.; Bhale, A. Analyst 1989, 114, 1029-1031.

[157.] Michael, D. J.; Joseph, J. D.; Kilpatrick, M. R.; Travis, E. R.; Wightman, R. M. Anal Chem 1999, 71, 3941-3947.

[158.] Wang, C.; Jia, G.; Taherabadi, L. H.; Madou, M. J. Microelectromechanical Systems, Journal of 2005, 14, 348-358.

[159.] Ranganathan, S.; McCreery, R. L. Analytical chemistry 2001, 73, 893-900.

[160.] Wightman, R.; Amatorh, C.; Engstrom, R.; Hale, P.; Kristensen, E.; Kuhr, W.; May, L. Neuroscience 1988, 25, 513-523.

[161.] Strand, A. M.; Venton, B. J. Analytical chemistry 2008, 80, 3708-3715.

[162.] Zestos, A. G.; Nguyen, M. D.; Poe, B. L.; Jacobs, C. B.; Venton, B. J. Sensors and Actuators B: Chemical 2013, 182, 652-658.

[163.] Schrlau, M. G.; Dun, N. J.; Bau, H. H. ACS nano 2009, 3, 563-568.

[164.] Singhal, R.; Bhattacharyya, S.; Orynbayeva, Z.; Vitol, E.; Friedman, G.; Gogotsi, Y. Nanotechnology 2010, 21, 015304.

[165.] Morton, K. C.; Morris, C. A.; Derylo, M. A.; Thakar, R.; Baker, L. A. Analytical chemistry 2011, 83, 5447-5452.

[166.] Hermans, A.; Wightman, R. M. Langmuir 2006, 22, 10348-10353.

[167.] Niwa, O.; Jia, J.; Sato, Y.; Kato, D.; Kurita, R.; Maruyama, K.; Suzuki, K.; Hirono, S. Journal of the American Chemical Society 2006, 128, 7144-7145.

[168.] Koehne, J. E.; Marsh, M.; Boakye, A.; Douglas, B.; Kim, I. Y.; Chang, S.-Y.; Jang, D.-P.; Bennet, K. E.; Kimble, C.; Andrews, R. Analyst 2011, 136, 1802-1805.

[169.] Niwa, O.; Tabei, H. Analytical Chemistry 1994, 66, 285-289.

[170.] Song, Y.; Agrawal, R.; Hao, Y.; Chen, C.; Wang, C. ECS Transactions 2014, 61, 55-64.

[171.] Kostecki, R.; Song, X.; Kinoshita, K. Electrochemical and solid-state letters 2002, 5, E29-E31.

[172.] VanDersarl, J. J.; Mercanzini, A.; Renaud, P. Advanced Functional Materials 2015, 25, 78-84.

[173.] Moretto, L. M.; Mardegan, A.; Cettolin, M.; Scopece, P. Chemosensors 2015, 3, 157-168.

[174.] Dengler, A. K.; McCarty, G. S. Journal of Electroanalytical Chemistry 2013, 693, 28-33.

[175.] Zachek, M. K.; Hermans, A.; Wightman, R. M.; McCarty, G. S. Journal of Electroanalytical Chemistry 2008, 614, 113-120.

[176.] Zachek, M. K.; Takmakov, P.; Moody, B.; Wightman, R. M.; McCarty, G. S. Analytical chemistry 2009, 81, 6258-6265.

[177.] Penmatsa, V.; Kim, T.; Beidaghi, M.; Kawarada, H.; Gu, L.; Wang, Z.; Wang, C. Nanoscale 2012, 4, 3673-3678.

[178.] Penmatsa, V.; Ruslinda, A. R.; Beidaghi, M.; Kawarada, H.; Wang, C. Biosensors and bioelectronics 2013, 39, 118-123.

[179.] Xu, H.; Malladi, K.; Wang, C.; Kulinsky, L.; Song, M.; Madou, M. Biosensors and Bioelectronics 2008, 23, 1637-1644.

[180.] Xi, S.; Shi, T.; Liu, D.; Xu, L.; Long, H.; Lai, W.; Tang, Z. Sensors and Actuators A: Physical 2013, 198, 15-20.

[181.] Kim, J.; Song, X.; Kinoshita, K.; Madou, M.; White, R. Journal of the Electrochemical Society 1998, 145, 2314-2319.

[182.] Donner, S.; Li, H.-W.; Yeung, E. S.; Porter, M. D. Analytical chemistry 2006, 78, 2816-2822.

[183.] Sánchez-Molas, D.; Cases-Utrera, J.; Godignon, P.; del Campo, F. J. Sensors and Actuators B: Chemical 2013, 186, 293-299.

[184.] Poon, M.; McCreery, R. L. Analytical Chemistry 1986, 58, 2745-2750.

[185.] Heien, M. L.; Phillips, P. E.; Stuber, G. D.; Seipel, A. T.; Wightman, R. M. Analyst 2003, 128, 1413-1419.

[186.] Gonon, F.; Fombarlet, C.; Buda, M.; Pujol, J. F. Analytical Chemistry 1981, 53, 1386-1389.

[187.] Roberts, J. G.; Moody, B. P.; McCarty, G. S.; Sombers, L. A. Langmuir 2010, 26, 9116-9122.

[188.] Michael, D. J.; Wightman, R. M. Journal of pharmaceutical and biomedical analysis 1999, 19, 33-46.

[189.] Hashemi, P.; Dankoski, E. C.; Lama, R.; Wood, K. M.; Takmakov, P.; Wightman, R. M. Proceedings of the National Academy of Sciences 2012, 109, 11510-11515.

[190.] Pathirathna, P.; Yang, Y.; Forzley, K.; McElmurry, S. P.; Hashemi, P. Analytical chemistry 2012, 84, 6298-6302.

[191.] Yang, Y.; Pathirathna, P.; Siriwardhane, T.; McElmurry, S. P.; Hashemi, P. Analytical chemistry 2013, 85, 7535-7541.

[192.] De Volder, M. F.; Vansweevelt, R.; Wagner, P.; Reynaerts, D.; Van Hoof, C.; Hart, A. J. Acs Nano 2011, 5, 6593-6600.

[193.] Khan, A. S.; Michael, A. C. TrAC Trends in Analytical Chemistry 2003, 22, 503-508.

[194.] Singh, A.; Jayaram, J.; Madou, M.; Akbar, S. Journal of the electrochemical society 2002, 149, E78-E83.

[195.] McCreery, R. L. Chem. Rev 2008, 108, 2646-2687.

[196.] Jenkins, G. M.; Kawamura, K. Polymeric carbons--carbon fibre, glass and char; Cambridge University Press, 1976.

[197.] Kostecki, R.; Schnyder, B.; Alliata, D.; Song, X.; Kinoshita, K.; Kötz, R. Thin Solid Films 2001, 396, 36-43.

[198.] Ranganathan, S.; Mccreery, R.; Majji, S. M.; Madou, M. Journal of the Electrochemical Society 2000, 147, 277-282.

[199.] Hirabayashi, M.; Mehta, B.; Vahidi, N. W.; Khosla, A.; Kassegne, S. Journal of Micromechanics and Microengineering 2013, 23, 115001.

[200.] Hashemi, P.; Dankoski, E. C.; Petrovic, J.; Keithley, R. B.; Wightman, R. Analytical chemistry 2009, 81, 9462-9471.

[201.] Kachoosangi, R. T.; Compton, R. G. Analytical and bioanalytical chemistry 2007, 387, 2793-2800.

[202.] Roberts, J. G.; Hamilton, K. L.; Sombers, L. A. Analyst 2011, 136, 3550-3556.

[203.] Chen, C.; Liang, B.; Ogino, A.; Wang, X.; Nagatsu, M. The Journal of Physical Chemistry C 2009, 113, 7659-7665.

[204.] Felten, A.; Bittencourt, C.; Pireaux, J.-J.; Van Lier, G.; Charlier, J.-C. Journal of Applied Physics 2005, 98, 074308.

[205.] Hardy, C. G.; Ren, L.; Tamboue, T. C.; Tang, C. Journal of Polymer Science Part A: Polymer Chemistry 2011, 49, 1409-1420.

ABSTRACT

DEVELOPMENT OF SINGLE AND ARRAY ELECTRO-CHEMICAL SENSORS FOR REAL-TIME TRACE METAL ANALYSIS IN AQEOUS ENVIRONMENTAL MEDIA

by

YUANYUAN YANG

May 2016

Advisor: Dr. Parastoo Hashemi

Major: Chemistry (Analytical)

Degree: Doctor of Philosophy

Detection of trace metals has great importance in environmental and biological applications. While traditional electrochemical techniques have played critical roles in this field, their usefulness is limited by temporal resolution, Hg toxicity and stability concerns. Recently, we developed a method using fast-scan cyclic voltammetry (FSCV) at carbon-fiber microelectrodes (CFMs) to achieve rapid measurement of metal ions with high sensitivity, selectivity, and stability. Through optimizations this method showed strengths in real-time trace metal analysis.

Analytical selectivity was improved via covalent functionalization on CFMs. We employed diazonium electrochemical reduction followed by click chemistry to create robust covalent attachments. After optimization and characterization with ferrocene as proof of principle of the modification, we showcased its application through grafting Cu(II) ionophores onto CFMs. The selectivity was further reinforced via inhibition of other species' adsorption at surface oxygen groups.

This stepwise functionalization approach served as a universal platform for elevating CFMs' selectivity, while retaining sensitivity, response, stability, and lifetime.

In parallel work, pyrolyzed photoresist film (PPF) microelectrode arrays (MEAs) were fabricated to extend the borderlines of FSCV towards simultaneous multi-analyte analysis. The PPF MEAs maintained CFM's carbon-fiber structures but provided more sensing channels. We employed a two-step pyrolysis process and a dual O_2 plasma treatment to improve fabrication repeatability, surface reactivity, and spatial geometry. Our technique has evident potential to achieve real-time simultaneous detection of various electroactive molecules and be employed for numerous applications in complex biological and environmental systems.

AUTOBIOGRAPHICAL STATEMENT

Yuanyuan Yang

EDUCATION

2011 – 2016	Wayne State University, Detroit, MI	**Ph.D., Chemistry**
2007 – 2011	East China University of Science and Technology, Shanghai, China	**B.S., Chemistry**

HONORS AND AWARDS

2015 Graduate Department Citation for Excellence in Teaching Service, Wayne State University, MI
2015 Graduate Student Professional Travel Award (GSPTA) – Wayne State University, MI
2014 Thomas C. Rumble University Graduate Fellowships, Wayne State University, MI
2014 ANACHEM Oral Presentation Citation – ANACHEM, Livonia, MI

PUBLICATIONS

1. **Yang, Y.**, Ibrahim, A. A., Hashemi, P. and Stockdill, J. L., Real-Time, Ultra-Selective Detection of Copper(II) using Ionophore-Grafted Carbon-Fiber Microelectrodes, *In preparation.*
2. **Yang, Y.**,* Yi, W.,* Hashemi, P., Cheng, M., A Novel Carbon Nanofiber Pyrolyzed Photoresist Microelectrode Array for Fast Scan Cyclic Voltammetry Analysis, *In preparation,* *Contributed equally.
3. **Yang, Y.**, Ibrahim, A. A., Stockdill, J. L. and Hashemi, P. "A Density-Controlled Scaffolding Strategy for Covalent Functionalization of Carbon-Fiber Microelectrodes." *Analytical Methods*, **2015**, 7: 7352-7357.
4. **Yang, Y.**, Pathirathna, P., Siriwardhane, T., McElmurry, S. P., Hashemi, P. "Real-Time Subsecond Voltammetric Analysis of Pb in Aqueous Environmental Samples." *Anal. Chem.* **2013***,* 85(15): 7535-7541.
5. Pathirathna, P., **Yang, Y.**, Forzley, K., McElmurry, S. P., Hashemi, P. "Fast-Scan Deposition-Stripping Voltammetry at Carbon-Fiber Microelectrodes: Real-Time, Subsecond, Mercury Free Measurements of Copper." *Anal. Chem.* **2012**, 84(15): 6298-6302.